

**Algorithms & Techniques for Studying *In Vitro* Oral Biofilms**

by

**Ting Liu Luo**

A dissertation submitted in partial fulfillment  
of the requirements of the degree of  
Doctor of Philosophy  
(Oral Health Sciences)  
in the University of Michigan  
2018

Doctoral Committee:

Professor Betsy Foxman, Co-chair  
Associate Professor Alexander H. Rickard, Co-chair  
Associate Professor Marisa C. Eisenberg  
Associate Professor Carlos González-Cabezas  
Associate Professor Carl F. Marrs

Ting Liu Luo

[tingluo@umich.edu](mailto:tingluo@umich.edu)

ORCID iD: 0000-0002-6103-1981

© Ting Liu Luo 2018

## **DEDICATION**

I dedicate this work to my parents

## **ACKNOWLEDGEMENTS**

To my dissertation committee co-chairs Dr. Alexander H. Rickard, and Dr. Betsy Foxman: Thank you for your unwavering support, guidance, and instruction not only these past five years in the doctoral program, but the two years prior when I was a Masters student. To my dissertation committee members Dr. Marisa C. Eisenberg, Dr. Carl F. Marrs, and Dr. Carlos González-Cabezas. Thank you for your full support, suggestions, and incredible personalized mentorship that you have provided. My years in this program would not have been as fulfilling without having each and every one of you on my committee.

To Dr. Marianne Zsiska and Dr. Benjamin Circello from Oral Care, Procter & Gamble. Thank you for dedicating time and effort.

Lab members – Dr. Usha Srinivasan, Sreelatha Ponnaluri, Kirtana Ramadugu, Erika Trumble, Jean Li, Elizabeth Boyd, Rachel Gicquelais and Freida Blostein from the Foxman Lab. Kyu Han Lee and Annie Gencay from the Gordon lab. Hannah Segaloff, Rich Evans, and Kate Sutcliffe from the Martin Lab. Derek Samarian, Jae Shin, Gregory Kruse, Anna Frick, Savannah Hatt, Deepti Bettampadi, Constanza Fernandez, Ethan Kolderman, and Betsy Salzman from the Rickard lab. And to everyone from the fifth floor labs. Thank you for being not only colleagues, but friends.

Funding sources – I am personally very grateful for the funding sources that supported me these past five years and made this work possible, including a grant from Procter & Gamble, Graduate Student Instructor tuition waivers, the Dave Striffler Scholarship for Dental Research, the Francis E. Payne Scholarship, The Blackerby Lectureship Fund, and Rackham Graduate School Travel Grants.

Thank you to all my cohort members that have supported each other throughout this journey, from competency exam to graduation. Thank you to Dr. Michael Hayashi for becoming an integral member of the Biofilm Architecture Inference Tool development team. Thank you Michael Vanek for illustrations of *in vitro* model systems in Chapter II.

To my sister Mulon Luo, thank you for your guidance and support, especially these past few years. And finally, to my father and mother, Mr. Ming Chyur Luo and Mrs. Yu Ying Tai. Thank you for the sacrifices that you have made to provide my sister and I all the opportunities we have been afforded in the last 27 years.

## PREFACE

A version of Chapter III is currently under review by the journal *Nature Scientific Reports* with the following authors: Ting L. Luo, Marisa C. Eisenberg, Michael A.L. Hayashi, Carlos Gonzalez-Cabezas, Betsy Foxman, Carl F. Marrs, and Alexander H. Rickard. Chapter II and Chapter IV are anticipated to be submitted in the near future for publication.

## Table of Contents

DEDICATION	ii
ACKNOWLEDGEMENTS	iii
LIST OF TABLES	xi
LIST OF FIGURES	xii
LIST OF APPENDICES	xiv
ABSTRACT	xv

### CHAPTER I: Introduction

Oral Diseases and Biofilms	1
Epidemiology of Caries & Periodontal Disease	2
The Role of Bacteria in Caries & Periodontal Disease	4
The Changing Paradigm of Oral Diseases	4
<i>In Vitro</i> Laboratory Model Systems	6
Role of <i>In Vitro</i> Laboratory Models in Dental Biofilm Research	6
Resurgence of <i>In Vitro</i> Laboratory Models	6
Considerations for Using <i>In Vitro</i> Laboratory Models	7
Limitations of Current Approaches in <i>In Vitro</i> Laboratory Models	8
Paucity of Model System Standard Protocols	8
Biased Imaging Strategies	8
Quantification of Digital Data	9
Overall Aims	10

## **Chapter II: *In Vitro* Model Systems for Developing Oral Microbial Communities**

Summary	13
Introduction	14
Past and Present: Oral <i>In Vitro</i> Biofilm Models	16
Relevance of Biofilm Model Systems to Health & Disease Research	21
Drip-fed Biofilm Models	23
Constant Depth Film Fermenter	23
Sorbarod Perfusion System	25
Angled Drip-Flow Biofilm Reactor	27
Flow-fed Biofilm Models	28
Modified Robbins Device (MRD)	29
Flowcells	30
Bioflux™ Model System	32
Integration of Model Systems with Microscopy and Bioinformatics	34
Confocal Laser Scanning Microscope (CLSM)	35
16S rRNA Community Profiling	37
Concluding Remarks and Future Directions	39

## **Chapter III: A Sensitive Thresholding Method for Confocal Laser Scanning**

### **Microscope Image Stacks of Microbial Biofilms**

Abstract	51
Introduction	52
Results	55

Consistency & Agreement of Thresholding Methods	55
Average Outcomes Following Each Thresholding Method	56
Visual Clarity of Biofilm Following Each Thresholding Method	57
Performance of the Three Automatic Thresholding Methods	58
Effect of Gain on the Three Automatic Thresholding Methods	59
Validation of BEM Threshold Range with Negative Controls	60
Assessment of BEM to Other Images & Bit-depths	61
Discussion	62
Methods	66
Biovolume Elasticity Method (BEM)	66
Otsu's Method	67
Iterative Selection Method (IS)	68
Manual Thresholding	68
Production of Biofilms	69
Image Acquisition	70
Converting Confocal Stacks to MatLab Readable Format	71
Post-thresholding Calculation of Core Biofilm Architecture	72
Sources of Additional Images Used for Validation	72
Comparison of 12-bit vs 8-bit Fluorescence	74
Comparing Manual & Automatic Thresholds	74
Comparing Biofilm Architectural Outcomes by Thresholds	75

## **Chapter IV: Introducing BAIT (Biofilm Architecture Inference Tool): A Software Program to Evaluate the Architecture of Oral Multi-Species Biofilms**

Abstract	92
Introduction	93
Methods	97
Development of BAIT	97
Validation of Outcomes Calculated by BAIT	98
BAIT as a Tool to Measure Architecture Changes after Treatment	98
Treatment Formulations & Study Design	99
Media & Inoculum Collection	100
Overnight Growth of Oral Biofilms	100
Post-growth Staining of Biofilms	101
Confocal Laser Scanning Microscopy	101
Statistical Analysis	102
Results	102
Validation of BAIT Scripts	102
Biofilm Sampling	104
Qualitative Visual Observations of Treatment Group Effects	104
Quantitative Water Treatment Effects	105
Quantitative Stannous 1,000 PPM Treatment Effects	106
Quantitative Stannous 3,439 & 10,000 PPM Treatment Effects	107
Discussion	107

## **Chapter V: Concluding Remarks & Future Directions**

Conclusions	123
Future Directions	126
Textural, Spatial, & Temporal Outcomes in BAIT	126
16S rRNA Community Profiling of <i>In Vitro</i> Dental Biofilms	128
Synthesizing All Outcomes	129
Personal Comments	129
<b>Appendices</b>	<b>132</b>
<b>References</b>	<b>146</b>

## LIST OF TABLES

### Tables

II.1	Examples of Fundamental & Applied Research of <i>In Vitro</i> Dental Biofilms	42
II.2	Open System Biofilm Models Relevant to Dental Biofilm Research	43
II.3	Sequencing Platforms for 16S rRNA Community Profiling	44
III.1	Biofilm Outcomes by Thresholding Method and by Treatment	76
III.2	Paired T-tests Between Thresholding Methods Stratified by Treatment	77
III.3	False Positive Noise Distribution of Negative Controls	78
IV.1	Outcomes Currently Available in BAIT	112
IV.2	Groups of Biofilm Images Quantified by BAIT	113
IV.3	BAIT Outcomes by Treatment Group and Stratified by Viewing Port Half	114
IV.4	Linear Mixed Effects Models of Each Biofilm Architecture Outcome	116

## LIST OF FIGURES

### Figures

I.1	Microcosm Dental Biofilm	11
I.2	Structural Heterogeneity of Biofilm	12
II.1	Constant Depth Film Fermenter System (Drip-fed System)	45
II.2	The Sorbarod Perfusion System (Drip-fed System)	46
II.3	The Angled Drip-Flow Biofilm Reactor (Drip-fed System)	47
II.4	The Modified Robbins Device (Flow-fed System)	48
II.5	Flowcells (Flow-fed System)	49
II.6	Bioflux™ System (Flow-fed system)	50
III.1	Visual Comparison of Different Methods to Threshold Biofilm Images	79
III.2	Thresholding Necessary to Remove Background Noise	81
III.3	Image Intensity Histograms Vary By Imaging Platform	82
III.4	MRI, Light Microscopy, and Fluorescence Microscopy Image Histograms	84
III.5	Image Intensity Histograms Vary by Confocal Operator	85
III.6	Thresholding Methods on Images from Different Platforms	87
III.7	Image Intensity Histograms of 8-bit & 12-bit Images	88
III.8	BEM Thresholding Scaled to 12-bit Images	89
III.9	26-neighborhood Connectivity Determination of Regions of Interest	91

IV.1	Graphical User Interface (GUI) Layout of BAIT	117
IV.2	Mock Dataset Used To Validate Outcomes Calculated by Scripts	118
IV.3	Representation of the 24-well Bioflux™ Plate & Imaging Strategy	119
IV.4	Validation of BAIT Using Three Confocal Oral Biofilm Images	120
IV.5	Stitched Images of Representative Biofilms by Group	121
IV.6	Immediate Effects of Treatments	122
V.1	Potential Application of BAIT to CLASI-FISH	131
A.1	Intensity Histograms of Red & Green Channels	141

## LIST OF APPENDICES

### APPENDICES

A.	Protocol using 24-well Bioflux™ to Develop Dental Biofilms	133
	Preparation of Pooled Saliva as Inoculum & Medium	133
	Growth of Dental Microcosm Biofilms	134
	Objective Imaging Strategy	137
	Harvesting Biofilm Cells for 16S rRNA Community Profiling	138
	Calculation of Weighted Viability	139
B.	Publications	142
C.	Poster Presentations	145

## Abstract

Dental caries and periodontal disease affect billions of people annually with a global prevalence estimated at 35% and 11%, respectively. Oral biofilms that develop on tooth surfaces and within gingival crevices are a major risk factor. Disease prevention efforts are focused on controlling the overgrowth of biofilms by removal (e.g., toothbrushing), antimicrobial-containing mouth rinses, and dentifrices. A number of laboratory (*in vitro*) models of biofilms are used to understand how biofilms develop and their response to mouth rinses and dentifrices.

However, there are two major limitations to currently available *in vitro* biofilm model systems. First, there is no biofilm model system validated for the development of representative dental plaque biofilms. Second, there is no standard approach to analyze biofilm images. Current techniques rely on thresholding algorithms that are not designed for fluorescent images. Combined, these limitations can lead to differences in quantification of biofilm outcomes and thus raise questions regarding the relevance of the model system to the “real-world”.

This dissertation seeks to bridge the gap between current laboratory techniques and software algorithms and provide investigators additional tools to conduct *in vitro* oral

biofilm studies. First, a distillation of model systems relevant to modern *in vitro* oral biofilm research is provided. Second, we adapted one of these described model systems, the 24-well Bioflux™ to reproducibly grow multi-species dental biofilms. An objective imaging strategy was further developed to capture all biofilm architectural features. Before analyzing biofilm images, a novel thresholding algorithm, the biovolume elasticity method (BEM), was developed to threshold fluorescent signal. Finally, a software package called Biofilm Architecture Inference Tool (BAIT) was built and evaluated to measure core architectural features of biofilms.

In summary, this dissertation describes the modification of a 24-well Bioflux system that facilitates the reproducible development of biofilms. For better visualization and quantification of *in vitro* biofilms, a novel thresholding algorithm was described. Finally, a software package integrating the BEM thresholding method was developed to measure architectural outcomes. The work presented here represents the outcome of a combinatorial approach to redefine techniques to study oral biofilms, and may also be relevant to the study of biofilms that exist outside the oral cavity.

## Chapter I

### Introduction

#### Oral Diseases and Biofilms

Dental caries and periodontal disease affect people in developing and industrialized nations alike (Sheiham, Williams et al. 2015). An estimated 3.9 billion people worldwide suffer from caries and periodontal disease, which often leads to decreases in quality of life, reduced productivity, and lost wages (Sanders, Slade et al. 2009, Harford and Chrisopoulos 2012, Marcenes, Kassebaum et al. 2013). A 2015 estimate puts the direct and indirect costs of oral health burdens at \$442 billion (Team 2015) with caries and periodontal disease being major contributors (Beikler and Flemmig 2011, Kassebaum, Bernabe et al. 2015). Early clinical symptoms are minor and often neglected until treatment is needed, inflating healthcare costs. Today, caries and periodontal disease remain a global public health challenge.

Microorganisms play a major role in the etiology of caries and periodontal disease. Historically, oral diseases were thought to be outcomes of only a few microbial species: acid-producing *Streptococcus sp.* and *Lactococcus sp.* for dental caries and *Porphyromonas gingivalis* and *Treponema denticola* for periodontal disease (Berry and

Henry 1977, Liljemark and Bloomquist 1996, Hajishengallis and Lamont 2012). Today, the paradigm is that oral health status is a function of the entire biofilm community consisting of up to 1,000 bacterial species and its interaction with the host. With the advent of Next-generation sequencing technologies, there is renewed focus on community ecology and its role in disease pathogenesis (Sbordone and Bortolaia 2003). Evidence from clinical studies, and animal/laboratory model systems indicate that dental caries and periodontitis result not from the activity of a few species but from the interaction of a dynamic consortia of species contained within dental biofilms (Marsh 2006). Thus, a strategy of creating and maintaining a healthy oral microbial community could translate into successful strategies to prevent and control dental caries and periodontal disease.

### **Epidemiology of Caries & Periodontal Disease**

Dental caries and periodontal disease cause the vast majority of human oral diseases (Petersen, Bourgeois et al. 2005). In 2010, in a ranking of the global burden of 291 diseases, untreated caries ranked first (Murray and Lopez 2017). The estimated global prevalence of dental caries was 35%, which translates to roughly 2.4 billion people (Murray, Ezzati et al. 2012, Kassebaum, Bernabe et al. 2015). Periodontitis was number six in that list with an estimated global prevalence of 11%. Over the past two decades, disability-adjusted life years (DALYs) attributable to untreated caries and periodontal disease increased roughly 20% (Marcenes, Kassebaum et al. 2013). Further, caries and periodontal disease are strong indicators of overall systemic health and have been linked to many chronic conditions including heart disease (Dhadse, Gattani et al. 2010), diabetes

(Torpy, Burke et al. 2008, Casanova, Hughes et al. 2014, Tavares, Lindefjeld Calabi et al. 2014), coronary heart disease (Geismar, Stoltze et al. 2006), endocarditis (Anolik, Berkowitz et al. 1981, Lockhart, Brennan et al. 2009), and preterm birth (Newnham 2005). Thus, caries and periodontal disease are significant public health challenges that have garnered significant attention.

Non-microbial risk factors for caries and periodontal disease include a combination of environmental and behavioral factors that affect the microbial composition of dental plaque, and genetic factors that affect overall host susceptibility. Environmental and behavioral factors include, diet, oral hygiene, socioeconomic status, and use of dental services (Vieira, Modesto et al. 2014). Some social risk factors are more predictive of caries depending on geography and population demographics. For example, a study showed a wider gap in caries burden between the upper class and the lower class in industrialized nations compared to developing nations (Schwendicke, Dorfer et al. 2015). Socioeconomic position also predicts prevalence and severity of periodontal disease (Borrell and Crawford 2012). Although heterogeneity of oral health is often congruent with socioeconomic heterogeneity, closing the socioeconomic gap does not necessarily remedy oral health disparities due to multifactorial risk factors and habitual poor oral hygiene (Grembowski, Conrad et al. 1987, Polk, Weyant et al. 2008). Thus, designing interventions to promote oral health has proven difficult in high-risk regions where dentition has traditionally been a relatively low priority in the community (Taani 2002, Wu, Ren et al. 2014).

## **The Role of Bacteria in Caries & Periodontal Disease**

Dental caries and periodontal disease are clinical outcomes of microbial processes (Takahashi and Nyvad 2008, Genco and Borgnakke 2013, Wade 2013). Acidic byproducts of bacterial fermentation cause demineralization of dentin, enamel, and cementum leading to the breakdown of dental hard tissue (Selwitz, Ismail et al. 2007). Tissue degradation in periodontal disease and caries can be exacerbated by chronic gingivitis or periodontitis induced by an inflammatory response from the host. Eventually, pocket formation, bone loss, and tooth loss occur (Dye 2012). Early studies have identified acid-producing *Streptococcus sp.* and *Lactococcus sp.* as causative agents linked to dental caries (Berry and Henry 1977). Likewise, many studies have linked the presence of *Porphyromonas gingivalis*, *Treponema denticola*, and *Tannerella forsythia* to periodontal disease (Liljemark and Bloomquist 1996, Hajishengallis and Lamont 2012). Due to how intimately oral conditions are predicated on the individual's oral microbial ecology, prevention efforts primarily focus on plaque control to reduce bacterial bioburden (Axelsson, Nystrom et al. 2004, Tonetti, Eickholz et al. 2015).

## **The Changing Paradigm of Oral Diseases**

The human oral cavity contains many surfaces that serve as distinct niches to microbes. These include the tongue, hard and soft palate, tooth enamel, buccal surfaces, palate, tonsils, and gums. Each of these niches supports compositionally diverse microorganisms including viruses, fungi, Archaea, protozoa, and bacteria coexisting in

complex community structures (Dewhirst, Chen et al. 2010, Palmer 2014). Historically, dental caries and periodontal disease were thought to fit the standard infectious disease paradigm: a single pathogen could cause disease. However, the simple presence of suspected pathogens are not necessarily predictive of disease and thus do not fulfill Koch's postulates (Bradshaw and Lynch 2013). For example, *Streptococcus mutans* and *Porphyromonas gingivalis*, which have traditionally been identified as causative agents of caries and periodontal disease, are present in the mouths of healthy individuals and increased abundance of these species is not necessarily predictive of dental disease (Kolenbrander, Palmer et al. 2006, Marsh, Moter et al. 2011).

The contemporary paradigm is that oral health status is a function of the entire oral bacterial community consisting of up to 1000 bacterial species, each interacting with one another as well as the host. The community of surface-attached microbes living within the intraoral cavity can be collectively referred to as biofilms. Biofilms are dynamic cellular arrangements of multiple species of microscopic organisms bound by extracellular polymeric substances (**Figure I.1**). Bacteria in biofilms are physiologically and architecturally different from their planktonic counterparts. Biofilms are estimated to be responsible for up to 80% of all human infections (Romling and Balsalobre 2012, Akers, Mende et al. 2014). In context of the oral cavity, biofilms can contribute to periodontal disease, caries, and host inflammatory conditions. Thus, successful prevention and control strategies should focus on creating and maintaining a healthy oral biofilm community.

## ***In Vitro* Laboratory Model Systems**

### **Role of *In Vitro* Laboratory Models in Dental Biofilm Research**

*In vitro* model biofilm systems enable researchers to monitor the development of biofilms over time while simulating *in vivo* parameters that are representative of the conditions within the human oral cavity. Oral biofilm models are highly controlled experimental systems characterized by the growth of microorganisms under continuous, semi-continuous, or closed flow (McBain 2009). Closed-flow systems were predominant at the turn of the 20th century and today still have many applications. However, continuous systems are favored over closed systems for multi-species dental biofilm research applications since the continuous delivery of media simulates salivary flow (Blanc, Isabal et al. 2014). Newer conceptual designs that improve upon model reproducibility and intraoral mimicry have also emerged, yielding more representative results. When conducted appropriately, *in vitro* model systems can provide expeditious and generalizable results for the study of dental biofilms.

### **Resurgence of *In Vitro* Laboratory Models**

The popularity of oral laboratory model systems peaked in the mid 1990's and then stagnated until a revival in the mid 2000's. Recently, interest in oral *in vitro* model biofilm systems has been reinvigorated (Tang, Yip et al. 2003, Salli and Ouweland 2015). Many factors contributed to this resurgence, such as higher-throughput and better *in vitro* model

designs. However, the resuscitation of interest in laboratory-based systems can mainly be attributed to the integration of increased computational capacities and 'omic' technologies, particularly 16S community profiling, into established oral *in vitro* model systems (Edlund, Yang et al. 2013). For example, with enhanced computer hardware and software, the ability to measure 3-dimensional architecture of biofilms becomes feasible. This ability allows for the development of computational models to predict the response of biofilms to external stimuli (e.g., changes in pH, presence of antimicrobials, or colonization of a particular microorganisms). Coupled with decreasing costs, oral *in vitro* model systems become a more appealing method to conduct experiments evaluating the effects of proposed anti-biofilm or antimicrobial agents on the development, community succession, and architecture of dental biofilms.

### **Considerations for Using *In Vitro* Laboratory Models**

Modeling biofilms in the oral cavity is biologically and technically challenging for a variety of reasons. Due to the heterogeneity of multiple overlapping niches contained within the oral cavity, the oral microbiome must be deconstructed to identify a locale of interest (Parahitiyawa, Scully et al. 2010, Xu, He et al. 2015). The choice of model systems presents an additional challenge. At present, most oral biofilm research is conducted using either *in vitro* or *in vivo* approaches, each with their own advantages and disadvantages (Haffajee and Socransky 2006). *In vitro* approaches use biofilm systems that are logistically easier to conduct at higher throughput, but may lack clinical relevance (Baehni and Takeuchi 2003, McBain 2009). *In vivo* approaches have typically lower

throughput and rely upon animal model systems that reproduce certain aspects of the human oral environment, but suffer from limitations due to differences in anatomy, physiology, and microbiology between animals and humans (Chun, Kim et al. 2010, Graves, Kang et al. 2012). Thus, sample size tradeoffs, costs, and generalizability between *in vivo* systems and laboratory *in vitro* model systems must be considered when choosing an appropriate model system.

## **Limitations of Current Approaches in *In Vitro* Laboratory Models**

### **Paucity of Model System Standard Protocols**

Currently, there are a plethora of *in vitro* laboratory models to study biofilms ranging from simple static plates to complex rigs containing multiple pieces of hardware (McBain 2009). The difficulty lies in selecting the best model system given one's objectives. Factors to consider include open or closed systems, inoculum type, medium, shear force, temperature, atmospheric content, and substratum. With so many parameters to consider, there are few standardized protocols for developing multi-species microcosm dental biofilms. Additionally, the adaptation of modern commercially-available model systems could be technically challenging, involving many parts and accessories (Gabriliska and Rumbaugh 2015).

### **Biased Imaging Strategies**

Another limitation relates to the natural heterogeneity of biofilms and the subjectivity of a human microscope operator. Microcosm dental biofilm architecture is remarkably diverse (**Figure I.2**) and can be difficult to characterize within the field of view of an objective lens. Time permitting, user subjectivity can be completely eliminated by imaging the entire substratum. However, this is normally not the case and sampling is required. Sampling frequently is not random or systematic, but defaults to the microscope operator locating the portion of the substratum that contains the most biomass. This strategy is marred by user subjectivity and can bias interpretation of results, especially if the operator is not blinded to treatment and control samples. An alternative to selective imaging is devising a schematic approach where each sample is imaged at fixed locations, regardless of presence of biofilm material.

### **Quantification of Digital Data**

Biofilm architecture is a construct that is difficult to characterize. It is simpler to qualitatively describe biofilm architecture rather than quantify it. For example, a biofilm may appear compact or fluffy, and may be described qualitatively as that. However, the degree of compactness or fluffiness is important for drug delivery kinetics and can provide insights into how biofilms behave in response to treatment. It is often difficult to gauge the magnitude of qualitative descriptors with a glance of a two-dimensional image. Computational algorithms can deconstruct digital data into its constituent pixels (2-dimensional images) or voxels (3-dimensional images) in order to quantify biofilm features that are traditionally thought of as qualitative. There are a few software packages that can

quantify biofilm images, such as COMSTAT (Heydorn, Nielsen et al. 2000), Phlip (Mueller, de Brouwer et al. 2006), Icy (de Chaumont, Dallongeville et al. 2012) and ImageJ (Collins 2007). To our knowledge, there is no software package dedicated solely to biofilm architecture and no standardized protocol for analyzing biofilm images.

### **Overall Aims**

At present, there are few standard protocols specific to commercially-available *in vitro* model systems for the development of dental biofilms. To our knowledge, there are no standard protocols that address the limitations of biased imaging strategies and image quantification. Given these limitations, the primary objective of this dissertation is to develop a standard protocol, from laboratory to analysis, for evaluating *in vitro* dental biofilm outcomes. This will bridge the gap between equipment and algorithms to address current limitations in laboratory dental biofilm research. The contents of this dissertation can be broken down into four aims. The first aim is to provide a historical distillation of *in vitro* model biofilms systems and its integration with modern technologies for the study of dental biofilms. The second aim is to adapt the 24-well Bioflux™ model system to reproducibly develop overnight supragingival plaque. The third aim is to develop a sensitive thresholding method called the Biovolume Elasticity Method (BEM), designed to maximize signal to noise ratio in fluorescent microscopic images. The fourth aim is to develop a software package, called the Biofilm Architecture Inference Tool (BAIT), which applies the BEM thresholding technique to calculate core architectural descriptors. Lastly, potential future work that builds off this project will be discussed. Overall, the work

presented in this dissertation will provide investigators a complementary hardware to software protocol to conduct generalized biofilm research within the laboratory.

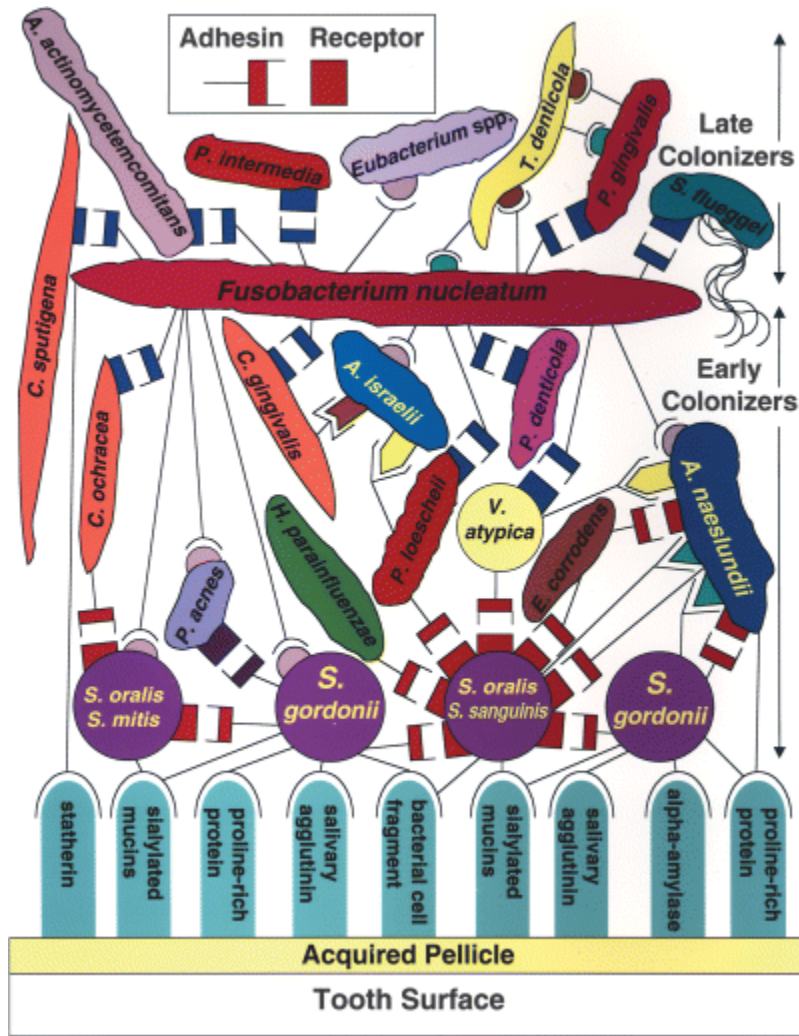


**Figure I.1. Microcosm Dental Biofilm.** A visual representation of a multi-species dental biofilm formed on a tooth and the types of resulting interactions. First, a conditioning film is acquired on the tooth surface. This pellicle consists of salivary proteins, polysaccharides, and mucins to which initial colonizers can attach. Depending on the time the biofilm remains undisturbed, ecological succession brings secondary and tertiary colonizers typically associated with disease. This community that can consist of hundreds of species that interact with one another through gene transfer events, cell-cell signaling, cross-feeding, and co-adhesion. Image acquired with permission from Kolenbrander et al. (Kolenbrander, Palmer et al. 2006).

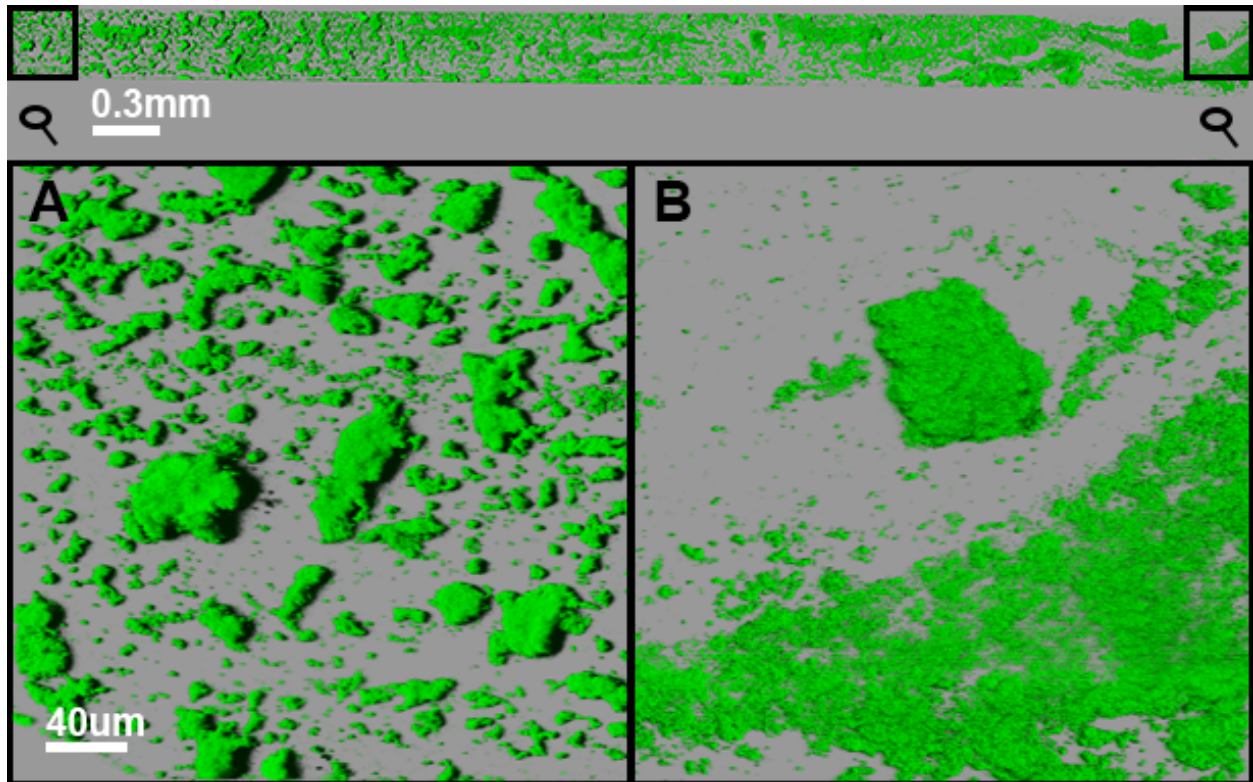


**Figure I.2. Structural Heterogeneity of Biofilm.** An oral biofilm developed over 22 hours using the 24-well Bioflux™ model system. The image contains the entire surface area of the glass substratum. The ends of the substratum most distal to each other are magnified to demonstrate structural heterogeneity of dental microcosm biofilms. Biofilms can be qualitatively described such as **A)** compact with large-chain islands, or **B)** fluffy with small fragmented archipelagos. Capturing the representative features of a biofilm within a sample is no trivial task, and is often chosen by the confocal operator.

## Chapter II

### ***In Vitro* Model Systems for Developing Oral Microbial Communities**

#### Summary

*In vitro* biofilm model systems provide a platform for oral health researchers to conduct fundamental or applied research on dental biofilms without the need for human or animal subjects. One of the earliest documented dental biofilm model systems was developed in the 1950's. Since then, developments in the last few decades have facilitated the simulation of intraoral conditions and allowed for increased generalizability of *in vitro* dental biofilm studies. In this chapter, we survey of model systems that are relevant to modern dental biofilm studies. These systems include the: constant depth film fermenter (CDFS), Sorbarod perfusion system, angled drip-flow reactor, modified Robbins device (MRD), flowcells, and the Bioflux™ system. The integration of contemporary model systems with technologies such as confocal laser scanning microscopy and 16S rRNA community profiling have revitalized interest in the field. These technologies enable quantification of biofilm architecture and community composition. How biofilm architecture and community composition respond to potential antimicrobials or anti-biofilm agents *in vitro* provide insight into the mechanisms underlying various

methods of biofilm control, and a method for evaluating new antibiofilm agents prior to *in vivo* evaluation.

## Introduction

The human oral cavity offers numerous surfaces for microbial species to form multi-species aggregated communities that are collectively referred to as biofilms (Marsh 2006). Biofilm communities are perpetually dynamic – component species are constantly interacting with the environment, the host, members of its own species, and members of other microbial species, leading to compositional changes in the biofilm over time (Hall-Stoodley, Costerton et al. 2004, Kolenbrander, Palmer et al. 2006, Wimpenny 2009). However, biofilm communities can be extremely recalcitrant to physical perturbations (e.g. brushing) and chemical treatments (e.g. antimicrobial) (Marsh 2010). In part due to their recalcitrance, biofilms are estimated to be responsible for >65% of all human infections (Davies 2003, Joo and Otto 2012). In the context of the oral cavity, biofilms contribute to periodontal disease, dental caries, infections, and inflammation, leading to debilitating decreases in quality of life (Jakubovics and Kolenbrander 2010). Collectively, these diseases cause a financial burden that is estimated to exceed 111 billion dollars in the USA in 2012 (Wall 2014). While clinical studies are the gold standard for evaluating approaches to control oral biofilms, their implementation is costly and logistically challenging (Bang and Davis 2007, Martin-Kerry, Lamont et al. 2015). Because of this, clinical research is often preceded by *in vitro* studies to offer insight into possible real-world treatment strategies (Krithikadatta, Gopikrishna et al. 2014). In particular, *in vitro*

biofilm model systems provide preliminary impressions on how biofilm development, succession, and architecture respond to environmental challenges under a defined set of controlled conditions (Kolenbrander, Palmer et al. 2006, Hojo, Nagaoka et al. 2009). Thus, *in vitro* biofilm systems can provide valuable insights into biofilm control and the role biofilms play in the etiology of persistent chronic oral conditions. Ultimately results garnered from *in vitro* studies serve as the foundational impetus to conduct *in vivo* clinical trials, underscoring the importance of laboratory-based models in dental research.

From a fundamental standpoint, *in vitro* model biofilm systems enable researchers to monitor the development of biofilms over time and identify functional roles of organisms within the biofilm state (Zhang 2017). Many of the available biofilm systems can simulate multiple *in vivo* parameters that are representative of the conditions within a human oral cavity (Coenye and Nelis 2010). This makes *in vitro* biofilm systems an appealing platform for exploratory studies that close knowledge gaps in human dental plaque biofilms without the need for human subjects. The closer the *in vivo* mimicry, the more generalizable the results gathered from *in vitro* model systems. As knowledge gaps are filled, *in vitro* model biofilm systems also can be harnessed for applied research with the practical directive of controlling dental plaque biofilm. Altering one parameter within a model system is a powerful method to study how biofilm develops *in vitro* (Fernandez, Aspiras et al. 2017). This can provide clues to how the component species interact with one another or other species within the oral cavity and can identify potential keystone species for oral biofilm development (Costerton, Geesey et al. 1978, Bradshaw, Marsh et

al. 1998, Diaz 2012). Examples of how *in vitro* model systems have been used in fundamental and applied dental biofilm research are detailed in **Table II.1**.

In this review, we provide a distillation of past models used to develop defined single-species, defined multi-species, and complex microcosms. This will be followed by a focus on select biofilm models and applicable integrated technologies that can be used to study microcosm growth under environmentally-germane conditions. A particular focus of discussion will be on biofilm models that are open (constant delivery of fresh media), multiple-throughput, and require small volumes to conduct experiments. Lastly, the impact and potential clinical relevance of biofilm model systems will be discussed along with limitations and future directions.

### **Past and Present: Oral *In Vitro* Biofilm Models**

Before the term biofilm was coined in the late 1970's (Costerton, Geesey et al. 1978), the aggregation of microbial communities on surfaces was described in two seminal papers focused on marine microorganisms, one by Henrici (Henrici 1933) and another by Zobell and Allen in the 1930s (Zobell and Allen 1935). However, probably in part because of the visually conspicuous nature of dental plaque, a significant number of *in vitro* biofilm model systems developed over the past half century have focused on oral biofilms. For example, relatively primitive oral biofilm models were developed as early as the 1950s (Pigman, Elliott et al. 1952, Pigman, Hawkins et al. 1955). Throughout the ensuing decades, newer conceptual designs improved on their predecessors to allow for

development of *in vitro* biofilms that are either (1) amenable to the study of fastidious dental microorganisms (Guggenheim, Giertsen et al. 2001, Thompson, Rybalka et al. 2015, Owens, Lynch et al. 2017) or are (2) able to grow biofilms that contain mixtures of species typically found in supragingival or subgingival human dental plaque (Edlund, Yang et al. 2013, Nance, Dowd et al. 2013). Past and present oral *in vitro* biofilm studies can be characterized by transition from fundamental to applied research within four arenas: (1) cariogenesis outcomes, (2) single-species plaque, (3) defined multispecies plaque, and finally, (4) microcosm multispecies plaque outcomes. Fundamental and applied research in the microcosm arena has recently gained traction due to technological advancements and methodologies that enable investigators to measure microcosm biofilm outcomes. Notably, these advancements enable interrogating community membership with 16S rRNA profiling and measuring biofilm architecture captured by a confocal laser scanning microscope.

The earliest fundamental model biofilm systems can be dated back to the early 1950's when Pigman and colleagues developed an artificial mouth model to induce cariogenesis on extracted teeth (Pigman, Elliott et al. 1952). This model is arranged vertically with sterile media drip-fed over an extracted human tooth inoculated with pooled human saliva and housed in an acrylic box. The media reservoir is positioned above the extracted tooth and media is delivered with a hypodermic needle. The artificial mouth model developed by Pigman is arguably the ancestor to contemporary drip-fed systems. This experimental setup was focused on identifying conditions that favor cariogenesis, and not particularly on plaque outcomes. Therefore, biofilms were developed at room

temperature and at times without the proper use of aseptic technique (Sissons 1997). From the 1950's to the 1960's, many *in vitro* oral studies used variants of Pigman's artificial mouth system with improvement modifications such as incubator cabinets at 35°C and sterilization with ethylene oxide (Pigman, Hawkins et al. 1955, Pigman, Brasher et al. 1962, Pigman and Newbrun 1962). Fundamentally, these studies linked common dietary sugars such as D-glucose and sucrose to cariogenicity. From the applied perspective, anticariogenic effects of compounds and dentifrice slurries can be evaluated by exposing tooth enamel with treatment concomitantly with conditions that would favor cariogenesis, such as supplementing bacteriological media with glucose (Pigman and Newbrun 1962). These models were used to demonstrate that fluorides reduced the rate of softening of enamel.

During the 1960's and 1970's, many key microbial species associated with oral diseases were identified. Consequently, model biofilm studies from the 1970s onward involved these organisms. Many of these studies were fundamental in nature, and focused on single-species surface-attachment, biofilm development, or dual-species interaction studies (Coulter and Russell 1976, Russell and Coulter 1977, Russell and Ahmed 1978). Although the popularity of multispecies microcosm studies have increased (Kinniment, Wimpenny et al. 1996, Foster and Kolenbrander 2004), single and small consortia oral biofilm studies still play a role in uncovering behavioral tendencies and interactions of keystone species. One such discipline that benefitted immensely from reductionist-based biofilm model systems is coaggregation or cell-cell interaction. Using an *in vitro* biofilm model, Palmer et al. built flowcells to test interspecific interactions

between *S. gordonii*, *S. oralis*, and *A. naeslundii*, known early colonizers of dental plaque. Independently, *A. naeslundii* and *S. oralis* were incapable of growing in a biofilm state within the model system. However, the dual-species culture of the two species resulted in abundant biofilm formation (Palmer, Kazmerzak et al. 2001). Coaggregation has been shown, using *in vitro* biofilm models, to be integral in biofilm formation in other studies as well (Nagaoka, Hojo et al. 2008, Rickard, Campagna et al. 2008, Walter, Schwab et al. 2008, Hill, Malic et al. 2010). This knowledge can pave the way to more directed applied studies such as interventions to disrupt coaggregation as a facilitator of biofilm control (Weiss, Lev-Dor et al. 1998).

Experiments using early model systems generally involved single or few species. This was in part due to technological limitations. However, studies involving small consortia communities provide inadequate understanding of how microbial communities function in their native environment (Rudney, Chen et al. 2012). Indeed, dental plaque exists as a dynamic ecosystem teeming with biodiversity, with estimates of the total number of native species ranging from hundreds to thousands (Marsh 2006, Zaura, Keijser et al. 2009, Dewhirst, Chen et al. 2010, Peterson, Snesrud et al. 2013). This prompted Sissons in his 1997 review on dental plaque biofilm model systems to remark: “an attempt to explain plaque behavior based on the properties of monocultures can be regarded somewhat as heroic.” (Sissons 1997). Through broad technological advancements, investigators acquired tools and methods to better characterize dental plaque grown from microcosm inoculum, most notably advances in microscopy and 16S community profiling (Tan, Lee et al. 2017). Somewhat unsurprisingly, the focus

consequently shifted from single-species and defined-species to microcosm-multispecies studies. In recent years, many fundamental validation and protocol studies emerged to gauge reproducibility and provide cursory microbiological results from oral microcosm biofilms (Edlund, Yang et al. 2013, Nance, Dowd et al. 2013, Samarian, Jakubovics et al. 2014). Oral microcosm biofilm studies will enable the measurement of different biofilm outcomes, such as biofilm architecture, microbial community profiles, and taxonomic spatial distribution (Gross, Beall et al. 2012, Valm, Mark Welch et al. 2012, Xiao, Hara et al. 2017).

The model systems focused upon in this review have been used in the past to study dental plaque biofilms and are the mainstay for current studies. These systems are all open biofilm models that constantly deliver fresh media to the site of biofilm development (McBain 2009). Canonically, model systems used to study dental plaque biofilms can be classified as drip-fed or flow-fed. Drip-fed systems deliver nutrient semi-continuously, whereas flow-fed systems deliver a constant laminar flow of nutrients. The drip-fed systems discussed are the constant depth film fermenter (CDFF), the Sorbarod perfusion system, and the drip flow biofilm fermenter. The flow-fed systems are the modified Robbins device (MRD), flowcells, and the Bioflux™ system. Many of these possess attributes that make them appealing candidates as model systems for modern dental plaque studies. All discussed model systems are compatible with confocal laser scanning microscopy and can be manipulated to harvest biofilm cells for microbial community profiling. Finally, all are multiple-throughput and many require small volumes for experiments. A summary of the discussed model systems is presented in **Table II.2**.

## Relevance of Biofilm Model Systems to Health & Disease Research

Model systems that are capable of developing environmentally-germane biofilms will provide more generalizable outcomes as it pertains to health and disease research. There are many parameters of the oral environment to consider for optimal *in vivo* mimicry. These parameters include shear force, bacteriologic media, atmospheric content, and substratum. Growth of biofilms under low shear mimics salivary or gingival crevicular flow (Blanc, Isabel et al. 2014), which is important for bacterial interactions (Huang, Li et al. 2011). One particularly important modification replaced bacteriologic medium with human saliva to feed *in vitro* oral biofilms (Yaari and Bibby 1976). The resultant oral biofilm is more representative of *in vivo* plaque as the bacterial composition is influenced by selective pressure of the physico-chemical properties and nutrients of human saliva, rather than artificial media. Another study delivered a gas mixture consisting of 95% atmospheric air and 5% carbon dioxide into the artificial mouth system (Dibdin, Shellis et al. 1976). This was designed to mimic the composition of expired breath. Lastly, choice of a substratum that represents human dentin and enamel is also important. Hydroxyapatite and glass are two surfaces commonly used to represent oral hard surfaces and as discussed before, there is no indication of differences in acquired pellicle formation and resultant biofilm development in either (Elliott, Pratten et al. 2005). Many of these *in vivo* parameters can be carefully controlled in modern studies involving model systems.

*In vitro* model systems are extraordinarily important to dental biofilm research from the perspective of both fundamental and applied research. With the development of *in vitro* biofilms that are increasingly representative to plaque that grows *in vivo*, investigators will gain a better platform to observe the role dental plaque plays in disease. Mounting evidence suggests that changes in the ecological and environmental factors drive plaque communities to impose etiologic roles in caries and periodontal disease (Aas, Griffen et al. 2008, Peterson, Snesrud et al. 2013). The importance of *in vitro* model systems lies within its ability to preserve and develop the polymicrobial community that is representative of the human oral microbiome. With that accomplished, researchers may be able to perform applied research studies to evaluate potential antimicrobial or anti-biofilm compounds. (Nance, Dowd et al. 2013, Kolderman, Bettampadi et al. 2015, Shin, Ateia et al. 2015). Additionally, investigators can use *in vitro* biofilm systems to study critical coaggregation interactions that occur between defined oral microbial species. For example, using a flowcell model, Eglund *et al.* discovered that *S. gordonii amyB* gene is upregulated in the presence of *V. atypica*, assisting the recruitment of *V. atypica* as an early colonizer to dental plaque (**Table II.1**). *V. atypica* and other periopathogens can then integrate with the maturing biofilm as secondary colonizers (**Figure I.1**). Thus, from the applied research perspective, targeting *S. gordonii amyB* expression or *V. atypica* colonization can prevent recruitment of periopathogens.

Animal models and human clinical trials also should be considered in oral health research. These two should complement promising results from *in vitro* experiments. Both offer the advantage of an *in vivo* environment and are important for validation of certain

hypotheses. However, compared to animal models and human clinical trials, *in vitro* models offer several considerable advantages for studying oral biofilms. One advantage is the affordability post development of a model system. Once a model system had been validated, costs to maintain the system and serially produce multiple runs decreases significantly and the throughput is increased due to the decreased per sample cost. Compared to the high costs associated with *in vivo* based research (Oz and Puleo 2011, Kantarci, Hasturk et al. 2015), validation for proof of concept and testing for efficacy of new anti-biofilm agents through *in vitro* model systems is time and cost saving. Another advantage over using animal models for biofilm research is that human oral biofilm-like community can be captured rather than a very different biofilm community that exists in the oral cavity of animal models such as mice (Coenye and Nelis 2010, Struillou, Boutigny et al. 2010). Currently, *in vivo* animal models for caries and periodontal disease often utilize single, or few select pathogens in high numbers unable to mimic the human biofilm community (Rivera, Lee et al. 2013, Chukkapalli, Easwaran et al. 2017). Lastly, *in vitro* systems can be extremely versatile. Key factors associated with biofilm disease pathogenesis such as nutrient availability, flow and shear rate, and time can be strategically controlled to help answer specific research questions regarding biofilm architecture, cellular organization, and mechanisms associated with biofilm growth, persistence and resistance.

### **Drip-fed Biofilm Models**

#### **Constant Depth Film Fermenter**

The constant depth film fermenter (CDFF) was first described by Peters and Wimpenny in 1988 as a means to develop freshwater biofilms at a defined thickness (Peters and Wimpenny 1988). The theory of maintaining the biofilm at a constant depth is to achieve a steady biofilm state within a reactor where measurable properties do not change significantly over time: perturbations to a steady state biofilm will be more interpretable and reproducible compared to the same perturbations applied to a non-steady state biofilm (Kinniment, Wimpenny et al. 1996). Mechanically, the CDFF is a chamber housing a rotating disc on the bottom. The rotating disc is embedded with customizable plugs where each plug is made of a material on which to develop biofilms. Media is drip-fed from above with inlets as the disc rotates to distribute media to each plug. Spent media is collected in a waste outlet located below the disc. The CDFF that keeps biofilms at a constant depth using a scraper blade that removes excess biofilm biomass and spent media as the disc rotates. (**Figure II.1**). Of the six systems reviewed, the CDFF has the highest throughput. The initial model described by Peters et al. held 25 plugs (Peters and Wimpenny 1988). Later models had the capacity of 75 plugs (Deng, van Loveren et al. 2005).

Initially created for freshwater biofilms, the CDFF has been applied successfully to the development of *in vitro* biofilms modeling dental plaque (McBain 2009, Hope, Bakht et al. 2012). Perhaps the most appealing aspect of the CDFF is the reproducibility of results. Replicate biofilms are kept at a constant thickness and are, theoretically, in a dynamic steady state. The CDFF has been used extensively for single-species (Deng,

van Loveren et al. 2005, Zanin, Goncalves et al. 2005, Metcalf, Robinson et al. 2006), defined consortia (Ledder, Madhwani et al. 2009, Fan, Wen et al. 2012, Owens, Lynch et al. 2017), and oral microcosm studies (Hope, Clements et al. 2002, McBain, Bartolo et al. 2003, McBain, Bartolo et al. 2003, Cenci, Pereira-Cenci et al. 2009, Abdulkareem, Memarzadeh et al. 2015). CDFFs are particularly well-equipped to conduct studies of antimicrobial challenges on mature dental biofilms, and biofilm growth monitoring. Because it is a high throughput system, biofilm biological replicates can be grown in the same chamber, and assigned to treatment or control groups post-growth. For example, Deng *et al.* grew *S. mutans* on 45 dentin plugs in a split CDFF chamber that was simultaneously treated with sodium fluoride or sodium fluoride/chlorhexidine formulations after the biofilm had matured (Deng, van Loveren et al. 2005). Sodium fluoride/chlorhexidine formulations conferred the most kill, lactic acid reduction, and remineralization of dentin compared to sodium fluoride alone. In another study, Feldman et al. monitored dual species *C. albicans* and *S. mutans* biofilm development on pre-treated hydroxyapatite discs (Feldman, Shenderovich et al. 2017). The discs were coated with a membrane designed to slowly percolate thiazolidinedione-8, a quorum sensing quencher. Biofilm development was hindered on discs containing the treatment.

### **Sorbarod Perfusion System**

In the mid 1990's, Hodgson *et al.* integrated Sorbarod filters with the conceptual framework of the perfused biofilm fermenter system (Hodgson, Nelson et al. 1995). The rationale for the development was to distinguish growth rates of bacteria in planktonic

phase from bacteria that had attached to a substratum. It was already evident that adhered bacteria had altered physiology from their planktonic counterparts and grew at different rates. The perfused biofilm fermenter system described by Gilbert *et al.* in 1989 (Gilbert, Allison *et al.* 1989) was inadequate for determining growth rate of adhered *S. aureus* and *P. aeruginosa* because the model tended to clog. To remedy this, Hodgson and colleagues inoculated Sorbarod filters with mid-logarithmic phase cultures and used the primed filters as the site of attachment and biofilm growth. The filters had wider average spaces between fibers than the 0.22 $\mu$ M membranes used in the perfused biofilm fermenter system, and therefore were less prone to clogging. The primed Sorbarod filter was then put below a drip of medium delivered by a hypodermic needle that was controlled by a peristaltic pump. The improved model system can be run continuously for up to ten days without issues. The principles of the Sorbarod perfusion system (**Figure II.2**) are very similar to the CDFF. As the site for biofilm development is the Sorbarod filter and not a solid surface, microscopy will require pre-imaging processing (See Rickard *et al.* (Rickard, Campagna *et al.* 2008).

Many studies have used the Sorbarod perfusion system design to study oral biofilms, particularly oral malodor. Because the system is stable for many days, it is often used for anaerobic and microcosm biofilm studies which require extended runtimes for growth. Taxa implicated in oral malodor generally include *Fusobacterium*, *Treponema*, *Haemophilus*, *Veillonella*, and *Porphyromonas* (Krespi, Shime *et al.* 2006). In oral malodor studies, a microcosm derived from dorsal tongue scraping is used as inoculum to grow representative communities believed to expel volatile sulfur compounds (VSC).

Time required for analogous steps in the biofilm development protocol is much longer for VSC producing communities. Initial attachment is 24-48 hours compared to 1 hour for studies modeling early supragingival plaque (Samarian, Jakubovics et al. 2014). Additionally biofilm development occurs over 96-120 hours as opposed to 20-24 hours. The Sorbarod perfusion system also has been used to develop dental biofilms inoculated from saliva (McBain, Sissons et al. 2005). McBain *et al.* concluded that the Sorbarod system was effective at maintaining a stable and reproducible oral biofilm community with relative abundances reflecting the initial starting inoculum.

### **Angled Drip-Flow Biofilm Reactor**

Unlike the CDF and Sorbarod systems, the drip-flow biofilm reactor is reclined at an angle. The angled biofilm reactor was first described by Xu *et al.* in the late 1990's as a means to develop *P. aeruginosa* biofilms (Xu, Stewart et al. 1998). Media is dripped from above at the portion of the reactor that sits highest. During use, the media flows downward coating a microscope slide layered with a substratum chosen by the investigator. The gravity-assisted flow of media creates a low shear environment that can be adjusted by elevating or depressing the angle of the system. At the bottom of the reactor is an outlet where effluent media traverses into a waste receptacle. Variations of the system have emerged through the years but the principles behind the system remain unchanged. A commercially-available reactor is produced by BioSurface Technologies (<http://biofilms.biz/products/biofilm-reactors/drip-flow-reactor>). In this model, the system has four or six individual parallel channels (**Figure II.3**). Care must be applied in sampling

biofilms over a large surface area. As demonstrated by Xu *et al.*, oxygen availability can influence heterogeneity of *P. aeruginosa* biofilms and if media flow across the slide is not uniform, then the development of a heterogeneous biofilm is expected (McBain 2009). This can be mitigated by unbiased biofilm sampling scheme, such as scraping biomass from the bottom of the slide.

Several studies have used the angled drip flow reactor to model single species and multispecies dental biofilms. Two studies coated the glass substratum with agents to determine if the agents possessed any anti-biofilm effects on *S. mutans* (Brambilla, Ionescu et al. 2014, Williams, Epperson et al. 2017). One agent was silver loaded into polymethyl methacrylate (PMMA) plates and the other agent was chlorhexidine loaded into dentin bonding systems. Silver PMMA plates were able to resist *S. mutans* biofilm formation in short-term washouts, but not long-term washouts. Chlorhexidine-loaded dentin adhesion bonds demonstrated variable results, leading authors to believe the variable chemical composition of the dentin binding systems masked the effects of chlorhexidine. The angled drip flow reactors also have been used for dentifrice studies on mature biofilms (Ledder, Sreenivasan et al. 2010, Ledder and McBain 2012). In those studies, microcosm biofilms were grown over 24 or 48 hours, followed by treatment regimens delivering dentifrice slurries every six hours for six days. In these studies, dentifrice treatments reduced culture counts and affected plaque community composition.

### **Flow-fed Biofilm Models**

## Modified Robbins Device (MRD)

First described by McCoy & colleagues in 1981, the modified Robbins device (MRD) allows reproducible biofilm formation for studying different types of biofilms under fluid shear conditions (McCoy, Bryers *et al.* 1981). MRD is commercially available through companies such as Biosurface Technologies Corporation (Bozeman, MT) and Tyler Research Corporation (Edmonton, Alberta, Canada). However, different versions of MRD can be made and customized in-house to fit the research design needed by independent laboratories. For example, Johnston *et al.* adapted the MRD with Malthus tubes to evaluate disinfection of biofilms (Johnston 1995). The principle behind the MRD is using individual coupons or discs attached to a plug that is inserted into a port. Coupons can be modified or built from different materials to resemble surfaces more akin to dental prostheses or tooth enamel. A peristaltic pump provides unidirectional media flow across all ports after the coupons are inoculated with microorganisms. Biofilm development occurs on the surfaces of the coupons as the system runs for a set amount of time. The throughput of the MRD varies by design. Low pressure and small volume MRDs offered by Tyler Research corporation range from 12-25 ports (<http://www.tylerresearch.com/low-pressure-devices>). The MRD equivalent offered by Biosurface Technologies has a throughput of 12 (<http://biofilms.biz/products/biofilm-reactors/bio-inline-biofilm-reactor>). A schematic of the physical system and direction of flow is illustrated in (**Figure II.4**).

The MRD has been used extensively to study oral biofilms, with many studies demonstrating its reproducibility at developing oral biofilms (Honraet and Nelis 2006,

Coenye, De Prijck et al. 2008, Noiri, Katsumoto et al. 2008, Sliepen, Van Essche et al. 2010, Blanc, Isabel et al. 2014, Yassin, German et al. 2016). The system and its detachable coupons proved to be particularly useful in evaluating efficacy of antimicrobials, antibiotics, disinfectants, and other agents. Coupons can be primed with the agent prior to biofilm development as in the study by Yassin et al. (Yassin, German et al. 2016). In the study by Yassin and colleagues, MRD coupons were prepared from a mixture of polymethyl methacrylate and sodium fluoride to create a copolymer that can be used for dentures while also releasing fluoride ions passively while worn. The investigators observed that mixed-species (*C. albicans*, *L. casei*, *S. mutans*) biofilm growth was inhibited by a factor of 10-fold on coupons containing the fluoride compared to biofilm growth on coupons that did not. Likewise, biofilms on coupons can be treated *post hoc* to evaluate efficacy of treatment after a biofilm has developed (Coenye, De Prijck et al. 2008). In 2008, Coenye et al. grew monospecies biofilms of *C. albicans*, *S. mutans*, *S. aureus*, and *P. aeruginosa* in a stainless steel MRD. After growth, the biofilms were treated with NitrAdine™, sonicated to remove biofilm from the coupons, and plated to determine efficacy of treatment in preventing regrowth. Similarly, Blanc *et al.* developed consortia biofilms on hydroxyapatite coupons to test antimicrobial efficacy of chlorhexidine, cetylpyridinium chloride, and sodium fluoride mouthwash rinses (Blanc, Isabel *et al.* 2014).

## Flowcells

The flowcell is the smallest in size of the six biofilm model systems described. Due to the compactness of the system, flowcells use small volumes of inocula and media for biofilm development. Flowcells are commercially-available through Stovall Life Science Inc. (Greensboro, NC), and Biosurface Technologies (Bozeman, MT), or can be constructed in-house for custom usage. Described by Palmer & Caldwell in the mid-1990s, the flowcell consists of two glass coverslips adhered to a rubber or silicone spacer (Palmer 1995). The main advantage of flowcells to study oral biofilms is the capability of observing changes to biofilm properties and architecture over time. This can be accomplished if the substratum of the flowcell is constructed from glass. With confocal or epifluorescent microscopy, morphological composition of bacteria and accumulation of biomass can be monitored over time. The throughput of flowcells vary by manufacturer. Stovall flowcells (<http://www.seilsci.com/Stovall/flow-cell.pdf>) contain three chambers and Biosurface flowcells (<http://biofilms.biz/products/microscopy-flow-cells/>) have throughputs ranging from 1-4 depending on application. A visual representation of the flowcell is presented in **Figure II.5**.

The flowcell has played a prominent role in oral biofilm research. In 2004, Foster *et al.* used a flowcell to test the efficacy of antimicrobials or anti-biofilm agents on dental biofilms. In that study, Foster and colleagues grew single species *S. gordonii* biofilms in saliva-conditioned flowcells and treated them with commercially available mouthwashes (Foster 2004). The experiment showed different active ingredients varied in antimicrobial efficacy, demonstrating the utility of flowcells in the expeditious evaluation of candidate compounds. Later, Foster and colleagues used the same saliva-conditioned flowcell for

consortia biofilms featuring four oral residents. These experiments showed that biofilm formation can depend on whether the microorganisms form coaggregates with each other in the planktonic phase (Foster and Kolenbrander 2004). The flowcell has also been used in studies to test pellicle formation on glass compared to hydroxyapatite. The results indicated that the two surfaces were similar and had no effect on biofilm attachment (Elliott, Pratten et al. 2005).

### **Bioflux™ Model System**

The Bioflux™ system, manufactured by Fluxion Biosciences (San Francisco, CA), is another continuous flow system used by investigators to model oral biofilms (Benoit, Conant et al. 2010, Samarian, Jakubovics et al. 2014). The system consists of three main parts: the consumable plates, the controller, and the software control interface. The software controls the flow rate expelled from each hose, the total runtime, and determines which pumps are active. The pneumatic pressure top creates an airtight environment within the Bioflux™ plate, allowing pressure to be applied only from the controller. This expels fluid from inlet well to output well at a fixed rate. A viewing port exists between the inlet and outlet wells and is where biofilm is developed under the prescribed flow rate. The Bioflux™ plate, similar to flowcells, can be imaged with inverted microscopy techniques during biofilm growth or after maturation. The 24-well Bioflux™ system is shown in **Figure II.6**.

Of all the systems described in this review, the Bioflux™ requires the least amount of media and inocula. Oral biofilms have been developed overnight at .2 dynes/cm<sup>2</sup>, which requires 380 uL of media per sample. Inoculum-wise, as little as 100 µL is needed. The low volumes required are especially advantageous for studies using donations of bodily fluid for media. Another advantage of the Bioflux™ system is its throughput. With evenly-distributed flow supplied by a computerized pneumatic pump and a heating plate that covers the entirety of the plate, multiple biofilms can be produced in parallel under the same environmental parameters. Additionally, the atmospheric contents of the interface can be controlled by fitting a Bioflux™ controller with a pressurized gas cylinder containing a defined gaseous mixture. Different plate models enable 3, 8, or 24 biological replicates of oral biofilms to be developed in parallel. When compared to the modified Robbins device, the Bioflux™ model system has comparable throughput. However, unlike the Bioflux™ system, each biofilm sample from the MRD are not biological replicates. This is because each peg is situated at a different distance downstream from the introduction of media. This results in a nutrient gradient that affects biofilm formation on pegs more distal to the media source (Johnston 1995). Biological replicates can be achieved with the flowcell model system as well as the drip reactor; however, with the throughput of those two systems, considerably more effort is required to accumulate a comparable sample size to the Bioflux™.

First described in 2010, Benoit *et al.*, used the throughput advantage of the Bioflux™ system to quickly screen several antimicrobials in their effectiveness on *P. aeruginosa* PAO1 flow biofilms (Benoit, Conant et al. 2010). Since then, the Bioflux™

system has been adapted for oral biofilm architecture and community studies. In 2013, Nance *et al.*, developed overnight microcosm biofilms seeded from salivary inoculum and tested the antimicrobial effectiveness of cetylpyridinium chloride (CPC) (Nance, Dowd *et al.* 2013). Using LIVE/DEAD™ staining, a dose-response viability gradient was observed between .001% and .5% w/v CPC. Also in the study, Nance established that the Bioflux™ system was capable of developing a dental biofilm that was compositionally very similar to early supragingival plaque. A standardized protocol for developing oral multi-species biofilms using the Bioflux™ system was described by Samarian *et al.* in 2014. Since then, the Bioflux™ system has been used to study the effects of other compounds on dental biofilms. In 2015, Kolderman *et al.* demonstrated the biofilm destabilization properties of L-arginine (Kolderman, Bettampadi *et al.* 2015). Lastly, the Bioflux™ system has been used in single-species studies. Ding *et al.* grew single-species *S. mutans* biofilms with flowing media and tested the antimicrobial peptide bactenecin (Ding, Wang *et al.* 2014). The group observed a significant decrease in viability.

### **Integration of Model Systems with Microscopy and Bioinformatics**

Since the first model biofilm systems were described in the 1950s, innovation in methodologies have enhanced the generalizability of oral biofilms grown *in vitro*. Today, investigators can cultivate an *in vitro* oral biofilm that is compositionally similar to the microbial community of plaque (Rudney, Chen *et al.* 2012, Nance, Dowd *et al.* 2013). The ability to replicate the *in vivo* to the *in vitro* is crucial to conducting representative studies without the need for human subjects. Two disciplines where technological advancements

have significantly augmented the value of laboratory model systems are microscopy and bioinformatics, particularly in the domain of 16S rRNA bacterial community profiling. Microscopy is the cornerstone behind the exploration of biofilm architecture, whereas bioinformatics techniques are becoming increasingly popular for characterizing the function of biofilm microbial communities as a whole.

### **Confocal Laser Scanning Microscopy (CLSM)**

Microscopy enables investigators to observe dental plaque biofilm while it is still attached to the substratum (Zaura-Arite, van Marle et al. 2001). Instead of destructively removing dental biofilm for downstream quantification, microscopy enables *in situ* quantification. For example, instead of culture viability counting, which often requires sonification of biofilm to remove it from its substratum, a confocal laser scanning microscope can take a digital snapshot of a biofilm stained with LIVE/DEAD™. Viability measured post-sonification may underestimate true viability due to the destructive nature of the harvesting process. Although the stains that comprise LIVE/DEAD™ are intercalating agents that renders microbial life inert, a cross-sectional measurement of the biofilm's viability can be achieved. Of more importance is that structural features of dental biofilms can only be visualized with the aid of microscopy. Understanding how dental plaque structure matures over time and observing how it responds in real-time to treatment have important implications for treatment delivery strategies (Wood, Kirkham et al. 2000).

Biofilm architecture captured with microscopy can also give clues to its microbial membership. Like the edifices that define the skyline of a metropolis, multi-species oral biofilms feature conspicuous architectural features interspersed along a heterogeneous topography. This complexity in biofilm structure is attributed to the heterogeneity of taxa found within dental plaque. The architecture of biofilms is an enticing research topic because certain physical attributes could indicate the prevalence of known pathogenic taxa. In a 2010 study, Zijngge *et al.* used fluorescent *in situ* hybridization to observe subgingival plaque on extracted teeth from four subjects diagnosed with periodontitis. They identified *Acintomyces* sp., *Tannerella forsythia*, *Fusobacterium nucleatum*, *Spirochaetes* sp., and *Synergistetes* sp. with dominant co-localizations, embedded in distinct formations within the subgingival plaque (Zijngge, van Leeuwen *et al.* 2010). Using a variety of microscopic methods, other studies also have investigated co-localization and spatial arrangement tendencies of pathogenic species within dental plaque (Dige, Nilsson *et al.* 2007, Ng, Kin *et al.* 2016). Understanding these biofilm structures and cellular arrangements could be important to biofilm control and therapeutic options. For instance, identifying coaggregation partners and targeting participating species could destabilize biofilm development (Rickard, Gilbert *et al.* 2003). Thus, considerable effort has been dedicated into identifying a disease-associated motif seen in biofilm architecture and its possible role in pathogenesis.

However, exploring biofilm architecture *in vitro* is challenging, as it requires a model system capable of growing an environmentally-germane biofilm, the hardware to visualize biofilms attached to a substratum and appropriate analytic tools. One popular

technology to directly visualize the physical architecture of a biofilm is confocal laser scanning microscopy (CLSM). CLSM technology captures a 3-dimensional stack of x-y planar images at user-defined z-interval distances and translates it into input for analytical software. Additionally, CLSM is amenable to the study of spatial relationship of species (taxa-specific fluorescent antibodies) and cells that are intact or damaged (LIVE/DEAD™). Multiple analytical software packages are publically available and offer a multitude of outcome measurements. Alternatively, customized in-house analysis can be performed from the raw digital data stored by confocal imaging. A computing environment such as Matlab (Natick, MA, USA) is necessary for the latter alternative and is described in more detail by Lewandowski *et al.* (Beyenal, Donovan et al. 2004). The also data can be used as input for 3D rendering software, such as Imaris (Zurich, Switzerland), which generates the topography of the physical biofilm and gives investigators insight to structural features of an intact dental biofilm in its natural state. Scanning electron microscopy (SEM) also can capture the 3-dimensional architecture of biofilms, but biofilms can suffer from architectural deformation during fixation steps prior to imaging (Bomchil, Watnick et al. 2003).

### **16S rRNA Community Profiling**

Biofilm research also has benefited from developments in sequencing which enable identification of all taxa present. The focal point of bacterial pathogenesis of oral diseases has shifted from individual causative agents to microbial community profiles that function as a unit within the intraoral cavity (Li, Zou et al. 2016, Vogtmann, Hua et al.

2018). There is mounting evidence that consortiums of species, and their interactions with the host, are responsible for initiating the pathway for soft and hard tissue destruction seen in periodontal disease and caries. For example, *Streptococcus mutans* and *Porphyromonas gingivalis*, which have traditionally been identified as causative agents of caries and periodontal disease, are present in the mouths of healthy individuals and increased abundance of these species is not necessarily predictive of dental disease (Kolenbrander, Palmer *et al.* 2006, Marsh, Moter *et al.* 2011, Whitmore and Lamont 2011). The present challenge is identifying community profiles, not individual species, most associated with disease.

A popular technique for constructing community membership within a sample is 16S rRNA sequencing. All prokaryotes possess the 16S rRNA gene coding for the 16S ribosomal RNA. Variations within the nine hypervariable regions of the 16S rRNA gene can be used to identify taxa (Janda and Abbott 2007). With more hypervariable regions sequenced within a read, a higher resolution taxonomic assignment can be achieved. Prior to the advent of next-generation sequencing (NGS), investigators relied upon technologies that produced low read counts of 16S rRNA sequences. These technologies included clone libraries (Diaz, Chalmers *et al.* 2006) and denaturing gradient gel electrophoresis (Strathdee and Free 2013), for the study of the oral microbiome. With NGS, massively parallel and deep sequencing capabilities emerged, enabling the oral microbiome to be quickly characterized (Behjati and Tarpey 2013).

To interrogate the microbiome of a biofilm grown *in vitro*, investigators harvest and prepare biofilm cells from their model system for integration with next-generation sequencing technologies. This involves removing biofilm material from substratum with sonification or turbulent shear with the Bioflux™ system. Unlike cell culture viability techniques, the destructive nature of removing biofilm is irrelevant for 16S rRNA community profiling. The objective is to retrieve a cross-sectional snapshot of the community at the time of harvest by sequencing 16S rRNA fragments of bacterial cells extant within the biofilm. There are numerous NGS platforms used for 16S profiling. Choice of sequencing platform depends on the investigator's research questions and involve trade-offs between read length, read depth, sequencing depth, and accuracy. Sequencing platforms relevant to oral microbiome studies are listed below in **Table II.3**. Bear in mind this is not an exhaustive list since NGS technologies that offer insufficient or superfluous read length (20Kb read lengths offered by PacBio) for the 16S rRNA gene are excluded.

### **Concluding Remarks and Future Directions**

The miniaturization of *in vitro* platforms operating on the microscale, combined with integration with imaging and 'omic' technologies have reinvigorated the appeal of laboratory biofilm model systems. A PubMed search on the key terms "animal model system dental" and "laboratory model system dental" indicates that animal and laboratory-based models have comparable numbers of publications count up until 2014. In 2014, 2015, and 2016, nearly double the number of publications relate to dental laboratory

model systems. This popularization of laboratory-based systems is likely owed to technologies that can be tethered to model systems, such as confocal laser scanning microscopy (CLSM) and 16S community profiling (Azevedo, Lopes et al. 2009, Valm, Mark Welch et al. 2012, Fritz, Desai et al. 2013). Combined with decreasing costs, *in vitro* model biofilm systems have become an appealing option for multi-species dental biofilm studies.

The future directions of *in vitro* model systems could involve a shift from developing representative dental plaque within the system to transplanting already-developed *in vivo* plaque into the system. There are *ex situ* hybrid studies that involve human participants wearing non-invasive oral prostheses housing bovine enamel chips. This enables testing hypotheses on mature dental plaque grown *in vivo* for better applied research. Another direction of *in vitro* model systems could incorporate a biological substratum for biofilm development, such as that developed using tissue culture techniques. There are multiple surfaces in the intraoral cavity including hard and soft palate, tongue, subgingival, buccal, and teeth. Glass and hydroxyapatite are representative of the hard surfaces of teeth, but are a poor model for attachment and development of subgingival plaque. Tissue culture of host epithelial cells, on the other hand, would more adequately represent the substratum of subgingival plaque (Guggenheim, Gmur et al. 2009). This will open a new subset of *in vitro* oral biofilm studies to include modeling of subgingival communities.

The development and validation of new biofilm model systems for applied dental biofilm research is a continual effort. The biggest challenge thus far in translating the *in vitro* model system findings into clinical practice has been the inability to form *in vivo*-like

biofilms in a laboratory setting. The fusion of old and new model systems implementing improved protocols are allowing investigators to get closer to mimicking the natural oral biofilm states and providing investigators the tools to more accurately measure dental biofilm outcomes.

**Table II.1. Examples of Fundamental & Applied Research of *In Vitro* Dental Biofilms.**

Studies that improve the understanding of dental biofilms are fundamental. Applied studies, on the other hand, are designed to intervene. *S. mutans* had been observed to cause dental caries through its acidogenic metabolism of sugar. Based on this fundamental understanding, applied studies can be designed with an intervention to limit *S. mutans* biofilm formation.

<b>Outcomes</b>	<b>Fundamental Study (Reference)</b>	<b>Applied Study (Reference)</b>	<b>Model System(s) Used</b>
Cariogenesis <sup>a</sup>	D-glucose and sucrose induce caries (Pigman, Brasher et al. 1962).	Fluoride slurry inhibits enamel softening (Pigman and Newbrun 1962).	Artificial Mouth
Single-Species Plaque	<i>S. mutans</i> biofilms fed sucrose induces caries (Deng and ten Cate 2004).	Chlorhexidine in dentin bonding systems can inhibit <i>S. mutans</i> biofilm formation (Brambilla 2017)	Constant Depth Film Fermenter, Angled Drip-Flow Reactor
Defined-Species Plaque	<i>S. oralis</i> and <i>A. naeslundii</i> biofilms grew more when co-cultured than alone (Palmer, Kazmerzak et al. 2001).	<i>S. gordonii</i> expression of <i>amyB</i> gene is increased in presence of <i>V. atypica</i> , paving way for <i>V. atypica</i> colonization (Egland, Palmer et al. 2004).	Flowcells
Microcosm Plaque	Community composition of <i>in vitro</i> biofilms can reflect that of microcosm donor (McBain, Sissons et al. 2005).	Exposure to L-arginine hydrochloride can alter biofilm community composition (Kolderman, Bettampadi et al. 2015)	Sorbarod Perfusion, Bioflux™

<sup>a</sup> Not a dental biofilm outcome, but listed to provide historical context and highlight the shift of focus to dental biofilm outcomes.

**Table II.2. Open System Biofilm Models Relevant to Dental Biofilm Research.**

Examples of model biofilm systems that have been used for the study of dental biofilms. General properties of each system is described, along with its nutrient delivery classification, year it was first described in literature, throughput, and volumetric scale.

Biofilm Model	Classification	Year <sup>a</sup>	General Properties	Throughput	Volumetric Range
<b>Constant depth film fermenter</b> (Peters and Wimpenny 1988)	Drip-fed	1988	-Scraper blade to smear media and keep biofilm at constant depth -Keeps biofilm in a steady state -Rotating disc embedded with plugs -Plug composites can be modified to simulate a different substratum -Can run for several days	<b>25</b> (Peters and Wimpenny 1988), <b>75</b> (Deng, van Loveren et al. 2005)	Liters
<b>Sorbarod perfusion system</b> (Hodgson, Nelson et al. 1995)	Drip-fed	1995	-Sorbarod filter substratum -Media perfuses through filter -Similar to CDFF -Can run for several days	<b>1</b> (Hodgson, Nelson et al. 1995), <b>5</b> (McBain, Sissons et al. 2005), <b>6</b> (Taylor and Greenman 2010),	Milliliters to Liters
<b>Angled drip-flow biofilm reactor</b> (Xu, Stewart et al. 1998)	Drip-fed	1998	-Reactor angled to allow drip to flow continuously across substratum -Gravity-assisted flow simulates low shear -Non-homogenous trickle flow can generate heterogeneous biofilms -Shear rate can be -Can run for several days	<b>4-6<sup>b</sup></b>	Milliliters to Liters
<b>Modified Robbins device</b> (McCoy, Bryers et al. 1981)	Flow-fed	1981	-Individual coupons or discs as substratum -Coupons customizable by investigator -Proximity of coupon to nutrient source a parameter to consider	<b>12, 25<sup>b,c</sup></b>	Liters
<b>Flowcells</b> (Palmer 1999)	Flow-fed	1995	-Rubber or silicone spacer bound by glass coverslips -Amenable to inverted microscopy -Can use other substrata but may jeopardize compatibility with microscopy	<b>1-4<sup>b,d</sup></b>	Milliliters to Liters
<b>Bioflux™</b> (Benoit, Conant et al. 2010)	Flow-fed	2010	-consumable plates etched with microchannels -software-controlled pneumatic pump -Glass-bottomed substratum -Amenable to inverted microscopy	<b>3,8,24<sup>e</sup></b>	Microliters to Milliliters

<sup>a</sup> Year that open system biofilm model was introduced for general biofilm research. The cited reference may not have used the biofilm model for dental biofilm research at the outset.

<sup>b</sup> Commercially available through Biosurfaces Technologies Corporation.

<sup>c</sup> Commercially available through Tyler Research Corporation.

<sup>d</sup> Commercially available through Stovall Life Science, Inc.

<sup>e</sup> Commercially available through Fluxion Biosciences

**Table II.3. Sequencing Platforms for 16S rRNA Community Profiling.** Compatible next-generation sequencers that have been used to characterize a dental microcosm biofilm grown *in vitro* are listed. The sequencing chemistry, expected read length, sequencing depth, and consensus accuracy of each platform is also described.

Sequencing Platform (Reference)	Sequencing Chemistry	Read Length	Sequencing Depth	Consensus Accuracy
<b>454 GS FLX+</b>  (Nance, Dowd et al. 2013, Kistler, Pesaro et al. 2015, Koopman, Roling et al. 2015)	Pyrosequencing	Up to 1000bp	700 Mb	99.997
<b>Illumina MiSeq</b>  (Koopman, Buijs et al. 2016) (Agnello, Cen et al. 2017)	Sequencing by synthesis	2x150, 2x250, 2x300	4.5-5.1 Gb, 7.5-8.5 Gb, 13.2-15 Gb	80% bases > 99.9 75% bases > 99.9 70% bases > 99.9
<b>Illumina HiSeq</b>  (Edlund, Yang et al. 2013)	Sequencing by synthesis	2x125	450-500 Gb	80% bases > 99.9
<b>IonTorrent PGM</b>  (Fernandez, Aspiras et al. 2017)	Ion semiconductor	Up to 400bp	Up to 2 Gb	>99.0

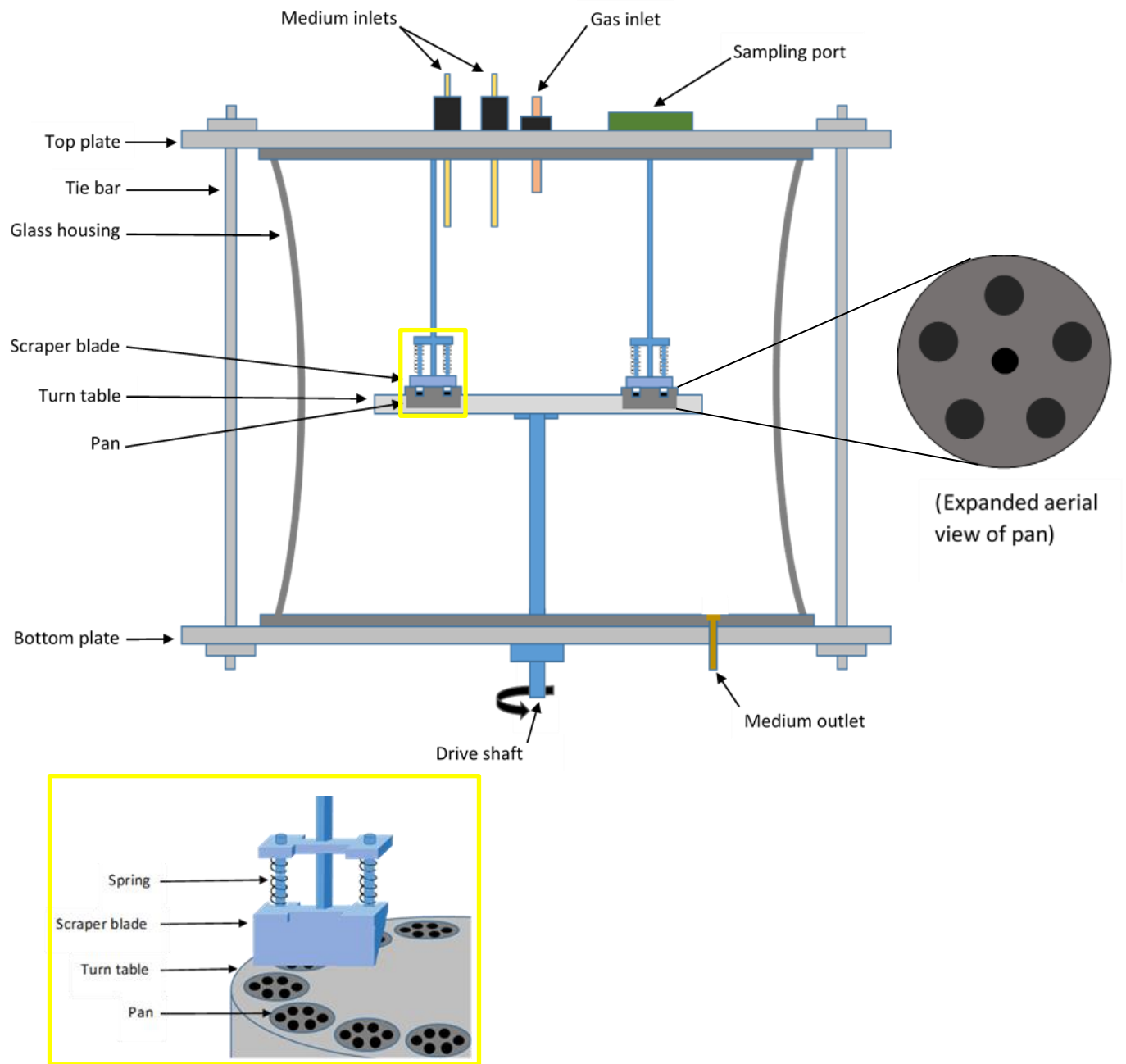


**Figure II.1. Constant Depth Film Fermenter System (Drip-fed System).** A side view of a typical CDFF is presented. A drive shaft rotates the turntable as medium is dripped onto the turntable. Biofilm is formed on substratum plugs that are inserted into slots on each pan (shown top-down on the right). Biofilms are kept at a constant depth (thickness) by a scraper blade that is positioned near the interface of biofilm development.

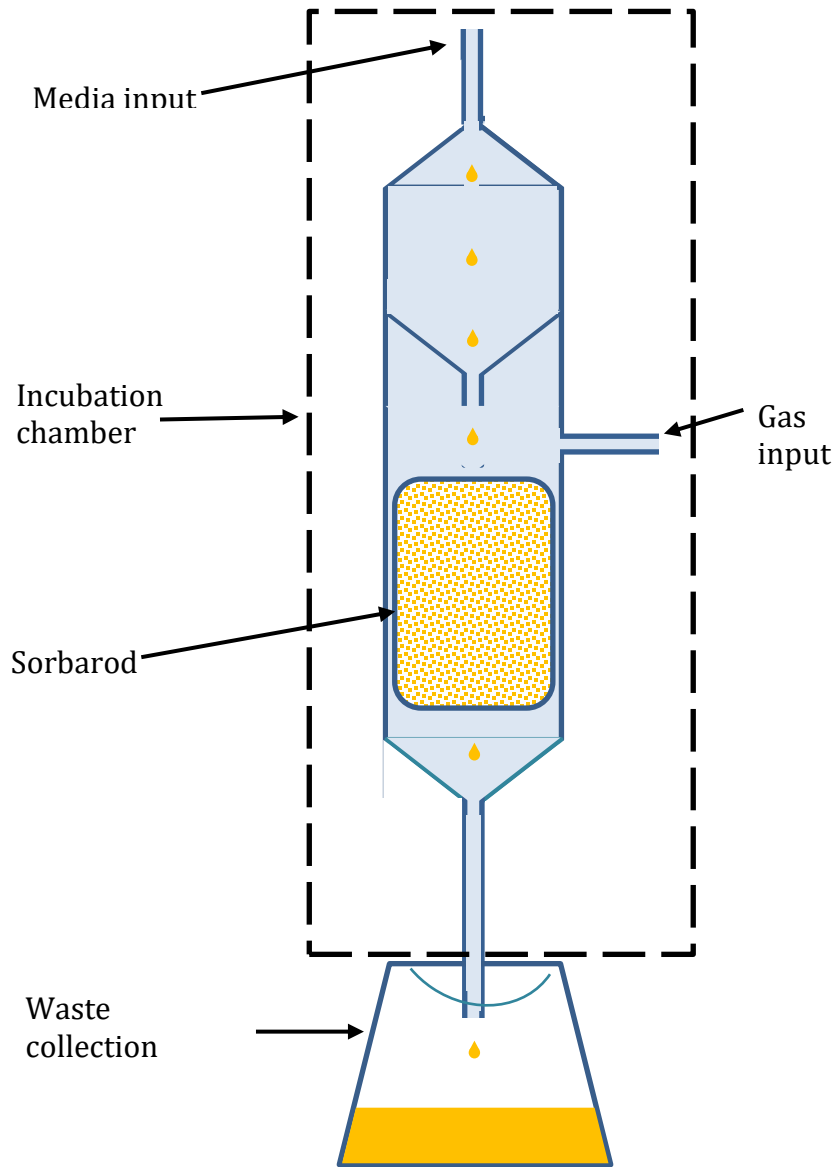


**Figure II.2. The Sorbarod Perfusion System (Drip-fed System).** A side view of a variant of the Sorbarod perfusion system is shown. Medium is dripped from above through the medium inlet. There the media percolates through the Sorbarod filters, where biofilm development occurs. Cells detaching from biofilm are washed away with the perfusate and collected after exiting from the medium outlet.

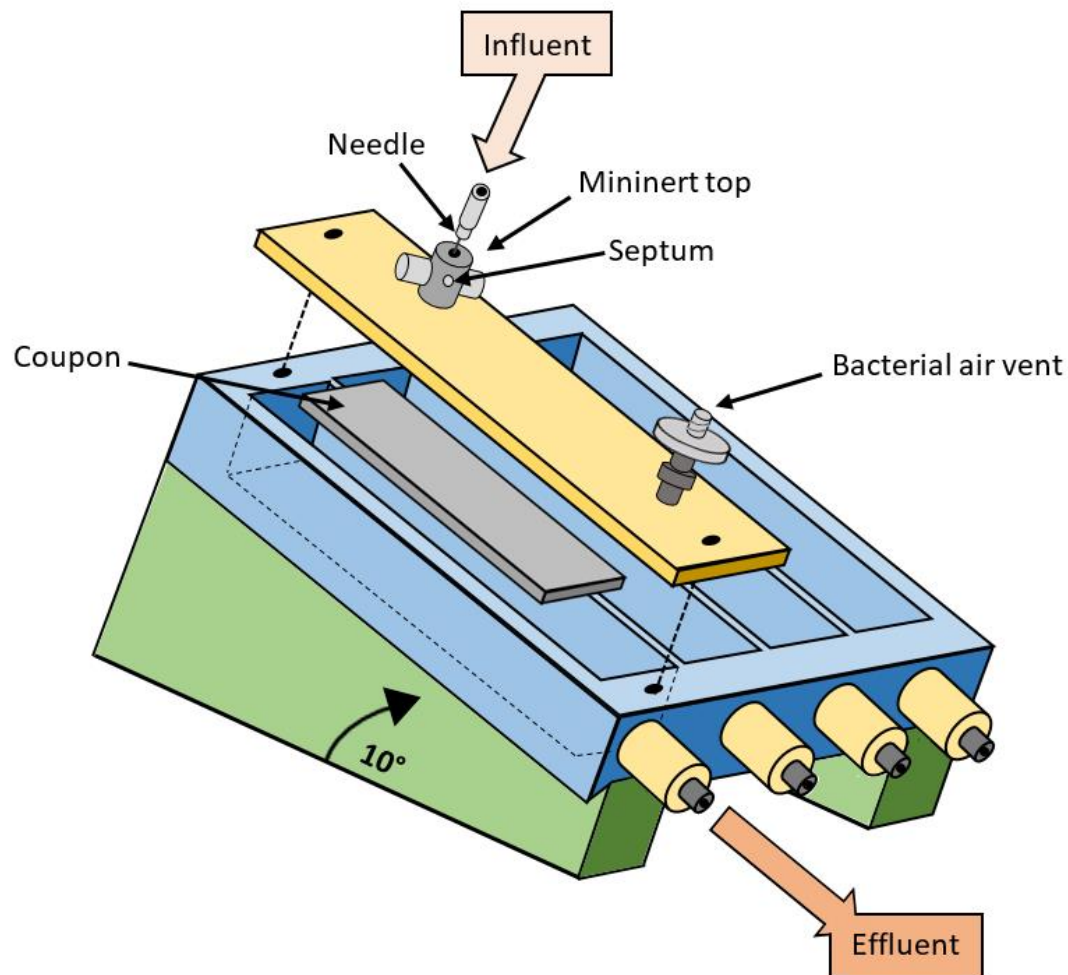


**Figure II.3. The Angled Drip-Flow Biofilm Reactor (Drip-fed System).** A perspective view of the angled drip-flow biofilm reactor is shown. The steepness of the angle can be modified by adjusting the biofilm reactor's hind legs. Medium is dripped from the medium inlet onto a microscope slide on the end that is elevated. With assistance of gravity, the media flows downward toward the effluent outlet, where spent media is expunged. Biofilm development occurs across the microscope slide.

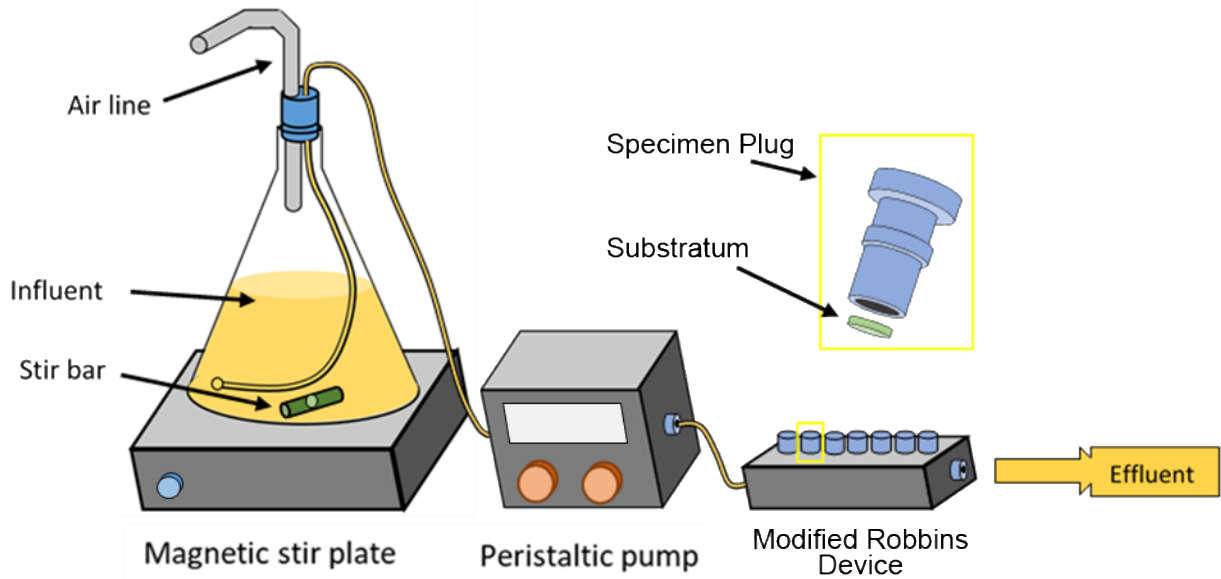


**Figure II.4. The Modified Robbins Device (Flow-fed System).** The side view of the MRD is shown. Flow of media is unidirectional and provided by a peristaltic pump. Plugs retrofitted with coupons are inserted into ports. Coupon inserts can be made of various materials. Biofilm development occur on the coupon surfaces. Coupons most distal from the medium inlet are fed media that had already bathed coupons that are more proximal to the medium inlet.

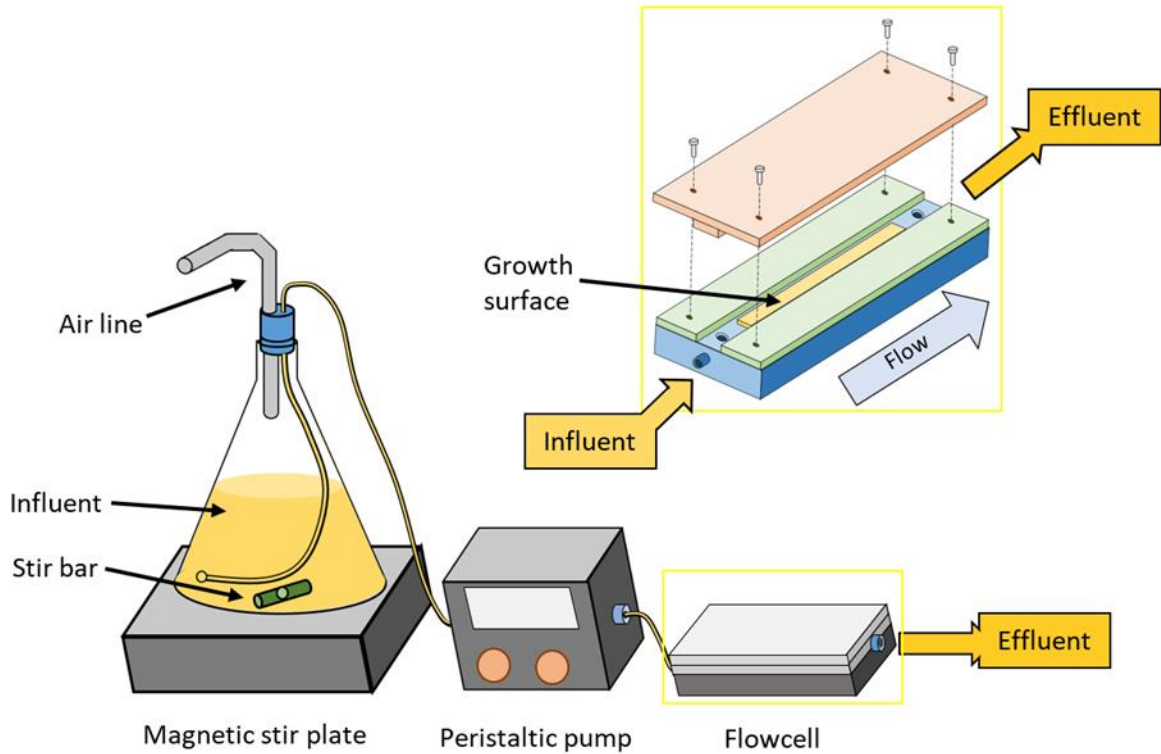


**Figure II.5. Flowcells (Flow-fed System).** A schematic of a basic flowcell is presented. Inoculum is pulsed into square capillaries or glass coverslip, where biofilm development occurs. The glass substratum can be coated with hydroxyapatite. A microscope objective can observe the system as it is running.

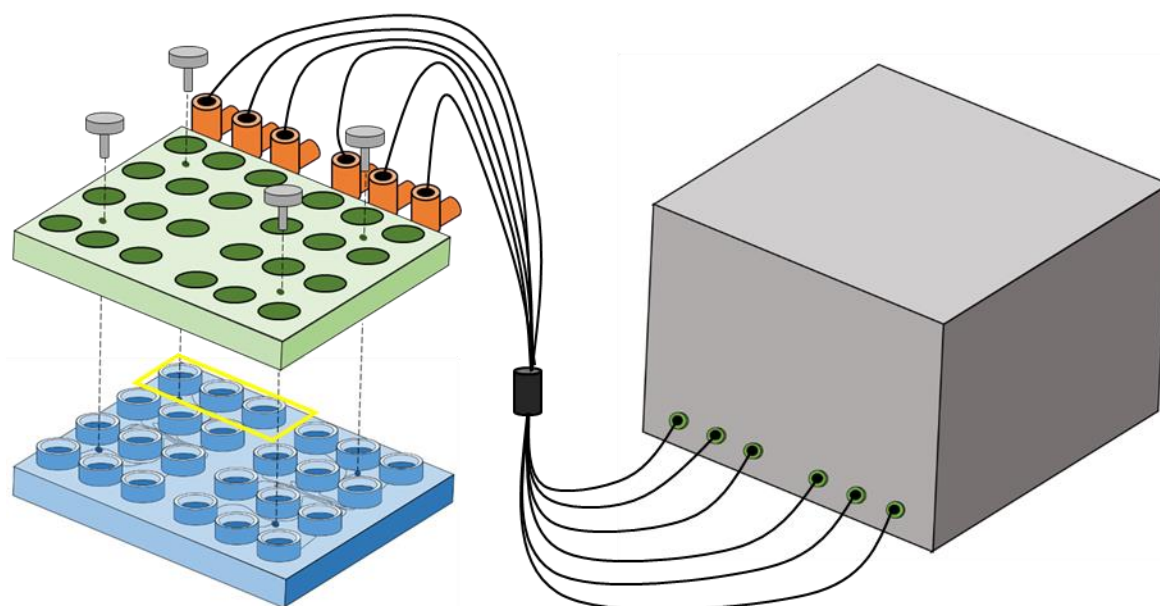
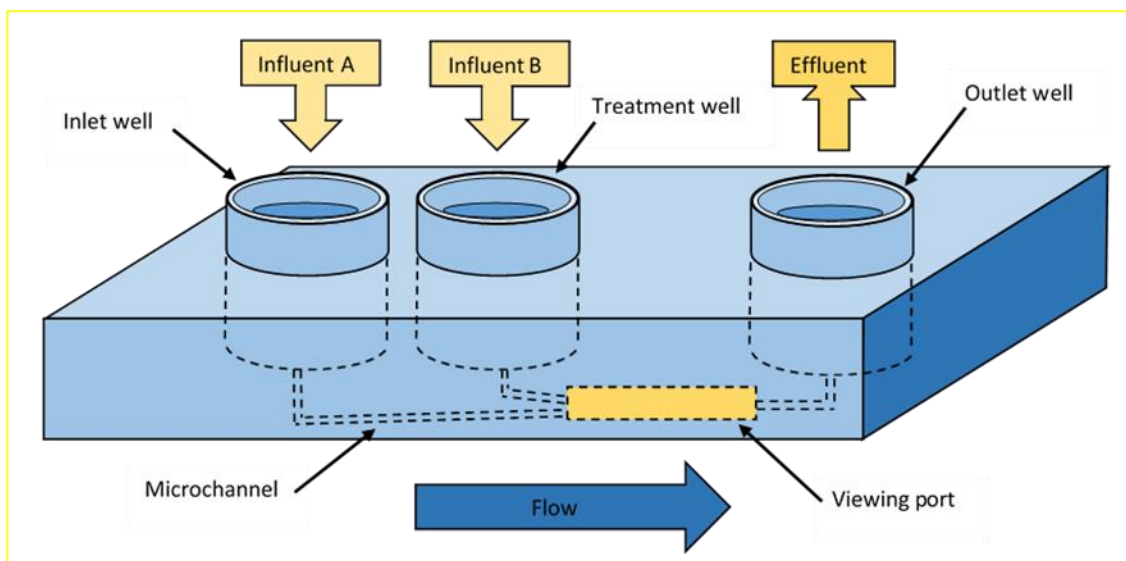


**Figure II.6. Bioflux™ System (Flow-fed system).** The 24-well Bioflux™ system is illustrated above, featuring the dual inlet system. The secondary inlet can be used for aqueous treatment formulations or products. The Bioflux™ system relies on an external control unit and commercially-available consumable plates. Each plate is laser-etched to provide micro-channels across each well. The substratum of Bioflux™ consumable plates is glass. The control unit flows media unidirectionally at a set shear force and can deliver treatment at set times specified by the investigator.

## **Chapter III**

### **A Sensitive Thresholding Method for Confocal Laser Scanning Microscope Image Stacks of Microbial Biofilms**

#### **Abstract**

Biofilms are surface-attached microbial communities whose architecture can be captured with confocal microscopy. Manual or automatic thresholding of acquired images is often needed to help distinguish biofilm biomass from background noise. However, manual thresholding is subjective and current automatic thresholding methods lead to loss of meaningful data. Here, we describe an automatic thresholding method designed for confocal fluorescent signals, termed the biovolume elasticity method (BEM). We evaluated BEM using confocal image stacks of oral biofilms grown in pooled human saliva. Image stacks were thresholded manually and automatically with three different methods; Otsu, iterative selection (IS), and BEM. Effects on biovolume, surface area, and number of objects detected indicated that the BEM was the least aggressive at removing signal, and provided the greatest visual and quantitative acuity of single cells. Thus, thresholding with BEM offers a sensitive, automatic, and tunable method to maintain biofilm architectural properties for subsequent analysis.

## Introduction

Biofilms are architecturally ornate surface-attached microbial communities that exist throughout nature (Wimpenny, Manz et al. 2000). The biological activities of biofilms vary by ecological niche (Dufour 2010, Diaz 2012) and particular attention has focused on the ability of biofilms to have deleterious effects (Costerton, Cheng et al. 1987, Yang, Liu et al. 2011). For example, in humans biofilms can cause chronic wounds and a multitude of diseases (Beikler and Flemmig 2011, Harriott and Noverr 2011, Mulcahy, Isabella et al. 2014). In industry and infrastructure, uncontrolled biofilm growth on ship hulls and on piping can interfere with function (Holm, Schultz et al. 2004, Pavissich, Vargas et al. 2010, Dombrowsky, Kirschner et al. 2013). Much of the biological activity of biofilms is attributable to community composition and biofilm architecture.

To quantify biofilm architecture, a three-dimensional dataset must be generated from biofilms with intact structural integrity. One tool that provides this capability is a confocal laser scanning microscope (CLSM), which can capture two-dimensional cross-sections of a biofilm to produce a three-dimensional representation (Palmer and Sternberg 1999). Cross-sections that make-up a confocal stack data often consist of 8-bit grayscale values from 0-255, which correspond to the intensity of signal captured, but images with higher bit depths can be generated (e.g. 12 bit, which corresponds to gray scale values from 0-4095). Following thresholding, the digital data contained within confocal stacks can be quantified by image analysis software such as COMSTAT (Heydorn, Nielsen et al. 2000), Icy (de Chaumont, Dallongeville et al. 2012), and PHLIP

(Mueller, de Brouwer et al. 2006), or imported to MatLab (Mathworks, Natick, MA) for customized analysis (Yang, Beyenal et al. 2000, Renslow, Lewandowski et al. 2011).

Thresholding allows pixels of a grayscale image to be classified as foreground biomass or background interstitial space, depending on its signal intensity (Unnikrishnan, Pantofaru et al. 2007, Mansoor, Patsekin et al. 2015, Vyas, Sammons et al. 2016). Thresholding can be performed on a two-dimensional image or a three-dimensional confocal stack (Beyenal, Donovan et al. 2004, Yerly, Hu et al. 2007). A threshold that is too low will lead to false positives that will infer spatial presence of biomass when there is none. Conversely, a threshold that is too high will lead to false negatives: missing measurement of true biomass emitting low-intensity signal. In either case, suboptimal thresholding will bias measured features of the biofilm architecture. Thresholding can be done manually or automatically. Manual thresholding relies on individual(s), often operating under guidelines, for visually determining thresholds. This method can be arbitrary and the reproducibility/generalizability of results can be affected by inter-operator subjectivity (Yang, Beyenal et al. 2000, Bergouignan, Chupin et al. 2009, Million, Sbrignadello et al. 2010). By contrast, automatic thresholding eliminates subjectivity in thresholding; however, algorithm selection can drive sensitivity/specificity of regions of interest detection and predicate the success or failure of downstream outcome measurement (van Aarle, Batenburg et al. 2011). Further, imaging platforms can affect algorithm performance (e.g. CLSM vs light microscopy) as well as within-platform acquisition parameters (e.g. gain, smart offset, and excitation energy in CLSM) (Yerly, Hu et al. 2007). In the absence of a consensus on the best algorithm to automatically

threshold CLSM images, manual thresholding has been used (Takenaka, Iwaku et al. 2001, Derlon, Grutter et al. 2016).

Two algorithms used for automatically thresholding images are Otsu and the iterative selection (IS) methods (Ridler 1978, Otsu 1979). Otsu's method selects a threshold that maximizes between-class (background vs. foreground) variance (Otsu 1979). Thus this method is particularly powerful for segregating foreground signal from background noise in images characterized with a bimodal intensity histogram (Yang, Beyenal et al. 2001, Yerly, Hu et al. 2007). The IS method has demonstrated the most congruency with manually-set thresholds for light and confocal biofilm images (Yang, Beyenal et al. 2001). This method seeks to find a threshold that maximizes the separation between mean background and foreground values (Ridler 1978). Functionally, Otsu and IS are similar and assume that histograms of image intensity values possess similarly-sized bimodal peaks that resemble a normal distribution (Rosin 2001, Xue 2012). CLSM images, however, are often characterized by unimodal histograms with long tails (Baradez 2003). These characteristics are poorly compatible with implicit assumptions of IS/Otsu's methods and are not well-matched for its use with confocal images (Rosin 2001, Baveye 2002). In the case of CLSM images with long tails, IS/Otsu sacrifice actual biofilm material in favor of maximizing the separation between apparent foreground and background. This limitation led us to develop an automatic thresholding method designed to cope with unique features of CLSM image histograms.

## Results

### Consistency and agreement within and between automatic and manual thresholding

The distribution of thresholds by treatment and control groups is summarized in **Table III.1**. The BEM thresholds for each image were lower than the thresholds calculated by IS and Otsu's methods or those set manually. Additionally, the BEM had the least variance of all the methods. Overall, manual thresholding was consistently more aggressive at removing signal than BEM, but less aggressive than IS and Otsu. Each method produced slightly higher average thresholds for images of biofilms that had been treated intermittently with water. The difference in average thresholds between water treated and control group images was not significant for all four methods.

Differences in magnitude between each pairwise combination of thresholding methods were evaluated with student's paired t-test and is summarized in **Table III.2**. Each pairwise method tested statistically significant, indicating magnitude differences between any two thresholding methods. Treatment status of oral biofilm images did not affect the conclusion that the four thresholding methods can be differentiated from one another in terms of magnitude. Although Otsu and IS mean thresholds were close to each other, the consistency of IS thresholds scoring two intensity units higher than Otsu thresholds on the same images minimized variance. Considering quantification and rendering, the significance of a two unit difference in threshold is negligible.

### Average Outcomes Following Each Thresholding Method

The post-thresholding architectural measurements are summarized in **Table III.1**. Regardless of thresholding method, the biofilms treated with water at 8 and 18 hours had lower end-stage biovolume, surface area, and number of objects detected. In all four thresholding methods, biovolume and surface area differences between the two sets of biofilms were significantly different as tested by student's 1-tailed heteroscedastic t-test with moderate effect sizes. For objects detected, the BEM automatic threshold and manual thresholds indicated significant differences between treatment and control biofilm images whereas IS and Otsu's methods did not. Following the implementation of the less conservative thresholding methods (BEM & manual), water treated biofilms had a significantly decreased number of objects than control biofilms. The higher thresholded image stacks, using Otsu and IS methods, filtered out low-intensity signal fragments that were picked up by BEM (**Figure III.1**).

The values derived using the BEM thresholding method for the average biofilm biovolume, surface area, and objects were consistently much greater than the other two automatic methods. In the control set, the number of objects detected increased roughly five-fold with BEM thresholds measuring an average of 19,435 objects. In the same set of 25 images, Otsu and IS thresholds yielded averages of 3,780 and 3,818 objects detected, respectively. Similarly, in the treatment set, the application of BEM thresholds increased the average number of objects detected four-fold compared to the other two

algorithms. In general, average biovolume, surface area, and objects detected from manual thresholding occupy a middle ground between BEM and IS/Otsu thresholds. Out of the three automatic methods, BEM was most similar to manual thresholding values.

### **Visual Clarity of Biofilm Following Each Thresholding Method**

**Figure III.1** shows three rendering modes of the same image after application of BEM, Otsu/IS, and manual thresholds. A shadow projection of the same image without thresholding is presented in **Figure III.2**. After applying thresholds, the image was projected with maximum intensity projection (MIP), blend, and thresholding. The BEM threshold of 10 differed visually from the Otsu and IS thresholds of 59 and 61, respectively (**Figure III.1**). The first row shows the MIP where each pixel's given intensity value is the maximum out of all pixels at that location across the entire Z-axis. For the demonstration image, there are 53 slices. Thus, each pixel location has a set of 53 values. As compared to the other methods, The BEM MIP reveals more biofilm material in small flocs attached to the acquired pellicle. Additionally, the center of the large biofilm mass contains more signal (vis-à-vis biofilm) compared to the Otsu and IS thresholded images. The manual threshold average of 31.8 is intermediary to the results seen in BEM and Otsu/IS thresholds. The second row shows a blend render where the intensity of each pixel value, across the Z-axis, are blended together with inclusion of transparency. This mode allows for shadows within a 3D environment. In this mode, tiny flocs of biofilm material picked up by BEM's lower threshold also are observed. Additionally, the cavitation in the middle of the biofilm is less pronounced.

The third row shows two renderings. The blue channel represents voxels that are removed by thresholding by each of the methods and the green channel represents voxels that are considered signal and true biovolume. The blue channel rendering has a transparency applied as to not mask the green signal render. Overall, the BEM-thresholded image captured the most biovolume, closely followed by manual threshold average. Additionally, the void space in the center of the large floc is less saturated with blue in the BEM image. The fourth row images are 4x snapshots of the high resolution render shown above where the focus is on the bottom left corner. At this magnification, it is evident that the blue haze that is removed by Otsu and IS thresholding is bacterial cells. There are numerous streptococcal signatures (multiple cocci cells arranged in chain-like morphology) that have been retained using the BEM method and lost with the other methods.

### **Performance of the Three Automatic Thresholding Methods**

The distribution and modality of the grayscale histograms differ by imaging platform used (light microscope, MRI, or CLSM). **Figure III.3** and **Figure III.4** support this assertion. As shown in the representative image, CLSM grayscale histograms were unimodal with a strong skew to the right resembling a power-law distribution (**Figure III.3**). The same distribution of grayscale intensity was also observed in other images containing fluorescent tags (**Figure III.3**, **Figure III.4**). Log transforming the frequency of these histograms is recommended to make low-frequency values relatively more comparable

to high frequency values. This will create a more manageable functional form for operators to threshold manually. In fluorescently-labeled images with the described histogram characteristics, IS thresholds are consistently two units higher than Otsu's thresholds. This precision was also observed in the 50 CLSM oral biofilm images in this study.

### **Effect of Gain on the Three Automatic Thresholding Methods**

An oral biofilm that presented complex architectures was chosen to serve as the biological replicate for CLSM image stack captured using three different gains (**Figure III.5**). The 726V gain image stack capture was not sensitive enough to capture biofilm biomass that was visually conspicuous and architecturally ornate through the objective lens. Acquiring an image stack with a 726V gain resulted in a grayscale histogram that was severely weighted toward the low-intensity values. In the portion of the histogram that was toward the higher intensity values, the log frequency values became erratic, indicating noise. For this scenario, where gain is insufficient, all three automatic thresholding methods were comparable. The Otsu, IS, and BEM methods calculated thresholds were 22, 24, and 29, respectively. The biovolume dropped precipitously as threshold increased due to low abundance of voxels containing signal. No voxels were saturated with high intensity (255) signal and the highest detected intensity was 230.

Using the Leica Look-Up-Table (LUT), a gain of 900V was used to generate an image stack that contained an "optimal" spread of intensity values between 0 and 255.

This “optimal” is achieved when biofilm starts showing saturated pixels in blue in the LUT, indicating the entire dynamic range of 8-bit intensities are utilized. The image stack derived from using the 900V gain resulted in an image that was visually representative of the biofilm observed by eye through the objective lens. At this gain, the grayscale histogram was still weighted toward the low-intensity portion, but not as severely as the 726V (**Figure III.5a** vs. **Figure III.5b**). The log frequency was more uniformly distributed across the intensity axis. In this gain-optimized image, the BEM-calculated threshold of 10 differed significantly from the thresholds calculated by Otsu (threshold of 85) and IS (threshold of 87). The maximum intensity projection of saturated voxels revealed its presence along the X-Y Cartesian coordinate system. It should be noted that the image histograms of all 50 biofilm images as well as all fluorescent-based micrographs in **Figure III.2** resembled the 900V image histogram.

In the image stack acquired with a gain of 1250V, the biofilm biovolume was noticeably greater, as visualized by eye, than viewed through the objective lens. The grayscale intensity histogram was similar in shape to the log-frequency histogram and both reveal a sharp peak at 0 and 255, but also a modality in the region of 20. At maximum gain, the BEM-calculated threshold of 8 remained disparate from Otsu and IS thresholds of 121 and 123, respectively. Additionally, the biovolume was least elastic to changes in threshold amongst the three tested gains. The MIP of saturated voxels reveals that over half the X-Y coordinates contained a saturated voxel.

### **Validation of BEM Threshold Range with Negative Controls**

Five images of varying depth were taken of a stained channel completely void of biofilm. Image acquisition parameters were identical to those used for biofilm images. The image histograms were then used to identify the distribution of false positive noise assuming each voxel should be classified as 0. **Table III.3** shows the percentage of voxels belonging to the first 11 intensity classes with 0 considered as interstitial space and 1-10 as false positives assuming no thresholding. Despite absence of biofilm material, approximately 3% of voxels were noise. The distributions of false positives are near identical. For the image with 53 slices, 401,152 voxels were false positives with 399,776 belonging to intensity bins of 1-10. In the demonstration image (**Figure III.1**, **Figure III.2**, **Figure III.3a**) of 53 stacks, the BEM calculated threshold was 10, reclassifying a hypothetical 99.66% of false positive biovolume correctly back into interstitial space. This indicates that a threshold range of 9-14 seen in all 50 of our biofilm images with varying depth is sufficient to remove the vast majority of imputed false positives. Thresholds in the higher ranges calculated from Otsu/IS automatic methods, and even manual methods, are thus unnecessarily high.

### **Assessment of BEM to Other Images & Bit-depths**

The BEM threshold provided the best visual detail of a mouse imaged with an MRI, plant cells image under epifluorescence, and single-species *Rothia mucilogenosa* fluorescence imaged under confocal microscopy (**Figure III.6**). For bit-depth, the current BEM criterion placed thresholds too low (**Figure III.7**). After adjusting 8-bit values

calculated with BEM to 12-bit values (8-bit threshold of 10 would equal the 12-bit threshold of 80) for 12 bit images, the BEM provided the best visual detail for *Rothia mucilogenosa* biofilm 12-bit images (**Figure III.8**).

## Discussion

The work presented here demonstrates the utility of a sensitive method to threshold image stacks of biofilms generated with a CLSM, which we called the biovolume elasticity method (BEM). BEM is a model-based approach that applies a criterion to the biovolume by threshold curve. Threshold is determined where biovolume becomes relatively inelastic to changes in threshold. We then compared our proposed method to two existing automatic methods – Otsu and iterative selection (IS), which rely on intensity histograms to calculate optimal thresholds. Otsu’s method is ubiquitous across many analytical packages and iterative selection had been shown in studies to be congruent with manually-set thresholds for biofilms captured with light microscopy and CLSM (Heydorn, Nielsen et al. 2000, Yang, Beyenal et al. 2001, Mueller, de Brouwer et al. 2006, de Chaumont, Dallongeville et al. 2012). However, these methods are optimized for distinct intensity histograms that poorly fit the functional form of CLSM-acquired images of biofilms using fluorescence-based tagging (Baradez 2003, Arce, Wu et al. 2013), resulting in high thresholds. At these elevated thresholds, our renderings showed that meaningful biofilm biomass is sequestered from the image stacks (**Figure III.1**), which could lead to biased analyses.

In 2001, Yang and colleagues compared five algorithms to threshold confocal biofilm images and concluded iterative selection (IS) was the most suitable method. The images used were of mono-species biofilms grown in a flow-cell reactor and captured with light microscopy and CLSM. They did not evaluate Otsu's method. Their work, suggesting that IS functioned well enough to potentially replace manual operators in such images, (Yang, Beyenal et al. 2001) motivated our inclusion of IS for comparison with BEM and Otsu. However, we discovered that the IS method was very similar to Otsu's method for all biofilm CLSM images. Yang and colleagues focused their panel of algorithms on light microscopy images, which are unimodal with the mode located at a middling intensity, which, as we show, will give different results from Otsu's method. However, for confocal images where the histogram is unimodal with a strong right-skew, Otsu's method and IS are less easily differentiated.

Reliability between the five biofilm image analysis operators, who performed manual thresholding, was evaluated with intraclass correlation coefficients (ICC) calculated with both the consistency and agreement arguments as outlined by Koo et al. and Kim (Kim 2013, Koo and Li 2016). Consistency measures whether operators' rank-order of ratings were similar whereas agreement measures whether the raters' ratings are similar in magnitude. A 95% confidence interval was calculated for each ICC value to determine significance from a null hypothesis of ICC=0. The intraclass correlation coefficients for absolute agreement and consistency amongst the five independent operators were .243 ( $-.040 < \text{ICC} < .517$ ) and .707 ( $.556 < \text{ICC} < .818$ ), respectively. This indicates that although the manual operators had preferences that lead to differences in

magnitudes, their rank-order of thresholding by image was similar. The high variance of manually-calculated thresholds indicate that some individual operators prefer higher or lower thresholds than other operators (**Table III.1**). However, within the set of images provided to them, they generally agree on which images should have the lowest thresholds and which images should have the highest thresholds. This highlights the concern that post-thresholding manual outcomes can vary depending on the nuances and preferences of an individual.

Manual thresholding serves to gauge the automatic methods, but is not the gold standard for comparison of threshold methods: that standard should be post-threshold renders that provide the most biologically-sensible representation of biofilm. As described in Baveye's comments to the 2001 study by Yang and colleagues, manual operators, when confronted with image histograms, tend to shy away from vigorous threshold values in favor of a compromise of what is intuitively deemed to be a reasonable balance between background and foreground (Yang, Beyenal et al. 2001, Baveye 2002). This is functionally inherent in algorithms used in IS and Otsu's methods and thus, the thresholds selected by manual operators using only image histograms may or may not be biologically relevant. Thresholds calculated using BEM were more inclusive of biologically relevant signal, such as streptococcal cells and visible micro colonies. Manual operators were less conservative than IS/Otsu, but not seemingly bold enough to place thresholds as low as BEM thresholds.

The BEM is not without limitation. For example, using BEM to threshold confocal biofilm image stacks flooded with too much saturated voxels is not recommended. At its current configuration, it is not recommended to apply BEM to 12-bit images, as the calculated thresholds were too low, leaving traces of background noise. Low threshold values calculated by the BEM is a product of stretching in the dynamic range from 256 to 4096 units in the x-axis. Slope elasticity is much more sensitive in 8-bit formats. However, after scaling the 8-bit thresholds to the dynamic range of a 12-bit image, the BEM-calculated thresholds successfully optimized background removal while retaining biofilm architecture. This underscores the importance of an adjustable criterion that is flexible between image formats. Otsu and IS performances can vary drastically between image formats, and is not adjustable due to their maximization criterions.

Our study highlights the importance of thresholding in defining biofilm properties. In particular, biofilm outcome measurements can be sensitive to thresholding methods. Automatic methods eliminate issues of operator subjectivity and inter-rater reliability that are inherent to manual methods, but are not a panacea to thresholding. Investigators must consider their image histograms and image-acquisition parameters prior to selecting an automatic method. For CLSM image stacks that produce unimodal histograms with an extended tail, the BEM is a sensitive alternative to IS/Otsu's and even manual methods. By calculating lower thresholds, the biovolume elasticity method minimizes data loss and retains low-intensity architecture.

## Methods

### Biovolume Elasticity Method (BEM)

The BEM is a model-based approach to image segmentation whereby parameters to the model are optimized based on *a priori* expectation of oral biofilm shape and size (Caicedo, Cooper et al. 2017). The optimal BEM threshold is calculated by plotting the biovolume as a function of threshold. First, biovolume is calculated as the sum of all foreground pixels after a threshold is applied. Thus, the biovolume plots (right column **Figure III.5**) are directly related to the histograms (left column **Figure III.3**): biovolume is simply the sum of the histogram values above the chosen threshold. However, plotting biovolume directly rather than using the histogram allows us to tune our approach based on the outcome measures we are aiming to estimate. The higher the threshold, the more stringent the criteria for a voxel to be classified as foreground, leading to decreased biovolume estimates.

Second, we plot biovolume across all 256 data points and fit a 2-term power curve which takes on the functional form of  $bv(t) = a * T^b + c$  where:

$bv$  = biovolume

$T$  = threshold

$a, b, c$  = fitted constants

A power curve was chosen because we expected biovolume by threshold curve to possess a long tail (Baradez 2003). Additionally, it provides excellent fits in the lower threshold region where our criterion is applied.

Third, the best-fit curve is differentiated to obtain the slope at each threshold, representing the sensitivity of biovolume estimation due to a unit change in threshold. Lastly, the criterion for selecting optimal threshold in our proposed biovolume elasticity method is the first instance where a one unit increase in threshold changes the slope by less than 10%:

$$\frac{bv'(T + 1) - bv'(T)}{bv'(T)} < 0.10$$

The 10% criterion is adjustable and was chosen for this study to select the most sensitive thresholds while eliminating over 95% of false positives in a negative control.

There are three assumptions of the BEM. The first is the image histogram of 8-bit grayscale values is unimodal with an extended tail (**Figure III.3a**). Second, the mode is located at intensity value of 0. Lastly, the entire dynamic range (0-255) is utilized without saturation of 255 voxels (**Figure III.5b**). The change in slope criterion can be tuned to scale for higher bit images.

### Otsu's Method

The threshold from Otsu's method was calculated using MatLab's graythresh function. Otsu's method seeks to maximize interclass variance, or equivalently, minimize intraclass variance. The formulation is detailed in the original proposal of the method (Otsu 1979). Otsu's method has two main assumptions. The first is that the image histogram is bimodal, indicating separation of grayscale intensities of foreground object and background. The second is that there is a clear sharp valley between the two modes. As the size of the peaks become more disparate in size to each other, or if the image is corrupted by noise, the identifiable valley becomes less transparent, and Otsu's method is more prone to error.

### **Iterative Selection Method (IS)**

The threshold from the IS method was calculated using a MatLab script coded to the specifications described by Yang et al (Yang, Beyenal et al. 2001). Briefly, IS places the threshold where the difference between mean intensity values of background pixels and mean intensity values of foreground pixels is maximized. This functionally provides the most contrast between objects and background. The IS has two assumptions. The first is that the image histogram is bimodal. The second is that the image possesses objects that have average mean intensity that is distinguishable from the average mean intensity of the background (Ridler 1978).

### **Manual Thresholding**

Manual thresholding was also performed on each of the 50 acquired images. Five operators with experience rendering biofilm images with Imaris (Bitplane, Zurich, Switzerland) manually thresholded each image. The manual operators were presented the grayscale intensity histograms of each image to manually threshold and were instructed to select a threshold value where the foreground intensity signal is linearly distributed. Operators were blinded to treatment status. The five manual thresholds for each image were averaged, rounded to the nearest integer, and used for biovolume, surface area, and object detection.

### **Production of Biofilms**

Ten oral biofilms were developed overnight using 24-well microfluidic plates on the Bioflux 200C (Fluxion Biosciences, San Francisco, CA). The 24-well system is an adaptation of the 48-well Bioflux™ system that has demonstrated reproducibility in developing biofilms representative of early supragingival plaque (Nance, Dowd et al. 2013, Samarian, Jakubovics et al. 2014). The 24-well system features a secondary inlet well which enables the introduction of a treatment regimen concomitantly with media infusion. We used the media and inoculum collection protocol described by Samarian et al. (Samarian, Jakubovics et al. 2014).

To inoculate a 24-well plate, cell-free saliva media (CFS) was flowed backwards from outlet wells to inlet wells to coat the viewing port. The CFS was incubated at room

temperature for 20 minutes to allow for acquired pellicle formation. Cell-containing saliva inoculum (CCS) was then added from outlet wells to inlet wells and incubated for 1 hour at 37°C to enable cells to adhere to the acquired pellicle. After incubation, the primary inlet wells were filled with 2 mL of CCS media and the secondary inlet wells were filled with 2 mL of sterile water. An automated protocol was set up with the Bioflux™ software to supply the viewing port with media at a constant flow rate of 0.4 dyne/cm<sup>2</sup>. Five samples were grown uninterrupted for 22 hours while another five samples were treated with water at 8 and 18 hours into its 22 hour growth phase. Each treatment regimen was at 2.0 dyne/cm<sup>2</sup> for two minutes.

At the end of the 22-hour growth, the remaining CCS media from the primary inlet well were aspirated and replaced with 1 mL of 1x PBS. The biofilm was washed at 0.4 dynes/cm<sup>2</sup> for 20 minutes. After washing, the remaining PBS in the inlet wells were aspirated and the biofilm was stained with 3.34 μM Syto-9 and 20 μM propidium iodide solution at 0.4 dynes/cm<sup>2</sup> for 40 minutes. The stained biofilms were subsequently washed by flowing PBS through the system at 0.4 dynes/cm<sup>2</sup> for 20 minutes.

### **Image Acquisition**

A Leica Model TCS SPE (Leica Microsystems, Buffalo Grove, IL) inverted confocal laser scanning microscope equipped with an air immersion objective lens (NA 0.85, 40x magnification, model HCX PL APO) was used to capture biofilm stacks from the Bioflux™ viewing ports. Excitation of stain mixture was achieved with a 488nm solid state laser.

Emission capture parameters were standardized for the stain concentration used in the experiment and unchanged between plates. Specifically, these parameters included: 15% laser intensity of the 488nm laser, 900V gain, -7.6% smart offset, and 1.00x digital zoom. Each biofilm channel was imaged five times at five locations along the viewing port using the same image acquisition parameters. To provide an objective methodology of imaging a heterogeneous biofilm, five locations of the viewing port imaged were determined *a priori* and correspond to roughly the beginning of the viewing port, 1<sup>st</sup> quarter, middle, 3<sup>rd</sup> quarter, and the end of the viewing port. Gains of 726V, 900V, and 1250V were applied to one confocal stack to determine the effects of gain increases on thresholding performances. Additionally, an empty channel was stained with Syto-9/propidium iodide mixture and imaged at various depths to evaluate background noise distribution.

### **Converting Confocal Stacks to MatLab Readable Format**

Archives containing the confocal images were converted to the MatLab .mat format using the MatLab Exporter plugin in Icy (de Chaumont, Dallongeville et al. 2012). Each image is represented by a X\*Y\*Z\*T\*C cell array in uint8 format where X,Y and Z represent a voxel in three-dimensional space, T represents a time point, and C represents channel. Contained within each cell is an 8-bit unsigned integer (0-255) corresponding to signal strength from image acquisition. Under the parameters of image acquisition, the only dimension that is variable is Z, which the confocal operator sets for each image depending on biofilm thickness at the location of image acquisition. The dimensions of X, Y, T, and C were constrained to 512, 512, 1, and 2 respectively. Since the biofilms used were highly

viable and all images were endpoint acquisitions, the red channel and time dimension were disregarded, leaving a three-dimensional cellular array for each image. Automatic and manual thresholds were then applied to cell array data using Matlab 8.5.

### **Post-thresholding Calculation of Core Biofilm Architecture**

Once a threshold is determined manually or automatically with BEM/Otsu/IS, voxels with signal below or equal to the threshold are converted to background and voxels with signal above the threshold are retained as foreground. The core architectural outcomes calculated post-thresholding were biovolume, and surface area, and the number of objects detected. Object detection was done using the MatLab `bwconncomp` function using a 26-connectivity neighborhood criteria (i.e. so that two voxels count as 'connected' if they touch at any face, edge, or corner). An illustration of this type of object connectivity is shown in **Figure III.9** where two voxels with different connectivity are considered to be individual objects and the total objects detected would be three. The total number of detected objects is the sum of all objects detached from other signal via 26-connectivity rule. Biovolume is calculated as the sum of all foreground voxels at a threshold. Similarly, surface area is calculated as the sum of exposed surfaces of all foreground voxels at a given threshold. All three outcomes are sensitive to thresholds.

### **Sources of Additional Images Used for Validation**

To assess the generalizability of BEM to images from different platforms, we used several images for comparison.

1) A confocal image of an oral biofilm grown over 22 hours with no treatment was selected as the representative CLSM image (**Figure III.1, Figure III.2** taken with a Leica TCS SPE).

2) A magnetic resonance image of a human brain was provided with the MatLab software.

3) A light microscopy image of prostate cancer cells from rats, taken as a series over time, was also provided with the MatLab software.

4) Three confocal images of an oral biofilm grown over 22 hours with no treatment were taken at one location using 726V, 900V, and 1250V gains with a Leica TCS SPE (**Figure III.5**). Additional images were taken to further study the modality and distribution of image histograms from different imaging platforms (**Figure III.4**). These images include:

5) A magnetic resonance image of a mouse acquired with a 2T Varian Unity/Inova MRI small animal imaging system equipped with Acustar S-180 gradients. The image shown was obtained with a 3D gradient echo pulse sequence with a TR of 20 ms, TE of 4 ms, flip angle of 20°, and isotropic voxel size of 200 microns.

6) A light microscopy image of plant cells (Leica-prepared slide - As3211 – *Convallaria rhizome*, tissue section fast green safranin) taken with a Leica SPE equipped with a DFC 310FX camera.

7) A confocal image of plant cells (Leica-prepared slide - As3211 – *Convallaria rhizome*, tissue section fast green safranin) taken with a Leica TCS SPE.

8) A confocal image of fluorescently-labeled *Rothia mucilagenosa* biofilm stained with DAPI (blue), AMCA (red), and labeled with anti-*Rothia* polyclonal antibody (green) taken with a Nikon A1R confocal microscope.

### **Comparison of 12-bit vs 8-bit Fluorescence**

To compare thresholding performance between 12-bit and 8-bit images, we furthered analyzed the fluorescence image of *Rothia mucilagenosa* biofilm stained with DAPI, AMCA, and labeled with anti-*Rothia* antibody (**Figure III.7**). This image was taken natively in 12-bit and converted to 8-bit using Icy bioimage analysis software. BEM, Otsu, and IS thresholds were calculated and applied to each 12-bit and 8-bit formats (**Figure III.8**).

### **Comparing Manual & Automatic Thresholds**

To compare magnitude differences between thresholding methods, a student's paired t-test was used to evaluate whether mean threshold difference of one method versus another method was zero. This analysis was performed for each pairwise set of thresholding methods and was stratified by treatment and control images.

### **Comparing Biofilm Architectural Outcomes by Thresholds**

Means of architectural outcomes post-thresholding between biofilms intermittently treated with water over 22 hours and biofilms grown over 22 hours were compared with Student's 1-tailed t-tests. The treatment and control groups had sufficient sample size with 25 images each. We hypothesized that biofilms treated intermittently with water will have lower biovolume, surface area and total number of objects detected. Since biofilm architecture is intrinsically heterogeneous and as a consequence of our pre-established positioning for biofilm imaging, we expected the treatment and control measurements to come from distributions with unequal variances. Thus a more conservative heteroscedastic assumption was made and applied to the t-tests. A two-tailed t-test was used to compare average thresholds between treatment and control groups since we believed there to be no differences in thresholds between the groups. Significance threshold was set at  $\alpha=.05$ .

**Table III.1. Biofilm Outcomes by Thresholding Method and by Treatment.** Otsu and IS thresholds are significantly higher than BEM and manual thresholds and with higher standard deviation. BEM thresholds have the lowest standard deviation. Measured biovolume, surface area, and objects detected is highest for BEM, followed by manual, Otsu, and IS. Significance in the number of objects detected between treatment and control is detected with BEM and manual thresholds and not detected with Otsu/IS thresholds. Treatment reduces biovolume and surface area in all four methods. Outcomes can vary by up to five-fold depending on threshold as in the case of objects detected in control images. Effect size between control and treatment groups is calculated with Cohen's D, which quantifies the standardized difference of two means.

<b>Outcomes by Method</b>	<b>Control Average (Standard Deviation)</b>	<b>Treatment Average (Standard Deviation)</b>	<b>Effect Size (p-value)<sup>a</sup></b>
BEM Threshold	11.360(1.411)	11.96(1.060)	0.234(.096)
Otsu's Method Threshold	64.520(13.257)	65.280(10.550)	0.032(.824)
IS Threshold	66.400(13.200)	67.280(10.450)	0.037(.795)
Manual Threshold <sup>b</sup>	28.688(6.279)	30.016(4.531)	0.120(.396)
BEM Biovolume	2,741,745(1,578,495)	1,783,828(637,768)	0.370( <b>.004</b> )
Otsu Biovolume	1,035,338(606,875)	618,107(261,824)	0.408( <b>.002</b> )
IS Biovolume	1,009,385(594,804)	601,211(260,313)	0.406( <b>.002</b> )
Manual <sup>b</sup> Biovolume	1,797,055(1,051,159)	1,089,955(392,289)	0.407( <b>.004</b> )
BEM Surface Area	2,512,276(1,132,122)	2,055,876(551,373)	0.248( <b>.039</b> )
Otsu Surface Area	1,272,407(621,281)	884,563(216,642)	0.385( <b>.003</b> )
IS Surface Area	1,256,817(619,135)	868,678(215,324)	0.386( <b>.003</b> )
Manual Surface Area	1,669,107(761,516)	1,283,350(310,629)	0.315( <b>.025</b> )
BEM Objects	19,435(10,451)	14,552(4,442)	0.291( <b>.020</b> )
Otsu Objects	3,780(1,939)	3,614(1,586)	0.047(.371)
IS Objects	3,818(1,951)	3,687(1,594)	0.037(.398)
Manual Objects	4,486(2,261)	3,406(815)	0.303( <b>.032</b> )

<sup>a</sup> Test performed was a 2-tailed student's t-test for thresholds and 1-tailed student's t-test for biofilm architectural outcomes.

<sup>b</sup> Manual threshold used for an image is the average value from five different operators for that image, rounded to the nearest whole number.

**Table III.2. Paired T-tests Between Thresholding Methods Stratified by Treatment.**

The null hypothesis states that the mean difference between sets of thresholds obtained from one method vs another method is zero. Since all 12 null hypotheses were rejected, we conclude that each thresholding method was different from one another and is unaffected by treatment status of the images operated on. Although mean thresholds for Otsu and IS were roughly 2 intensity values apart, IS thresholds were consistently 2 units higher than Otsu thresholds applied to the same image, minimizing standard deviation and producing significant effects.

Pairwise Thresholding Method Comparison	Control Images (n=25)			Treatment Images (n=25)		
	Mean Threshold	Group 1 - Group 2 (95% confidence interval)	p-value	Mean Threshold	Group 1 - Group 2 (95% confidence interval)	p-value
Manual avg <sup>1</sup> . vs BEM	28.69/11.36	17.33(14.47,20.19)	<0.01	30.02/11.96	18.06(16.09,20.02)	<0.01
Manual avg. vs Otsu	28.69/64.52	-35.82(-39.44,-32.22)	<0.01	30.02/65.28	-35.26(-38.48,-32.04)	<0.01
Manual avg. vs IS	28.69/66.40	-37.71(-41.30,-34.13)	<0.01	30.02/67.28	-38.26(-40.45,-34.08)	<0.01
BEM vs Otsu	11.36/64.52	-53.16(-59.01,-47.31)	<0.01	11.96/65.28	-53.32(-57.89,-48.75)	<0.01
BEM vs IS	11.36/66.40	-55.04(-60.87,-49.21)	<0.01	11.96/67.28	-55.32(-59.85,-50.79)	<0.01
Otsu vs IS	64.52/66.40	-1.88(-2.02,-1.74)	<0.01	65.28/67.28	-2.00(-2.12,-1.88)	<0.01

<sup>1</sup>For an image's individual manual threshold value, the five values given by our five operators were averaged.

**Table III.3. False Positive Noise Distribution of Negative Controls.** Five images of varying depths were taken of a sterile channel containing LIVE/DEAD™ stain. The theoretical percentage of all voxels belonging to intensity value 0 for all five images is 100.00. Over 95% of voxels are correctly labeled as intensity value 0. Less than 5% of remaining voxels are false positives that are incorrectly labeled as biovolume. The vast majority (>95%) of false positives can be eliminated by setting a threshold of 10.

		Images of Stained Channel By Depth				
		20 slices	40 slices	53 slices	60 slices	80 slices
Intensity Value (0-255)	0	96.05	97.36	97.11	96.32	96.68
	1	1.55	1.05	1.10	1.45	1.32
	2	0.95	0.64	0.70	0.80	0.80
	3	0.58	0.38	0.42	0.54	0.48
	4	0.35	0.23	0.25	0.32	0.29
	5	0.21	0.13	0.15	0.19	0.17
	6	0.12	0.07	0.08	0.11	0.10
	7	0.07	0.05	0.05	0.06	0.05
	8	0.04	0.03	0.03	0.03	0.03
	9	0.02	0.01	0.01	0.02	0.02
	10	0.01	<0.01	<0.01	<0.01	<0.01

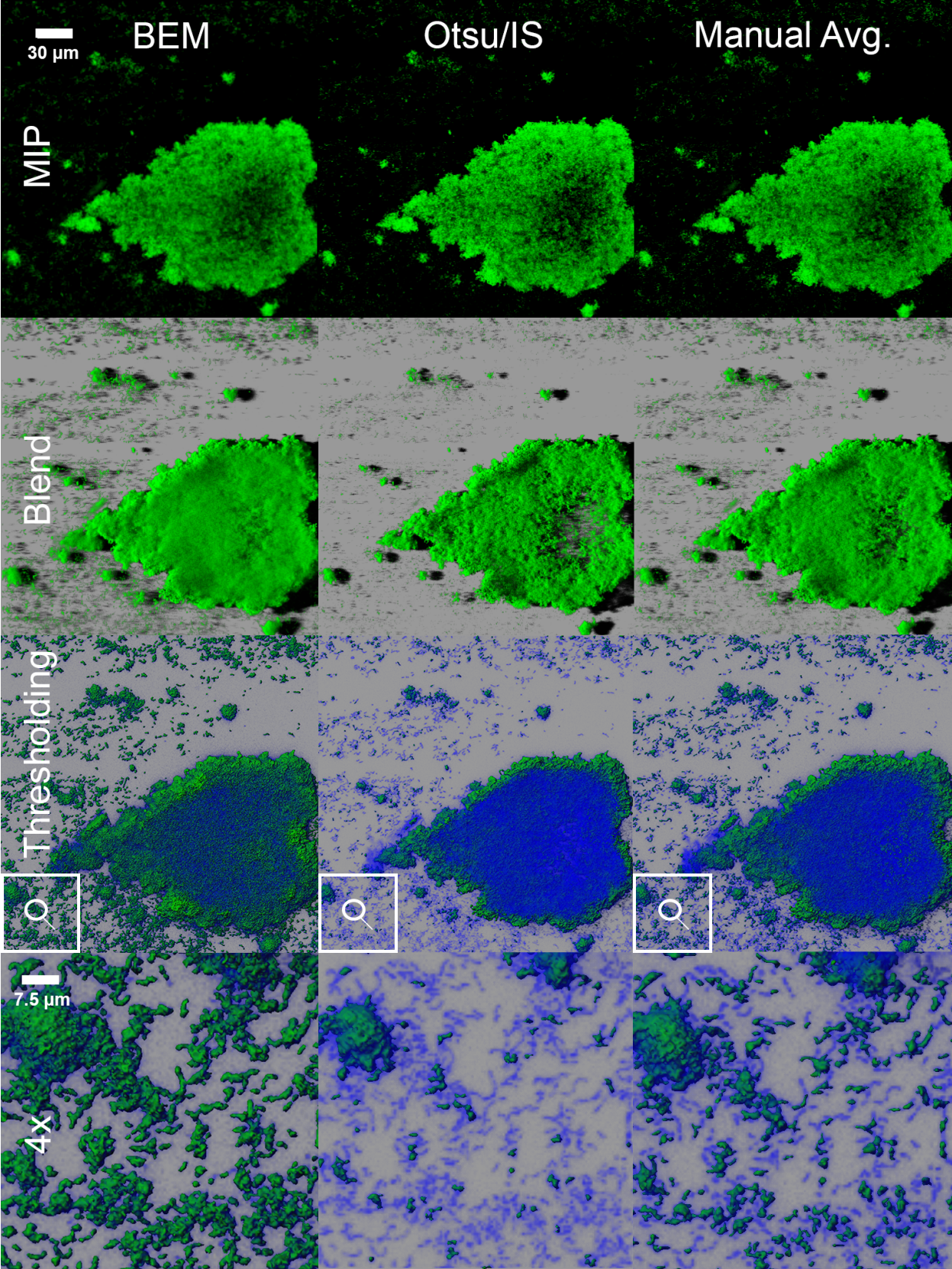


**Figure III.1. Visual Comparison of Different Methods to Threshold Biofilm Images.**

The maximum intensity projection, blend of all intensity values, and segmentation are shown from a top-down viewing angle. The first, second, and third columns are the projection of the same confocal laser scanning microscopy image stack that is rendered after applying threshold selected by the BEM, Otsu/IS, and manual operators' average, respectively. The MIP and blend projections show Otsu and IS methods threshold out the most biovolume, followed by manual and BEM methods. The segmentation projection shows biovolume that is above threshold in green, and biovolume that is thresholded out as blue. The fourth row is a magnification from the lower left corner of the thresholded image stacks and shows that Otsu and IS methods are too conservative in their thresholds. Low-intensity Streptococcus chains are thresholded out, leading to underestimates of actual biovolume. Manual threshold average is comparable to BEM threshold in all three projection modes.

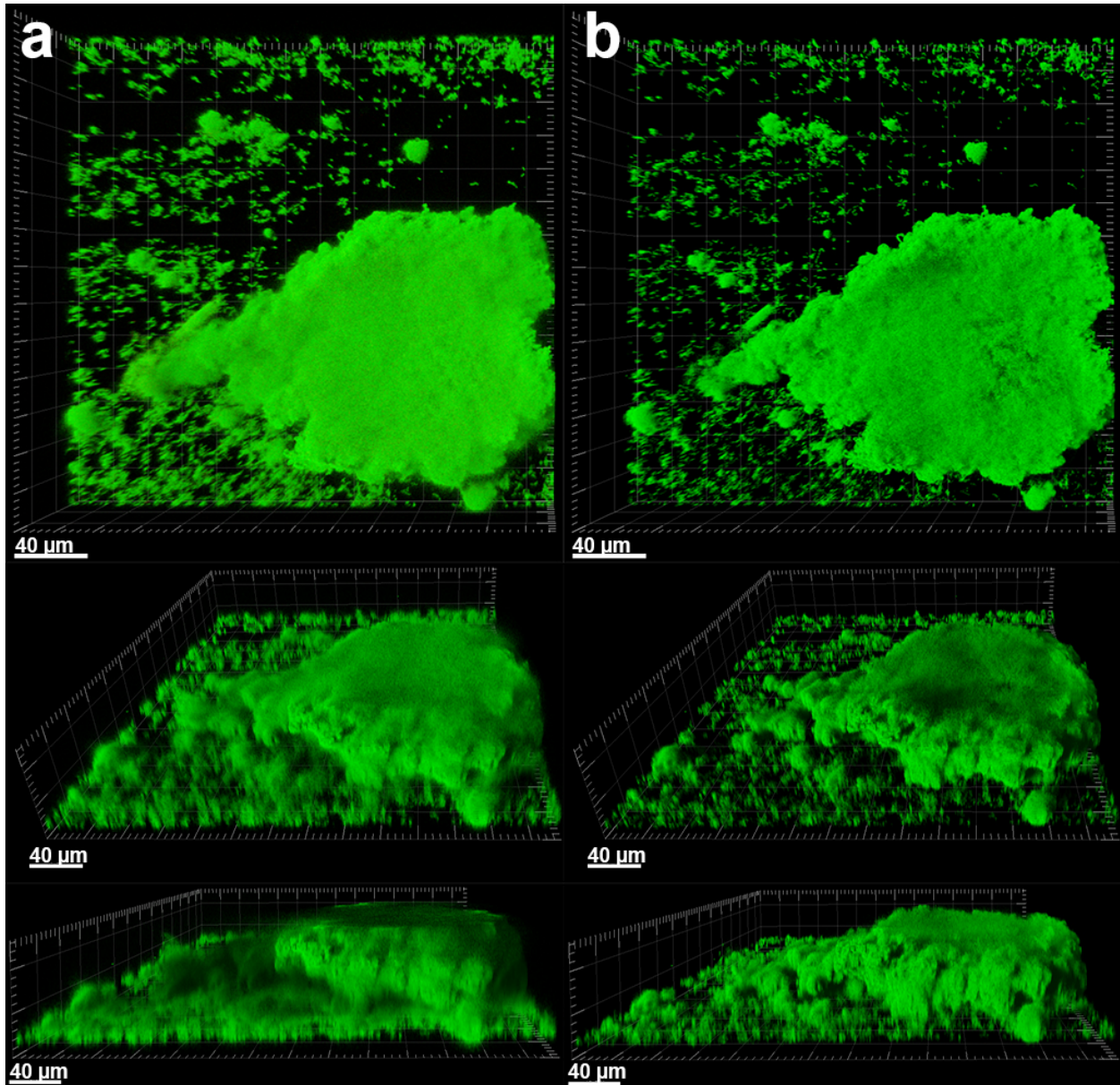


**Figure III.2. Thresholding Necessary to Remove Background Noise.** The figure shows a sample CLSM image stack of a biofilm grown over 22 hours in the Bioflux™ system with a top-down, angled, and side perspective views. **A)** Image that is not thresholded is visually compared to **B)** image that is thresholded with the biovolume elasticity method. Images that had been thresholded display higher visual acuity of biofilm structure. Background noise that decreases image sharpness is evident in images that have not been thresholded.

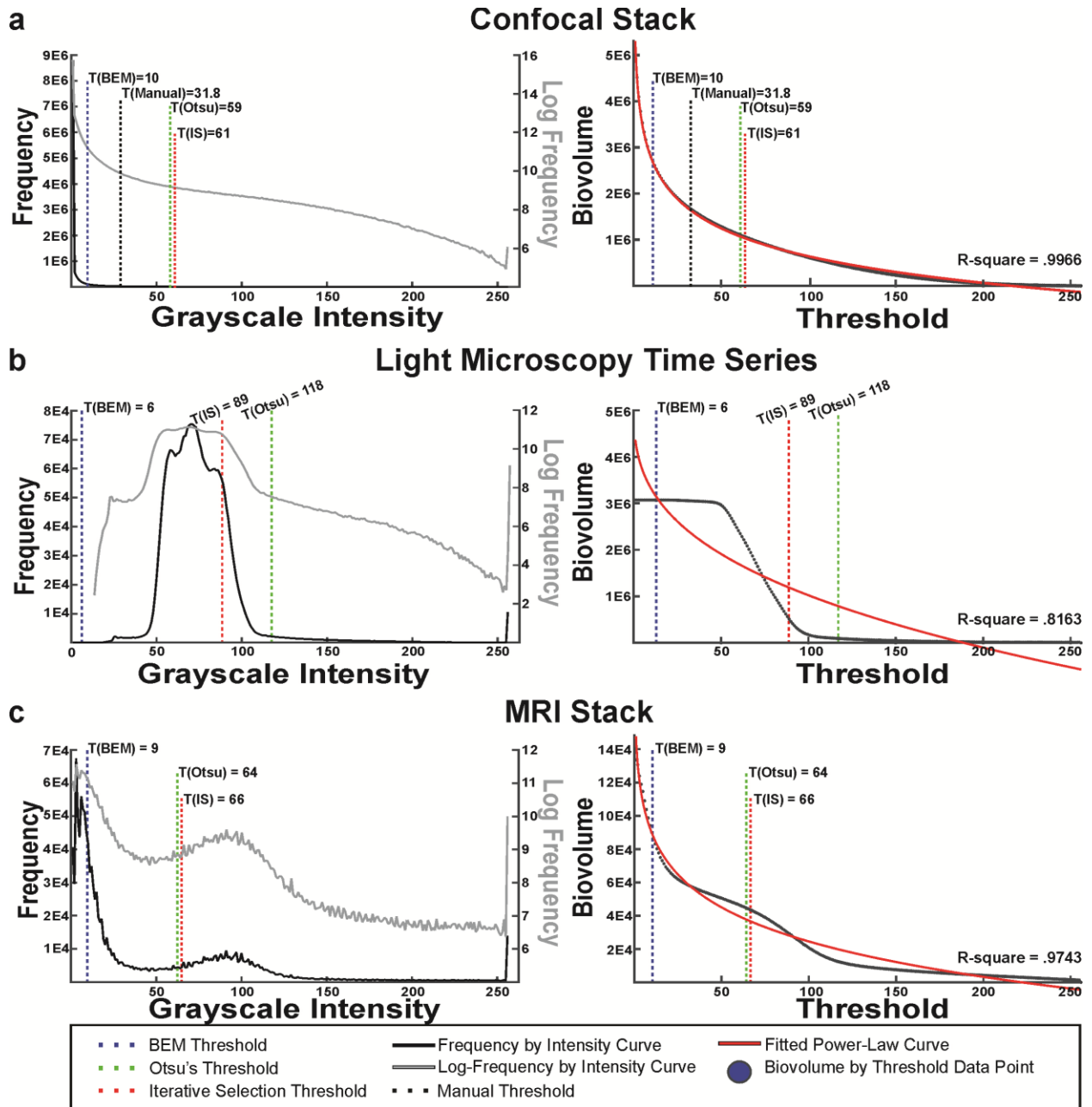


**Figure III.3. Image Intensity Histograms Vary By Imaging Platform.** The left column shows 8-bit grayscale intensity histograms of images taken from different platforms. The right column shows the biovolume as a function of threshold and a fitted 2-term power curve with the functional form  $bv(t) = a * T^b + c$ . The Biofilm Elasticity Model (BEM) threshold is determined by first instance of a <10% change in slope of fitted power curve as threshold increases by 1. **A)** A sample CLSM image stack of a biofilm grown over 22 hours. The grayscale histogram shows a unimodal distribution with a heavy skew to the right. The BEM and manual thresholds are less conservative than Otsu and IS. The fitted power law curve had a near perfect correlation coefficient with the biovolume by threshold data points. **B)** A light microscope image of cells shows a more classical unimodal histogram. The BEM is the least conservative. Otsu's and IS methods set higher

thresholds with Otsu setting the highest. The correlation coefficient between the fitted power curve and data is the lowest amongst the three imaging platforms. **C)** A sample MRI stack of the human brain shows bimodality in the grayscale histogram. The BEM sets the most conservative threshold whereas Otsu and IS thresholds are higher and comparable. The correlation coefficient between the fitted curve and data is high.

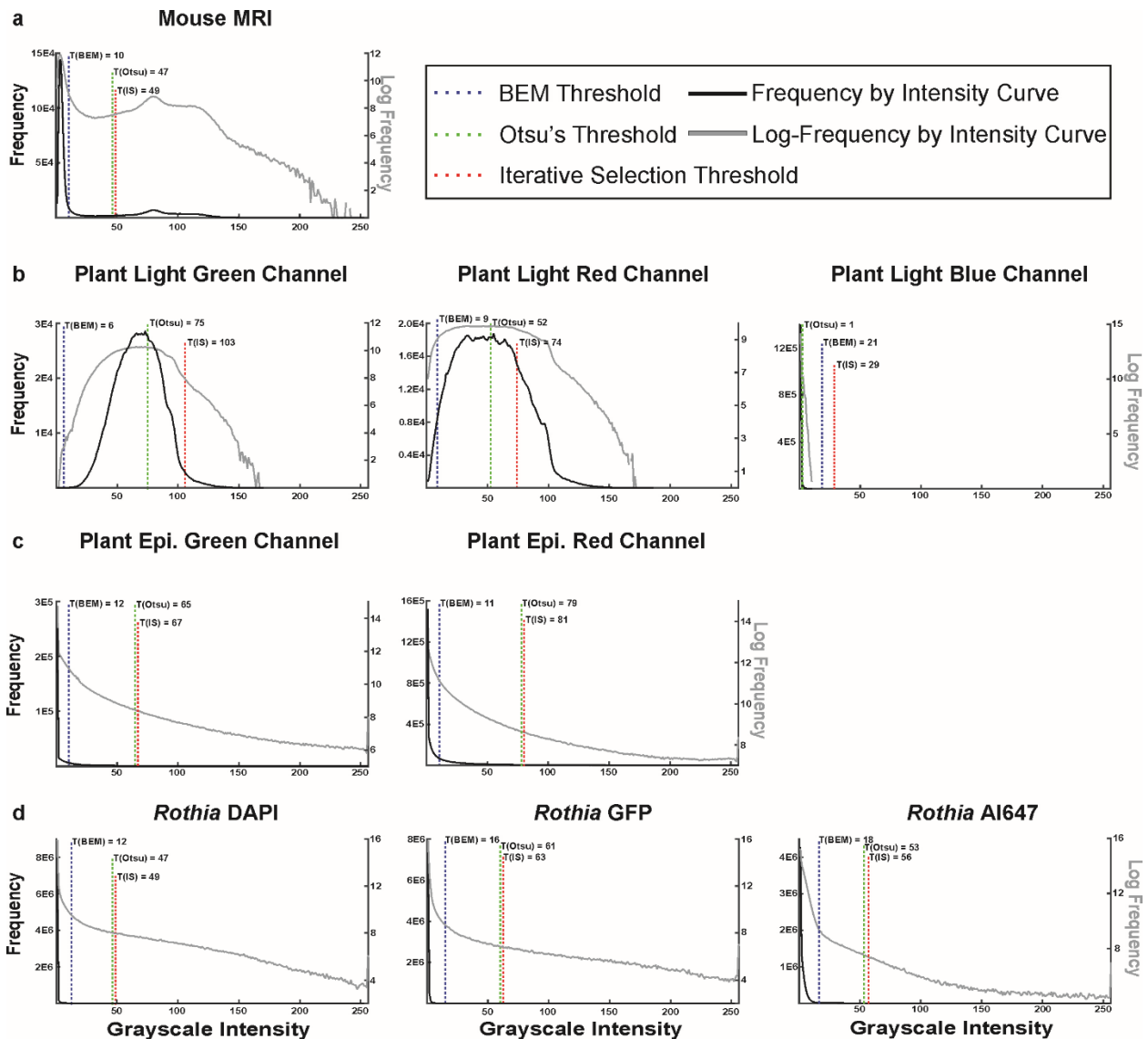


**Figure III.4. MRI, Light Microscopy, and Fluorescence Microscopy Image Histograms.** **A)** The mouse MRI image histogram was a hybrid between bimodal and unimodal. There were two visible peaks, but of unequal sizes. **B)** Light microscopy of plant cells was deconstructed into RGB channels. Image histograms of the red and green channel were unimodal with a normal distribution. Image histogram of the blue channel revealed negligible amount of signal. **C)** The same plant cells were visualized under confocal microscopy. The image histograms of the red and green channel revealed unimodality with peak at 0 and an extended tail. **D)** *Rothia mucilagenosa* biofilm under three different fluorescence tags showed image histograms resembling that of **C)**. In all platforms, BEM threshold was the least aggressive out of the three automatic methods. Otsu and IS thresholds were very similar for MRI, and fluorescence-based microscopy, but were differentiated in light microscopy.

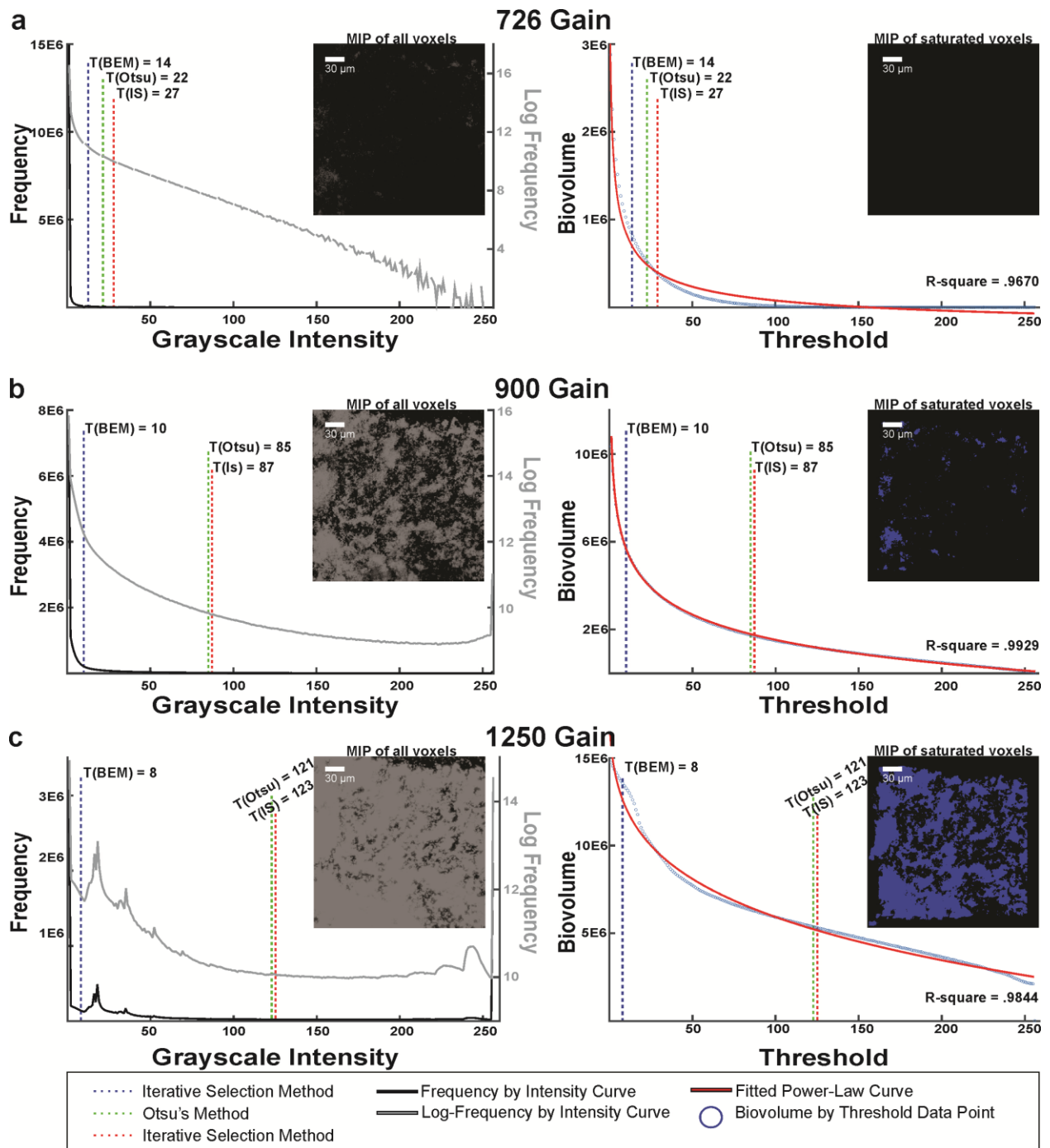


**Figure III.5. Image Intensity Histograms Vary by Confocal Operator.** Three biological replicates were imaged with identical image acquisition parameters except for gain. The first column shows grayscale histograms as well as the maximum intensity projection of the biofilm image. The second column shows biovolume as a function of threshold, the fitted power law curve, and the maximum intensity projection of saturated voxels. **A)** Scenario where signal sensitivity is too low, yielding no saturated voxels. In this scenario, the BEM, Otsu, and IS are comparable in threshold detection. **B)** Scenario where signal sensitivity is optimized by a confocal operator for the stain mixture, producing saturated

voxels. BEM selects for a lower threshold compared to Otsu and IS methods. **C)** Scenario where signal sensitivity is too high. BEM threshold selection is no longer applicable whereas Otsu and IS methods show robustness to operator error or inexperience. Correlation coefficients are high in all three scenarios, with the highest belonging to the image optimized by an operator.

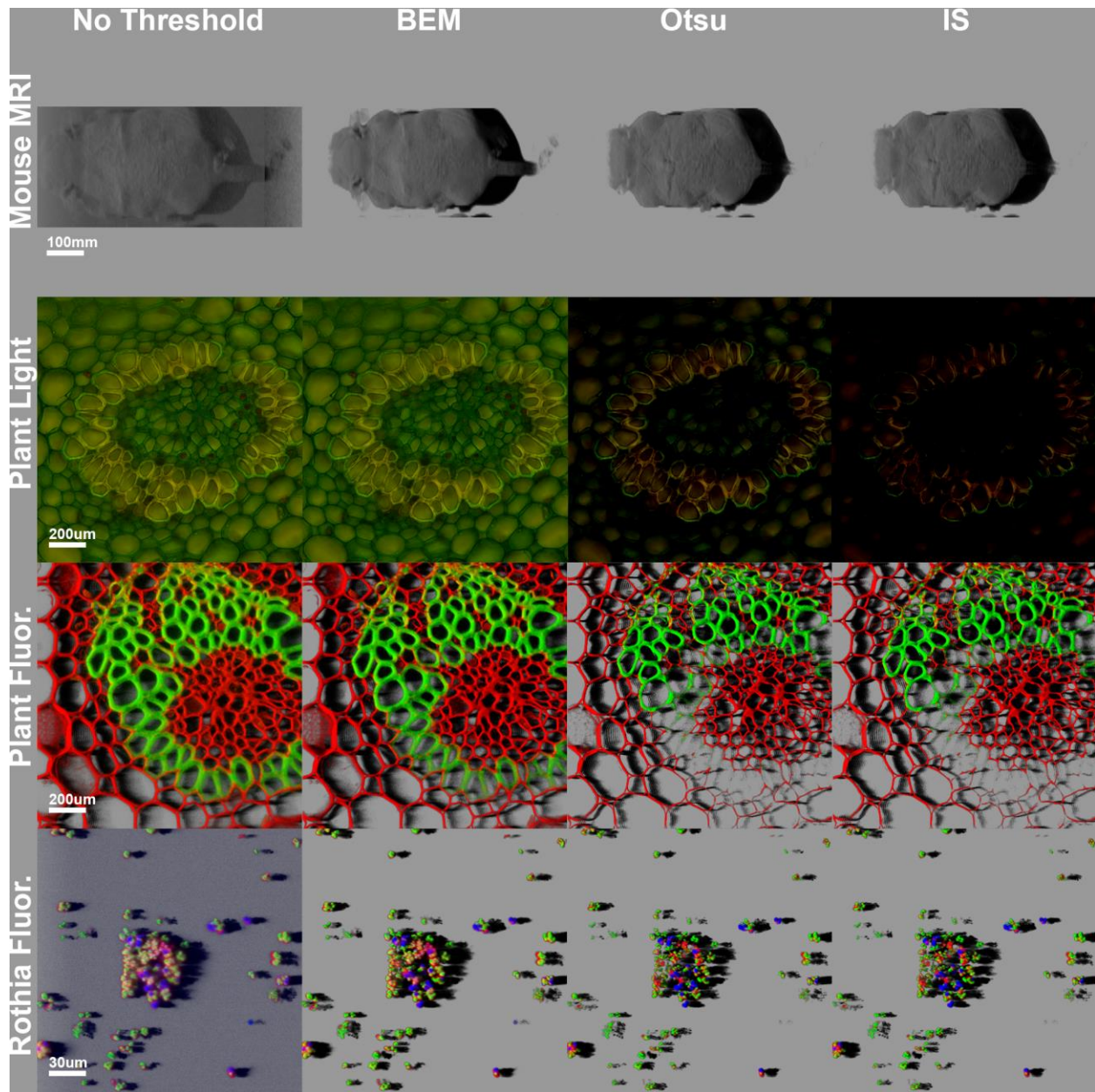


**Figure III.6. Thresholding Methods on Images from Different Platforms.** Thresholding was visibly necessary for three of the four images. Background noise contributing to image fuzziness was evident in mouse MRI, plant confocal, and *Rothia mucilagenosa* biofilm fluorescence. Difference between no threshold and BEM threshold of plant light micrograph was minimal. BEM maintained the most structural integrity of mouse MRI (cartilage of ears and tail), plant confocal, and *Rothia mucilagenosa* biofilm. Otsu and IS were too aggressive and removed biologically meaningful signal in all four images.

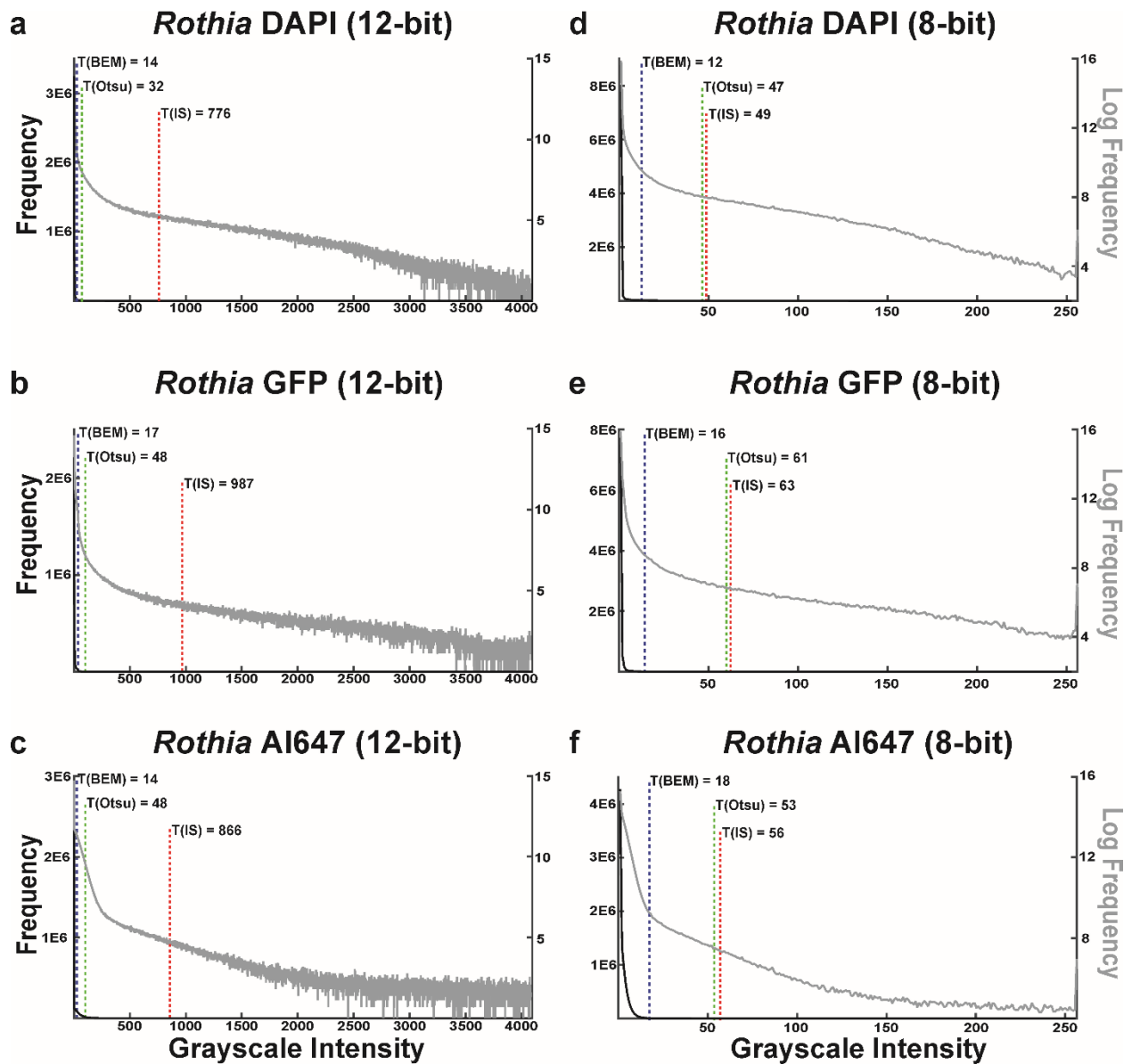
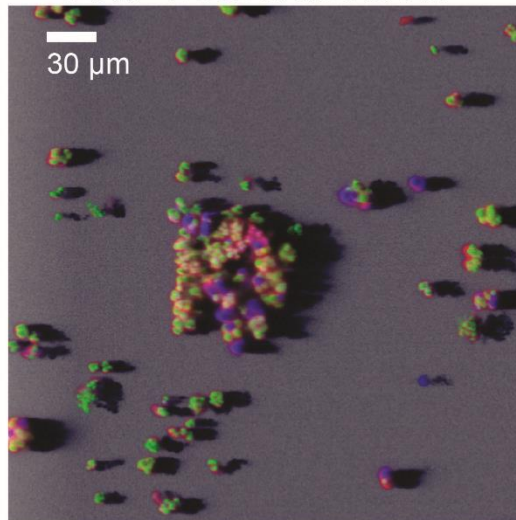


**Figure III.7. Image Intensity Histograms of 8-bit & 12-bit Images.** Dynamic range (X-axis) was larger for 12-bit images compared to 8-bit images. As a distribution, the image histograms were similar between formats: a unimodal histogram with peak at 0 and an extended tail. BEM thresholds were relatively unchanged between formats. Otsu thresholds were mildly higher and IS thresholds were distinctly lower in 8-bit format compared to 12-bit format.

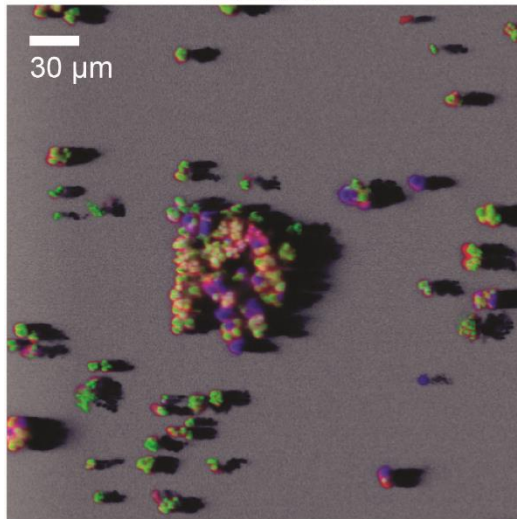
# Thresholds

	<u>DAPI</u>	<u>GFP</u>	<u>AI647</u>
<u>No Threshold</u>	0	0	0
<u>BEM</u>	14	17	14
<u>BEM Scaled</u>	96	128	144
<u>Otsu</u>	32	48	48
<u>IS</u>	776	987	866

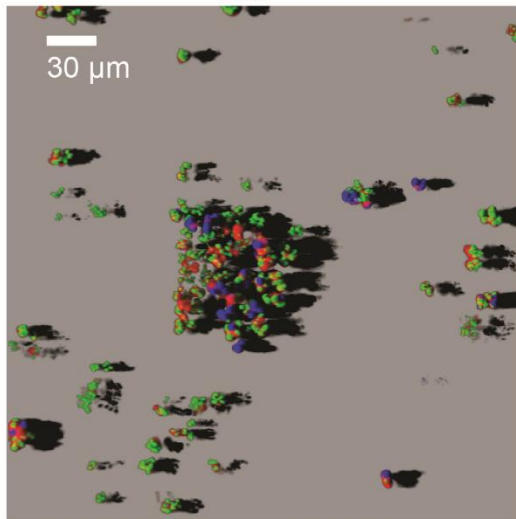
# No Threshold



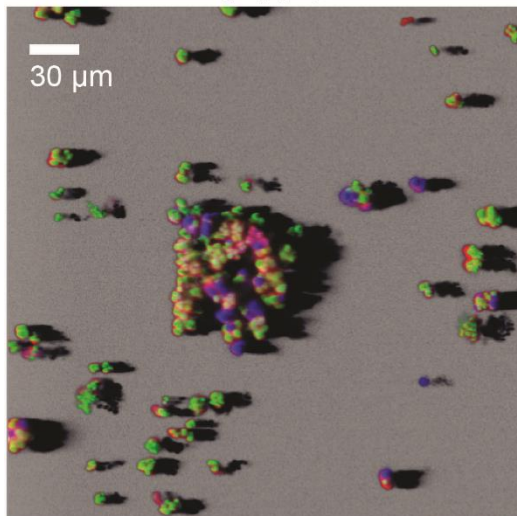
# BEM



# IS



# Otsu



# BEM Scaled

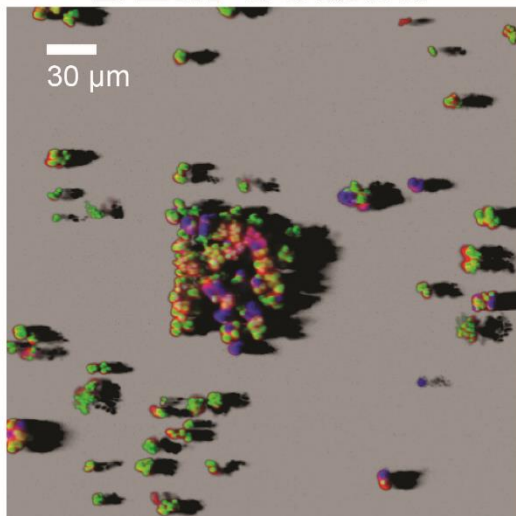


**Figure III.8. BEM Thresholding Scaled to 12-bit Images.** BEM and Otsu left traces of background noise whereas IS did not. IS was too conservative, compromising the architectural integrity of *Rothia mucilagenosa* biofilm. BEM threshold from 8-bit scaled to 12-bit was the best. It eliminated all visible background false positives and retained architecture of *Rothia mucilagenosa* biofilm.

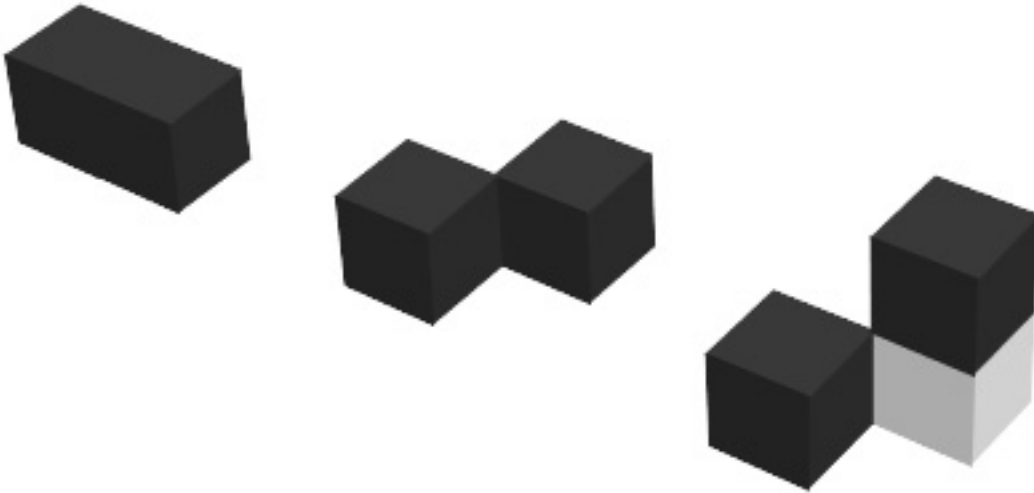


**Figure III.9. 26-neighborhood Connectivity Determination of Regions of Interest.** All three objects below are considered separate Regions of Interest (ROIs) with a biovolume occupying 2 voxels. The object on the left has two voxels on the same plane connected by a plane at an interface. The middle object has two voxels on the same plane connected by a line. The object on the right has two voxels on different planes connected by a point.

## Chapter IV

### Introducing BAIT (Biofilm Architecture Inference Tool): A Software Program to Evaluate the Architecture of Oral Multi-Species Biofilms

#### Abstract

*In vitro* model systems are used to study biofilm growth and predict the effects of anti-biofilm interventions within the human oral cavity. Many *in vitro* biofilm model systems use confocal laser scanning microscopy (CLSM) in conjunction with image analysis tools to study biofilms. The aim of this study was to evaluate the usefulness of a new image analysis software developed in-house that we call BAIT (Biofilm Architecture Inference Tool) to quantify the architecture of oral multi-species biofilms after anti-biofilm interventions using an automated 24-channel Bioflux™. Differences in biofilm architecture were compared between untreated biofilms and those treated with water (negative control), sodium gluconate (“placebo”), or stannous fluoride (SnF<sub>2</sub>). The 24-well Bioflux™ microfluidic system, which has two inlets, was inoculated with pooled human saliva and biofilms developed over 22h in filter sterilized 25% pooled human saliva. During this period, biofilms were treated with water, sodium gluconate, or stannous SnF<sub>2</sub> (1,000, 3,439, and 10,000 PPM Sn<sup>2+</sup>) after 8h and 18h post-inoculation. After 22h of growth,

biofilms were stained with LIVE/DEAD™, imaged with CLSM, and analyzed with BAIT. Biofilm biovolume, total number of objects, surface area, fluffiness, connectivity, convex hull porosity, and viability were calculated with BAIT. Image analysis showed oral biofilm architecture was significantly altered by 3,439 and 10,000 PPM stannous treatment regimens, resulting in decreased biovolume, surface area, number of objects, connectivity, and viability, while fluffiness increased ( $p < 0.01$ ). In conclusion, BAIT was shown to be able to rapidly measure the changes in biofilm architecture and evaluate possible antimicrobial and anti-biofilm effects of candidate agents.

## **Introduction**

Biofilms are cellular assemblages of multiple species of microorganisms that are arranged in complex three-dimensional architectures (Stoodley, Sauer et al. 2002). The contained biofilm bacteria are physiologically different from their planktonic counterparts (Mah and O'Toole 2001) and this is evidenced by their intrinsic tolerance to antimicrobials (Foley and Gilbert 1996). Biofilms are estimated to be responsible for up to 80% of all human infections and contribute to the etiology of periodontal disease and caries (Marsh, Moter et al. 2011, Romling and Balsalobre 2012, Akers, Mende et al. 2014). Dental caries and periodontal disease cause the vast majority of human oral diseases (Petersen, Bourgeois et al. 2005). In 2010, in a ranking of the global burden of 291 diseases, untreated caries ranked first and periodontal disease ranked sixth (Marcenes, Kassebaum et al. 2013).

For many dental plaque studies, *in vitro* model systems are used to capture snapshots of biofilms during and/or after development and/or following anti-biofilm interventions (such as treatment with an antimicrobial) under defined conditions (Salli and Ouwehand 2015). In this study, we used a 24-well Bioflux™ system to develop oral biofilms under flowing salivary conditions. The biofilm devices were seeded with a salivary inoculum and sterile saliva was used as the growth medium. A similar 48-well Bioflux™ system has been previously described to develop dental biofilms that are compositionally similar to early supragingival plaque (Nance, Dowd et al. 2013, Samarian, Jakubovics et al. 2014). An advantage to the 24-well system is its dual inlet feature, enabling delivery of potential treatment compounds while media flows uninterrupted. This two-inlet feature facilitates the study of both biofilm development and biofilm regrowth following a candidate anti-biofilm treatment.

Biofilm architecture is an umbrella-term used to describe the two and three-dimensional properties of biofilms and is based on cellular arrangements and features, including thickness, porosity, irregularity and fragmentation (Bridier, Dubois-Brissonnet et al. 2010, Zijngé, van Leeuwen et al. 2010, Hu 2013). Digitization of microscope images have enabled software assisted quantification techniques for 2-dimensional images, such as measuring biofilm accumulation (Larimer, Winder et al. 2016) or using gray level correlation to estimate structural heterogeneity of biofilms (Milferstedt, Pons et al. 2009). With the advent of confocal laser scanning microscopy (CLSM), 3-dimensional outcomes can also be measured (Bridier, Meylheuc et al. 2013, Shukla and Rao 2013). Some outcomes, such as biovolume are relatively straightforward to define; others such as

porosity are not. While there are many image analysis packages available, including COMSTAT (Heydorn, Nielsen et al. 2000), Phlip (Mueller, de Brouwer et al. 2006), Icy (de Chaumont, Dallongeville et al. 2012), and ImageJ (de Carvalho and da Fonseca 2007) that provide approaches to measure biofilm architecture, measurement is still not a trivial task. For example, the measurement of biofilm architecture relies on a suitable thresholding approach to maximize foreground (biofilm) signal from background noise (Yerly, Hu et al. 2007, Rojas, Rueda et al. 2011). Indeed, we recently developed an image thresholding approach that maximizes signal to noise ratio so that biofilm biomass is readily discerned, and this is included in the software package that we developed in this study. We also coded in-house algorithms for measuring biofilm biovolume, total number of objects, surface area, fluffiness, connectivity, convex hull, and unweighted viability. Outcomes such as fluffiness, convex hull, and viability are seldom included in currently available packages. Together, the scripts were coded into a workflow and compiled into the software package we have called BAIT (Biofilm Architecture Inference Tool) that enables users to quickly quantify measures that describe biofilm architecture.

The primary aim of this study was to evaluate the performance of a new analysis software called BAIT. Proof of concept for BAIT was achieved by inputting three tiers of datasets into the software. The first dataset included a synthetic image stack manually generated. This small mock dataset contained measurements that can be hand-calculated. Outcome measurements calculated by BAIT can then be compared to expected values. The second dataset included large image stacks of oral biofilms. These biofilm images are visibly distinct from one another and its expected quantification by

BAIT can be predicted visually. This is to test the rigor of the algorithms to large datasets where outcomes can't be calculated manually, but can be visually differentiated. Finally, to test the feasibility of the software for *in vitro* oral biofilm studies, an experiment was devised to test the antibiofilm properties of a candidate compound. Hundreds of oral biofilm images were generated to test the stability of BAIT when inputted with a large volumes of data.

The candidate compound chosen for the experimental validation of BAIT is stannous fluoride ( $\text{SnF}_2$ ) (Tinanoff, Hock et al. 1980, Camosci and Tinanoff 1984). Stannous fluoride is commonly used in oral healthcare products and it is known for its anti-cariogenic and antimicrobial effects.  $\text{SnF}_2$  is also an attractive compound to study because few investigations have examined its effects on dental biofilm development. One study estimated biofilm biomass before and after treatment with  $\text{SnF}_2$  using a crystal violet based staining and quantification technique and found that stannous fluoride did not reduce biofilm adherence in an *in vitro* model (Reilly, Rasmussen et al. 2014). Another study showed that stannous fluoride dentifrice was effective at reducing biomass, viability and composition of a three-species oral biofilm (Cheng, Liu et al. 2017). Unfortunately, anti-biofilm studies of  $\text{SnF}_2$  and other anti-biofilm agents seldom focus on the complex architecture of oral biofilms. Understanding changes in oral biofilm architecture could have profound impact in developing more efficacious agents. For instance, altering dental plaque biofilm architecture through antimicrobial or anti-biofilm treatments could result in changes to biofilm regrowth (Bakke 1986) and/or biofilm instability leading to sloughing and cell detachment (Flemming and Wingender 2010).

## Methods

### Development of BAIT

MatLab 8.5 was used to code all scripts used in the BAIT package. Individual scripts for biovolume, surface area, number of objects, fluffiness, connectivity, convex hull porosity, and viability were coded. The measurement descriptors are defined in **Table IV.1**. The software graphical user interface integrating all scripts was compiled with MatLab runtime environment (**Figure IV.1**). MatLab cellular array .mat files are compatible for use with the BAIT software. For standardization and convenience with MatLab, the .mat cellular array data format was chosen as the compatible input file type for BAIT. As of this current version of BAIT, only the .mat file format is compatible. Confocal .lif archives were converted to .mat files using the MatLab Exporter plugin in the software package ICY (de Chaumont, Dallongeville et al. 2012). To be noted, the final dimensions of each .mat file compatible with the current version of BAIT is (X,Y,Z, T, C) where X,Y and Z denote Cartesian coordinates, T is fixed at 1, and C denotes channels. Channel 1 is the propidium iodide channel and Channel 2 is the Syto-9 channel. Confocal stacks in 8-bit, 12-bit, and 16-bit formats are compatible for import into BAIT. Here, confocal images in 8-bit format were studied as these types of images are more amenable to our previously described thresholding technique (Luo 2018). In this study, all steps

were performed on a Sager NP9377-S laptop equipped with two Nvidia GeForce™ GTX 970m graphics cards in SLI.

### **Validation of Outcomes Calculated by BAIT**

To verify results calculated by BAIT, a mock cellular array dataset was created and imported into BAIT. Specifically, a visual schematic of two objects was created with an online voxel builder app (<http://voxelbuilder.com>). The mock dataset contains a voxel-space small enough to calculate outcomes by hand (**Figure IV.2**). Next, the visual schematic was deconstructed into binary data and manually inputted as a MatLab cellular array data compatible with BAIT. The hand-calculated results were compared to BAIT results.

In addition to the manually constructed mock-data set, three confocal oral biofilm images illustrating a visually conspicuous gradient of biovolume were chosen to validate the MatLab workflow to real data with voxel-space occupying millions of voxels. The images were classified as voluminous, moderate, and sparse, based on the amount of biofilm biovolume that was visually evident.

### **BAIT as a Tool to Measure Architecture Changes after Treatment**

A total of 615 confocal images with representatives from each treatment group (**Table IV.2**) were converted to .mat files and imported into BAIT. Prior to quantification,

the biovolume elasticity method was applied to distinguish background interstitial space from foreground biomass (i.e. thresholding). Other thresholding methods available in BAIT include Otsu's method and iterative selection. A comparison of thresholding techniques for fluorescence microscopy was compared in a previous work (Luo 2018). BAIT's 'Analyze All' functionality was used to calculate all six biofilm architecture outcomes for each group of image stacks described in **Table IV.2**. The BAIT output of results were exported as a .csv and analyzed in Microsoft Excel (Microsoft, Redmond WA).

### **Treatment Formulations & Study Design**

Biofilms developed in a Bioflux™ system were treated with either SnF<sub>2</sub> at different concentrations, sodium gluconate at different concentrations ("placebo" control), or deionized water (negative control) at 8h and 18h of growth or received no treatment (**Table IV.2**). Because sodium gluconate is required to maintain stannous fluoride in solution, "placebo" treatments containing sodium gluconate but lacking SnF<sub>2</sub> were used. Four comparison groups were used to evaluate the effects of a treatment with water or a treatment with different concentrations of stannous fluoride. Specifically, the 22h untreated group was matched to water-treated group; placebo 1,000 was matched with stannous 1,000; placebo 3,439 was matched with stannous 3,439, and placebo 10,000 was matched with stannous 10,000. The placebo treatment groups only contained the needed amount of sodium gluconate to keep 1,000, 3,439, or 10,000 PPM stannous

stable in solution. Sodium gluconate and/or stannous fluoride solutions were adjusted to pH 5.8.

### **Media & Inoculum Collection**

Saliva batches were collected from at least five non-smoking healthy individuals that had not eaten or drank for the last two hours (except water) and had not taken antibiotics the last three months. Individual saliva samples were pooled together. Cell-containing saliva (CCS, the inoculum) and cell-free saliva (CFS, growth media) were prepared according to previously established protocol (Samaritan, Jakubovics et al. 2014).

### **Overnight Growth of Oral Biofilms**

One mL of CFS was added to the outlet wells of 24-well Bioflux™ plates and flushed through the viewing port at 1.0 dyne/cm<sup>2</sup> for one minute (**Figure IV.3**). The plate was then incubated for 20 minutes at room temperature to develop an acquired salivary pellicle. The remaining CFS in the outlet wells were then aspirated and replaced with 100 uL of CCS. CFS media for the run and applicable treatment formulations were then added to inlet one and inlet two of the biofilm system, respectively. The plates were inoculated by flowing CCS in reverse from the outlet well at 1.0 dyne/cm<sup>2</sup> for 12 seconds and incubated at 37°C for one hour to enable attachment of cells to the acquired pellicle. After incubation, the automated protocol was initiated. Our automated protocol continuously supplied CFS from inlet 1 (**Figure IV.3**) to the site of biofilm development at 0.4 dyne/cm<sup>2</sup>.

At hours 8 and 18, treatment was delivered from inlet 2 at 2.0 dyne/cm<sup>2</sup>. The protocol ended after 22 hours of growth under flowing conditions.

### **Post-growth Staining of Biofilms**

After the automated protocol terminated, the remaining CFS and treatment formulations from the first inlet wells were aspirated and replaced with one mL of phosphate buffered saline (PBS, pH 7.4). The overnight biofilm was washed with PBS for 20 minutes at 0.4 dyne/cm<sup>2</sup> from inlet one wells. After wash, the remaining PBS in inlet one wells were aspirated and replaced with a LIVE/DEAD™ stain mixture containing 3.34 μM Syto-9 and 20 μM propidium iodide solution in PBS. The biofilm was stained for 40 minutes under a flow of 0.4 dyne/cm<sup>2</sup>. After staining, the plate was washed with PBS from inlet one for 20 minutes at dyne/cm<sup>2</sup> and the biofilms were subsequently imaged using a CLSM.

### **Confocal Laser Scanning Microscopy**

A Leica (Model TCS SPE) inverted confocal laser scanning microscope (CLSM) equipped with an air immersion objective lens (NA 0.85, 40x magnification, model HCX PL APO) was used to capture biofilm stacks along the viewing port. Excitation of stain was achieved with a 488nm laser and emission capture parameters (640-700nm for red and 500-550nm for green) were standardized for the stain concentration used in the experiment and unchanged between plates. Five image stacks (with 1 μm z-sections)

were captured for each sample at predetermined locations (imaging schematic shown in **Figure IV.3**), representing approximately a third of the surface area of the viewing port.

## **Statistical Analysis**

Comparisons of outcome means between groups were evaluated with student's t-test to evaluate treatment effects. In order to determine if treatment effects are differential across the viewing port, comparisons were also stratified by image proximity from inlet forks by excluding images 4 and 5 for the 1<sup>st</sup> half of the viewing port and images 1 and 2 for the 2<sup>nd</sup> half of the viewing port (**Table IV.3**).

## **Results**

### **Validation of BAIT Scripts**

The BAIT outcomes were validated with mock data as shown in **Figure IV.2**. The voxel-space of the mock data was small to ensure ease of manual measurements. **Figure IV.2** contains one object in the green channel and one object in the red channel. The green object is 12 voxels in size and the red object is 14 voxels. Based on the arrangement of these voxels, the green object has 66 exposed voxel surfaces and the red object has 70. Fluffiness and connectivity were then calculated from biovolume, surface area, and number of objects measurements. The convex hull volume of an object was calculated as the volume of the polyhedron generated when the straight lines are

drawn from object vertices. For the green object the expected convex hull volume was 16 voxels; for the red object, the convex hull volume was 21.33 voxels. These values were used to calculate convex hull porosity, the proportion of the convex hull volume that was devoid of biomass. The expected convex hull porosities for the green and red object are 0.25 and 0.34, respectively. Unweighted viability is a measurement that incorporates green and red channels; the expected viability of the sample data was 0.46. It should be noted that for this type of viability measurement, the intensity of green and red channels was not used as weights for viability calculation. The sample data were used as input in BAIT and the calculated outcomes matched all results calculated manually.

The three images chosen to illustrate a visually conspicuous gradient of biovolume (voluminous, moderate, and sparse), as well as the image metrics measured using BAIT, are shown in **Figure IV.4**. The biovolume outcomes reflected what was expected with the 'voluminous' image measuring 1,925,598 voxels and the 'sparse' image measuring 2,463 voxels (**Figure IV.4**). Like biovolume, surface area and number of objects detected matched what could be deduced upon visual inspection. What is less visually obvious is connectivity (average size of an object) and fluffiness (surface area to biovolume ratio). In **Figure IV.4**, 'voluminous' and 'moderate' had comparable connectivity and fluffiness while 'sparse' had markedly increased fluffiness and decreased connectivity. The convex hull porosity of the 'voluminous' and 'moderate' biofilms were similar at 0.70 and 0.69, respectively. However, the 'sparse' image had a convex hull porosity measure of 0.50, suggesting the objects in that image are more regular and contain less oblong protrusions than the objects in the other two images. The unweighted viability of the three biofilms

was high (>99% indicating the presence of more than 99 green voxels per red voxel), and this is evidenced visually by the amount of green fluorescent signal compared to red fluorescent signal from each biofilm.

### **Biofilm Sampling**

Each biofilm sample was imaged five times at five fixed locations (**Figure IV.3**). The imaging locations were evenly distributed across the viewing port for each image. A total of 123 biofilms were imaged in this study generating a total of 615 confocal image stacks. The distribution of samples by treatment group were as follows: 20 untreated, 18 water, 18 placebo 1,000, 19 stannous 1,000, and 12 each of placebo 3,439, stannous 3,439, placebo 10,000, and stannous 10,000. One sample from each group was manually imaged across the entire viewing port to generate Figure 5. The entire viewing port could be covered by 14 lengths of the objective lens' viewing field, thus the 5 images per sample strategy covers roughly 36% of the viewing port.

### **Qualitative Visual Observations of Treatment Group Effects**

**Figure IV.5** shows a visual representation of oral biofilms from each treatment group imaged across the entire viewing port. The panels show the effects of water, 1,000 Sn<sup>2+</sup>, 3,439 Sn<sup>2+</sup>, and 10,000 Sn<sup>2+</sup> treatments. The most notable decrease in biofilm growth occurred in the biofilms treated with 3,439 and 10,000 PPM Sn<sup>2+</sup>. In particular, the architecture of the 10,000 PPM Sn<sup>2+</sup> group had the least visible biovolume while the 1,000

PPM Sn<sup>2+</sup> group had the most. The 1,000 PPM Sn<sup>2+</sup> group contained small fragments of biovolume that was comparable to the 22h untreated group, but less confluent. The effect of 1000 PPM Sn<sup>2+</sup> was visually more pronounced in the second half of the viewing port. Water and sodium gluconate treatment also appeared to change the biofilm architecture. Biofilm fragments in the 1,000 PPM placebo group were larger than the 22h untreated group. The higher the concentration of sodium gluconate, the more pronounced this observation was. In the 10,000 PPM placebo group, large islands of biovolume were present, particularly at the tail end of the viewing port.

### **Quantitative Water Treatment Effects**

Water effects on biofilm architecture were measured using BAIT by comparing outcomes from biofilms treated with water at 8 and 18 hours into development to biofilms that were grown for 22 hours uninterrupted. Treatment with water had significant effects on biofilm outcomes. A total of 20 untreated and 18 water-treated samples were imaged at the end of each period, yielding 5 images per sample matched by proximity from inlet forks. Significant decrease in biovolume, objects detected, and surface area were found in all water-treated samples. Fluffiness and viability, on the other hand, significantly increased (**Table IV.3**). Stratification by image location revealed that water-treated biofilm in the 1<sup>st</sup> half of the viewing port contributed for most of the differences detected. For instance, the average biovolume decrease between water-treatment and untreated groups was 29.87% across the entire viewing port, while for the first half of the viewing port it was 39.1%. Viability was the only significant outcome in the second half of the

viewing port. In the linear mixed effects model where fixed effects of imaging location (proximity from the inlet fork) and random effects of sample were accounted for, treatment with water had no appreciable effect on transformed-outcomes (**Table IV.4**). The direction of effects in the linear mixed effects model were all concordant to the direction seen in the 2-sample t-tests.

### **Quantitative Stannous 1,000 PPM Treatment Effects**

The treatment effects of 1,000 PPM  $\text{Sn}^{2+}$  were measured using BAIT by comparing differences from biofilms treated with a placebo formulation that was identical to 1,000 PPM  $\text{Sn}^{2+}$  without the presence of  $\text{SnF}_2$ . Comparing images across the entire viewing port, biofilms treated with 1,000 PPM  $\text{Sn}^{2+}$  resulted in significantly higher number of objects detected and fluffiness (**Table IV.3**). Restricting analysis to viewing port halves, there was evidence that 1,000 PPM  $\text{Sn}^{2+}$  effects on biofilm development were differentially distributed across the viewing port. As opposed to water treatment effects in the first half of the viewing port, 1,000 PPM  $\text{Sn}^{2+}$  treatment had the most detectable effects on biofilm development in the second half of the viewing port. In this region biofilm that had been treated with 1,000 PPM  $\text{Sn}^{2+}$  had lower biovolume, surface area, connectivity, and higher fluffiness compared to biofilms that had been treated with the placebo 1,000 PPM  $\text{Sn}^{2+}$  formulation. However, the difference in the number of objects detected in the second half of the viewing was not significant between  $\text{Sn}^{2+}$  and placebo. In the first half of the viewing port, 1,000 PPM stannous had significant effects on number of objects

detected. In the linear mixed effects model, 1,000 PPM Sn<sup>2+</sup> group had no effect on any of the biofilm outcomes (**Table IV.4**).

### **Quantitative Stannous 3,439 & 10,000 PPM Treatment Effects**

Using BAIT, the effect of 3,349 and 10,000 PPM Sn<sup>2+</sup> treatment was determined by comparing samples treated with stannous at 8 and 18 hours into development to samples treated with placebo treatments at the same time points. The majority of biofilm analysis outcomes, regardless of location within the viewing port, were significantly different. Formulations containing stannous ions reduced biofilm biovolume, surface area, connectivity, total number of objects, and viability (**Table IV.3**). Additionally, stannous treatments increased biofilm fluffiness. The only outcome that was not significantly different was convex hull porosity, suggesting that stannous treatments at high concentrations did not affect object irregularity. Stratifying the analysis to viewing port halves, % change in outcomes indicated no differential effects based on region of viewing port imaged. The effect size of stannous increased using 10,000 PPM Sn<sup>2+</sup> formulation compared to 1,000 and 3,439 PPM Sn<sup>2+</sup>, suggesting a dose response. The linear mixed effects model detected significance in all biofilm outcomes as well. The beta estimates also suggested a dose response to stannous ions as described and shown in **Table IV.4**.

## **Discussion**

In this study, we introduce the Biofilm Architecture Inference Tool (BAIT), a software package that can rapidly quantify the architecture of biofilms captured with a confocal laser scanning microscope. The software integrates a graphical user interface along with automation to provide users an intuitive interface to analyze biofilm architecture. BAIT was designed to be the post-imaging standard in a workflow that also includes an automated *in vitro* model system to study oral biofilms. We also adapted a 24-well Bioflux™ system to reproducibly grow multi-species oral biofilms treated with water, sodium gluconate, and stannous-containing formulations. Our study demonstrates that pairing a microfluidic *in vitro* model system with BAIT enables investigators to quickly evaluate the effects of candidate treatment formulations on biofilm development.

The biofilm architectural outcomes chosen for inclusion in BAIT are those expected to determine how well a treatment retards biofilm development and consequently affects host-biofilm homeostasis. Biovolume is a representation of the bioburden of a biofilm. In lieu of CLSM technology, total bioburden of biofilms has been estimated with techniques such as crystal violet assays (Luo, Rickard et al. 2015, Xu, Liang et al. 2016). The lower the biovolume measure, the more retarded the growth. Biofilm surface area, fluffiness, and convex hull porosity have implications for biofilm metabolic activity and overall physiology of the biofilm as it determines how exposed the biofilm is to the bulk-liquid phase (Bester, Kroukamp et al. 2011). Higher surface area and relative surface area to volume ratio could determine aggregate exposure to a nutrient or an antimicrobial. The higher the fluffiness, the greater the effect of an antimicrobial by mitigating the limitation diffusion phenomena of thick biofilms (Stewart 2003). The total number of objects

measured, and connectivity are estimates of biofilm fragmentation. Biofilm fragmentation has been estimated by the ratio of perimeter length over surface area, enhancing solute transfer by reducing average distance of diffusion (Battin, Kaplan et al. 2003). Similarly to fluffiness and surface area, fragmented biofilms can enhance antimicrobial delivery.

At its current stage in development, BAIT only contains outcomes calculated from a binary image stack that have undergone thresholding. These belong to a class of outcomes called areal parameters, which describe the biofilm architecture in context of morphology (volume, surface area, number of objects, porosity, etc.) (Beyenal, Donovan et al. 2004). We envision that future versions of BAIT will have the capacity to calculate outcomes dependent on the image stack's intensity histogram. This will allow for measurements of another class of outcomes called textural parameters, which characterize heterogeneity of biofilms using variations in signal intensities (Beyenal, Donovan et al. 2004, Beyenal, Lewandowski et al. 2004, Milferstedt, Pons et al. 2008).

In addition to the development of BAIT, we also adapted a variant of a published microfluidic system to demonstrate the anti-biofilm properties of stannous fluoride within the model system, simulating environmentally-germane conditions. The development of a workflow script with validated algorithms to quantify biofilm features was also integral to accommodate the significant confocal data it generated. Overall, the 24-well Bioflux™ model system was capable of reliably developing oral multi-species biofilms over the course of 22 hours, similar to the 48-well system, using identical preparations. The difference is the inclusion of a second inlet well that enabled the automatic delivery of

exogenous aqueous treatment solutions to the site of biofilm development. With the addition of this feature, candidate formulations and their effects on biofilms can be evaluated more conveniently than the traditional 48-well system, which requires halting biofilm development and manually adding treatment to the sole inlet.

The decision to evaluate the effects of stannous fluoride on biofilm architecture was motivated by past literature documenting its antibacterial effects on key oral species (Yoon and Berry 1979, Ellingsen, Svaton et al. 1980, Tinanoff 1995). In our study, we discovered that at sufficient concentrations, stannous fluoride can serve as a mild antimicrobial as indicated by viability measurements using BAIT. However, the more significant result was that at 3,439 PPM  $\text{Sn}^{2+}$  (the concentration of stannous in dentrifice), the periodic exposure of stannous fluoride solutions to developing nascent oral biofilms seemingly retarded or inhibited biofilm development and biofilm architecture. Of relevance, also, end-stage treatment with the highest concentrations of stannous fluoride did not demonstrate any immediate biofilm control effects seen to the extent revealed in periodic exposure treatment regimens (**Figure IV.6**). Together our results suggest that the efficacy of stannous fluoride's anti-biofilm properties is contingent on the maturity of the oral biofilm. With the destruction and removal of dental plaque biofilms that is accompanied with brushing, the addition of stannous fluoride to oral healthcare products could prove effective at retarding dental plaque development.

In conclusion, using BAIT, we can rapidly measure the changes in biofilm architecture and evaluate possible antimicrobial and anti-biofilm effects of candidate

agents. We envision that BAIT will enhance understanding of the effects of anti-biofilm and antimicrobial agents, ultimately shedding light on possible clinical outcomes following the use of such agents.

**Table IV.1. Outcomes Currently Available in BAIT.** Biofilm architectural outcomes available in BAIT are defined and coded to the following specifications. All outcomes are calculated on binary cellular array data post-thresholding. The biovolume elasticity thresholding method was applied to each image prior to quantification.

<b>Architectural Outcome</b>	<b>Description</b>
<i>Biovolume</i>	Sum of all voxels post-thresholding.
<i>Number of Objects</i>	Sum of all foreground objects that are separated from other foreground signal obeying a 26-connectivity rule
<i>Surface Area</i>	Sum of all exposed surfaces (i.e. dimensionless, not just the bulk-fluid exposed surface of the biofilm) of voxels post-thresholding.
<i>Fluffiness</i>	Surface area to biovolume ratio of all voxels within an entire image
<i>Connectivity</i>	Average biovolume per object.
<i>Convex Hull Porosity</i>	Following the removal of objects less than 100 voxels a convex hull mesh is applied to each object. The volume of this meshed object is defined as the convex hull volume. The convex hull porosity is the proportion of void voxels within the convex hull volume
<i>Viability</i>	BEM thresholding was applied to both the red channel and the green channel, yielding a binary image for each. Viability is calculated as the proportion of green voxels amongst all green and red voxels

**Table IV.2. Groups of Biofilm Images Quantified by BAIT.** Treatment schedule is described for each group to evaluate effects of water, sodium gluconate, and stannous fluoride treatments on oral biofilm architecture.

Group	Formulation			Final Concentrations	
	Water (Grams)	Sodium Gluconate (Grams)	Stannous Fluoride (Grams)	Sodium Gluconate (mMol)	Sn <sup>2+</sup> (PPM)
<b>Water</b>	100	0	0	0	0
<b>Placebo 1000 PPM</b>	99.348	.652	0	2.989	0
<b>Stannous 1000 PPM</b>	99.216	.652	.132	2.989	1000
<b>Placebo 3,439 PPM</b>	98.736	1.264	0	5.795	0
<b>Stannous 3,439 PPM</b>	98.282	1.264	.454	5.795	3439
<b>Placebo 10,000 PPM</b>	96.324	3.676	0	16.852	0
<b>Stannous 10,000 PPM</b>	95.004	3.676	1.320	16.852	10000

**Table IV.3. BAIT Outcomes by Treatment Group and Stratified by Viewing Port Half.** Respective treatment groups are compared to its appropriate baseline groups to evaluate effects of water, Sn<sup>2+</sup> 1,000, Sn<sup>2+</sup> 3,439, and Sn<sup>2+</sup> 10,000 effects. Results are also stratified by location of biofilm development. Water, Sn<sup>2+</sup> 3,439, and Sn<sup>2+</sup> 10,000 treatments have significant overall effects on biofilm architecture. Sn<sup>2+</sup> 1,000 treatments effects are more predominantly detected in the 2<sup>nd</sup> half of the viewing port.

Entire Viewing Port		Water Effect		Sn <sup>2+</sup> 1000 Effect		Sn <sup>2+</sup> 3439 Effect		Sn <sup>2+</sup> 10000 Effect	
Outcome		22 hr. growth (n=100)	Water (n=90)	Placebo 1,000 (n=90)	Sn <sup>2+</sup> 1,000 (n=95)	Placebo 3,439 (n=60)	Sn <sup>2+</sup> 3,439 (n=60)	Placebo 10,000 (n=60)	Sn <sup>2+</sup> 10,000 (n=60)
<b>Biovolume</b>		2,225,952	1,561,029	1,504,714	1,522,859	1,578,658	53,594	1,421,197	11,958
% change	p-value	-29.87	<0.01	1.20	0.92	-96.6	<0.01	-99.2	<0.01
<b>Number of Objects</b>		32,011	23,636	22,188	28,311	29,279	2,411	25,922	772
% change	p-value	-26.16	<0.01	27.60	0.04	-91.8	<0.01	-97.0	<0.01
<b>Surface Area</b>		2,656,538	2,096,775	2,035,852	2,166,362	1,963,659	112,970	1,868,002	32,532
% change	p-value	-21.07	<0.01	6.41	0.52	-94.3	<0.01	-98.3	<0.01
<b>Fluffiness</b>		1.35	1.52	1.59	1.82	1.37	3.40	1.55	4.47
% change	p-value	12.19	<0.01	14.47	<0.01	148.0	<0.01	187.8	<0.01
<b>Connectivity</b>		78.42	70.29	68.18	57.92	51.57	16.57	50.77	6.64
% change	p-value	-10.32	0.17	-15.1	0.07	-67.9	<0.01	-86.9	<0.01
<b>Convex Hull</b>		0.69	0.71	0.71	0.71	0.65	0.67	0.64	0.66
% change	p-value	3.1	0.10	0.2	0.90	1.9	0.62	2.9	0.55
<b>Viability</b>		0.9872	0.9942	0.9955	0.9950	0.9996	0.9760	0.9990	0.9201
% change	p-value	0.7	<0.01	-0.0	-0.79	-2.4	<0.01	-7.9	<0.01
<b>1<sup>st</sup> Half of Viewing Port</b>		Water Effect		Sn <sup>2+</sup> 1000 Effect		Sn <sup>2+</sup> 3439 Effect		Sn <sup>2+</sup> 10000 Effect	
Outcome		22 hr. growth (n=60)	Water (n=54)	Placebo 1,000 (n=54)	Sn <sup>2+</sup> 1000 (n=57)	Placebo 3,439 (n=36)	Sn <sup>2+</sup> 3439 (n=36)	Placebo 10,000 (n=36)	Sn <sup>2+</sup> 10000 (n=36)
<b>Biovolume</b>		2,773,916	1,688,084	1,740,974	1,992,875	1,789,587	64,812	1,684,122	18,052
% change	p-value	-39.1	<0.01	14.5	0.33	-96.4	<0.01	-98.9	<0.01
<b>Number of Objects</b>		37,684	24,997	24,767	34,280	31,818	3,201	29,160	1,086
% change	p-value	-33.7	<0.01	38.4	0.03	-89.9	<0.01	-96.3	<0.01
<b>Surface Area</b>		3,189,567	2,238,238	2,266,805	2,685,027	2,183,431	142,978	2,144,665	47,523
% change	p-value	-29.8	<0.01	18.4	0.15	-93.5	<0.01	-97.8	<0.01
<b>Fluffiness</b>		1.27	1.51	1.53	1.70	1.33	3.31	1.51	4.41
% change	p-value	18.5	<0.01	11.2	0.15	148.8	<0.01	193.2	<0.01
<b>Connectivity</b>		83.70	72.04	71.96	63.56	54.61	16.36	54.14	6.80
% change	p-value	-13.9	0.14	-11.7	0.28	-70.0	<0.01	-87.4	<0.01
<b>Convex Hull</b>		0.67	0.70	0.71	0.70	0.65	0.70	0.63	0.66
% change	p-value	4.8	0.09	-1.8	0.54	8.6	0.09	3.8	0.54
<b>Viability</b>		0.9873	0.9938	0.9934	0.9941	0.9996	0.9667	0.9989	0.9343
% change	p-value	0.7	0.06	0.0	0.80	-3.3	0.02	-6.5	<0.01
<b>2<sup>nd</sup> Half of Viewing Port</b>		Water Effect		Sn <sup>2+</sup> 1000 Effect		Sn <sup>2+</sup> 3439 Effect		Sn <sup>2+</sup> 10000 Effect	
Outcome		22 hr. growth (n=60)	Water (n=54)	Placebo 1,000 (n=54)	Sn <sup>2+</sup> 1000 (n=57)	Placebo 3,439 (n=36)	Sn <sup>2+</sup> 3439 (n=36)	Placebo 10,000 (n=36)	Sn <sup>2+</sup> 10000 (n=36)
<b>Biovolume</b>		1,771,609	1,411,601	1,326,207	940,614	1,305,436	405,15	1,062,772	2,632
% change	p-value	-20.3	0.06	-29.1	<0.01	-96.9	<0.01	-99.8	<0.01
<b>Number of Objects</b>		28,264	22,830	20,231	20,788	26,284	1,296	21,392	271
% change	p-value	-19.2	0.08	2.8	0.82	-95.1	<0.01	-98.7	<0.01
<b>Surface Area</b>		2,274,604	1,971,009	1,871,617	1,542,311	1,711,102	71,968	1,485,230	9,226
% change	p-value	-13.3	0.13	-17.6	0.04	-95.8	<0.01	-99.4	<0.01
<b>Fluffiness</b>		1.45	1.54	1.64	1.94	1.44	3.55	1.61	4.58
% change	p-value	6.5	0.19	18.0	<0.01	146.0	<0.01	184.3	<0.01
<b>Connectivity</b>		71.80	67.48	66.1	51.5	47.3	16.1	47.1	6.1
% change	p-value	-6.0	0.55	-22.1	<0.01	-66.0	<0.01	-87.1	<0.01
<b>Convex Hull</b>		0.71	0.72	0.72	0.73	0.66	0.66	0.63	0.63
% change	p-value	1.2	0.51	1.8	0.41	-0.6	0.88	1.3	0.86
<b>Viability</b>		0.9863	0.9941	0.9974	0.9965	0.9996	0.9902	0.9992	0.9168
% change	p-value	0.8	0.03	-0.1	0.59	-0.9	<0.01	-8.2	0.01

**Table IV.4. Linear Mixed Effects Models of Each Biofilm Architecture Outcome.**

Results are controlled for random effects of plate and fixed effects from imaging proximity to inlet junctions. Seven different models were tested, corresponding to each outcome. Count outcomes were log-transformed, ratio outcomes were square-root-transformed, and proportion outcomes were arcsin-transformed. Stannous 3,439 and stannous 10,000 PPM treatments had significant effects in all architectural outcomes except for convex hull porosity. All significant effects are in the direction of biofilm control. High concentrations of sodium gluconate decreases convex hull porosity, making the biofilm objects less irregular. Imaging location also has significant effects. The more downstream biofilm development is from the nutrient source, the more compromised the biofilm.

Effects	Estimate	t-value	p-value	Estimate	t-value	p-value
	<b>Log Biovolume (R<sup>2</sup> = 0.91)</b>			<b>Sqrt Connectivity (R<sup>2</sup> = 0.89)</b>		
Distance*	-0.26	-8.56	<0.01	-0.20	-6.77	<0.01
Water	-0.33	-0.91	0.35	-0.42	-0.74	0.45
Placebo 1,000	-0.10	-0.28	0.76	-0.11	-0.19	0.84
Placebo 3,439	0.02	0.05	0.76	-0.98	-1.51	0.13
Placebo 10,000	-0.59	-1.43	0.15	-1.14	-1.75	0.08
Stannous 1,000	-0.18	-0.50	0.60	-0.81	-1.41	0.16
Stannous 3,439	-5.16	-11.37	<0.01	-3.50	-4.91	<0.01
Stannous 10,000	-7.84	-17.27	<0.01	-4.77	-6.68	<0.01
	<b>Log Number of Objects (R<sup>2</sup> = 0.87)</b>			<b>Arcsin Convex Hull (R<sup>2</sup>=0.40)</b>		
Distance*	-0.20	-8.36	<0.01	0.01	1.98	0.05
Water	-0.23	-0.94	0.34	0.03	0.92	0.35
Placebo 1,000	-0.08	-0.32	0.73	-0.00	-0.01	0.97
Placebo 3,439	0.22	0.78	0.43	-0.08	-2.19	0.03
Placebo 10,000	-0.30	-1.05	0.29	-0.11	-2.90	<0.01
Stannous 1,000	0.09	0.34	0.72	0.00	0.06	0.94
Stannous 3,439	-3.55	-11.34	<0.01	-0.00	-0.11	0.89
Stannous 10,000	-5.28	-16.85	<0.01	0.03	0.51	0.59
	<b>Log Surface Area (R<sup>2</sup> = 0.90)</b>			<b>Arcsin Viability (R<sup>2</sup>=0.62)</b>		
Distance*	-0.22	-7.80	<0.01	0.01	2.17	0.03
Water	-0.22	-0.67	0.49	0.03	1.06	0.28
Placebo 1,000	-0.06	-0.20	0.83	0.01	0.28	0.77
Placebo 3,439	-0.07	-0.18	0.84	0.04	0.97	0.32
Placebo 10,000	-0.58	-1.57	0.11	0.03	0.82	0.40
Stannous 1,000	-0.08	-0.24	0.80	-0.02	-0.52	0.59
Stannous 3,439	-4.31	-10.64	<0.01	-0.13	-3.08	<0.01
Stannous 10,000	-6.87	-16.95	<0.01	-0.23	-5.58	<0.01
	<b>Sqrt Fluffiness (R<sup>2</sup> = 0.86)</b>					
Distance*	0.02	5.51	<0.01			
Water	0.07	1.19	0.23			
Placebo 1,000	0.03	0.46	0.64			
Placebo 3,439	-0.06	-0.87	0.37			
Placebo 10,000	0.01	0.15	0.86			
Stannous 1,000	0.08	1.38	0.16			
Stannous 3,439	0.65	9.11	<0.01			
Stannous 10,000	0.88	12.33	<0.01			

\*Distance predictor modeled continuously (1-5) with 1 indicating the image closest to the inlet fork and 5 indicating image furthest.

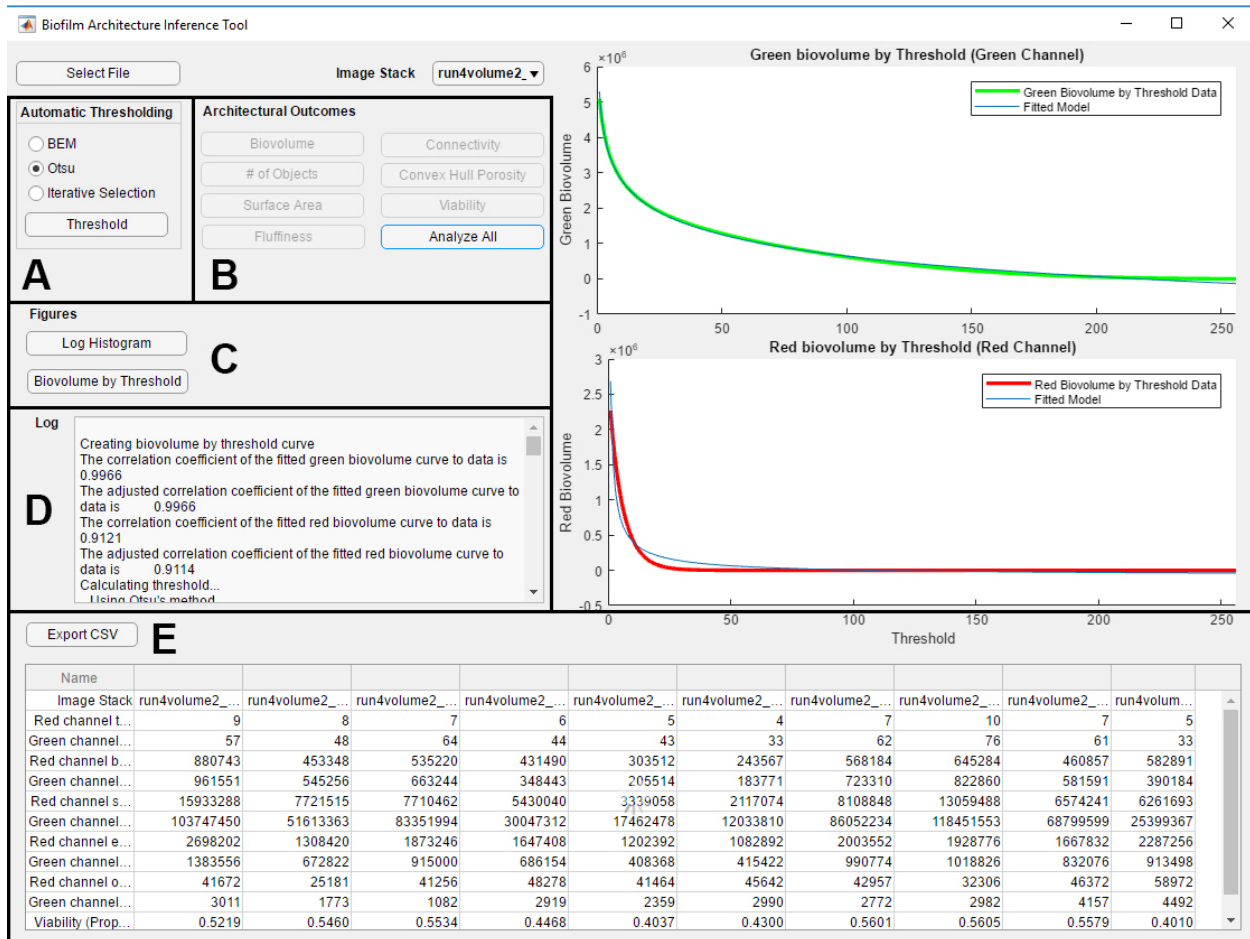


**Figure IV.1. Graphical User Interface (GUI) Layout of BAIT.** The layout of the Biofilm Architecture Inference Tool (BAIT) graphical user interface. Boxed regions indicate functionalities of BAIT. After loading a .mat cellular array archive of confocal stacks, images can be: **A)** automatically thresholded, **B)** analyzed for each architectural outcome, and **C)** visualized by its log intensity histogram or biovolume by threshold curve. **D)** All individual outcome measurements are kept in a log file. **E)** The 'Analyze All' functionality calculates all outcomes for each image and presents it in a spreadsheet that can be exported.

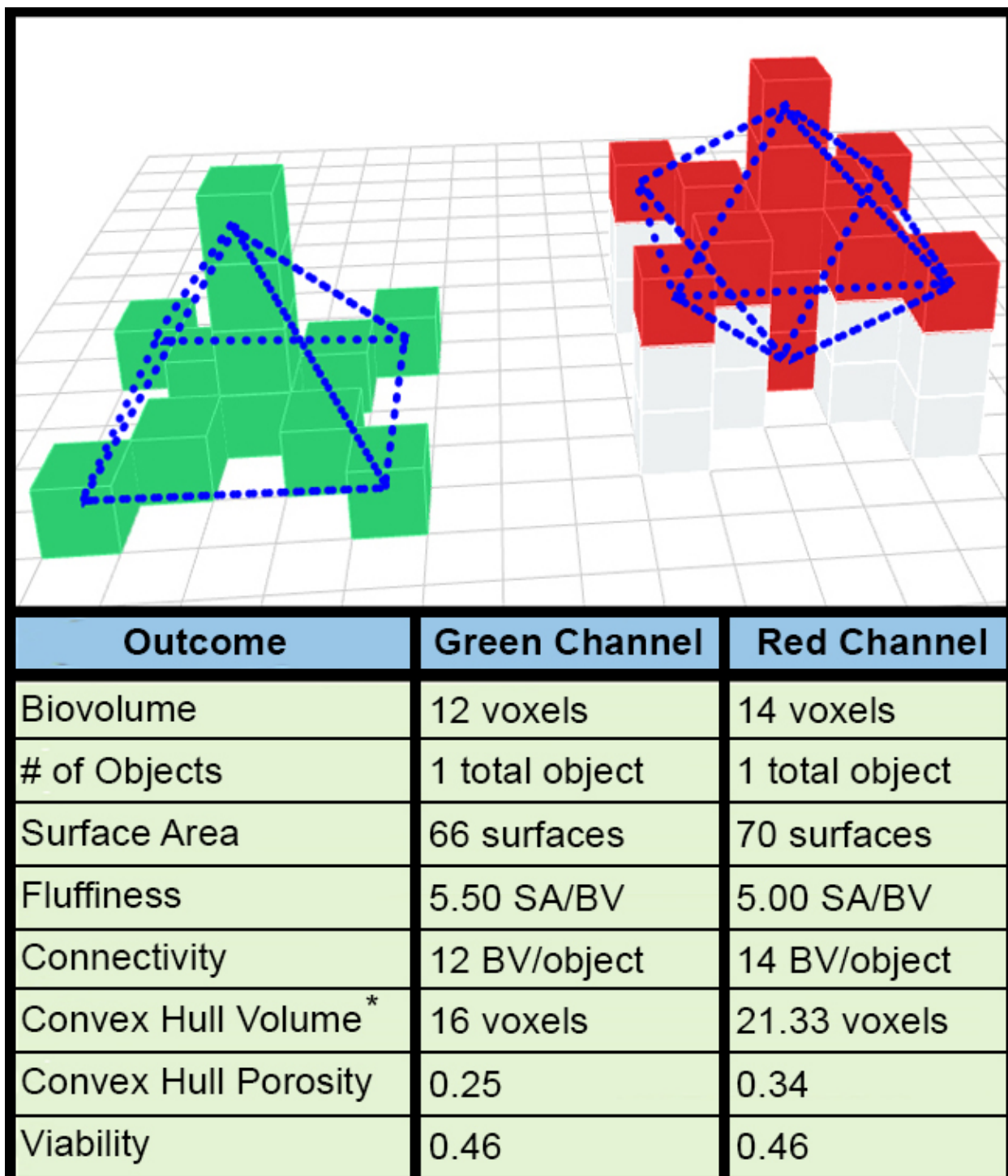


**Figure IV.2. Mock Dataset Used To Validate Outcomes Calculated by Scripts.** Cellular array dataset containing two biofilm objects were created for MatLab script validation. Voxel-space is small enough to calculate biofilm architectural outcomes manually. Outcomes were calculated for both green and red channels and expected values listed. Outcomes calculated by BAIT were identical to outcomes calculated manually.

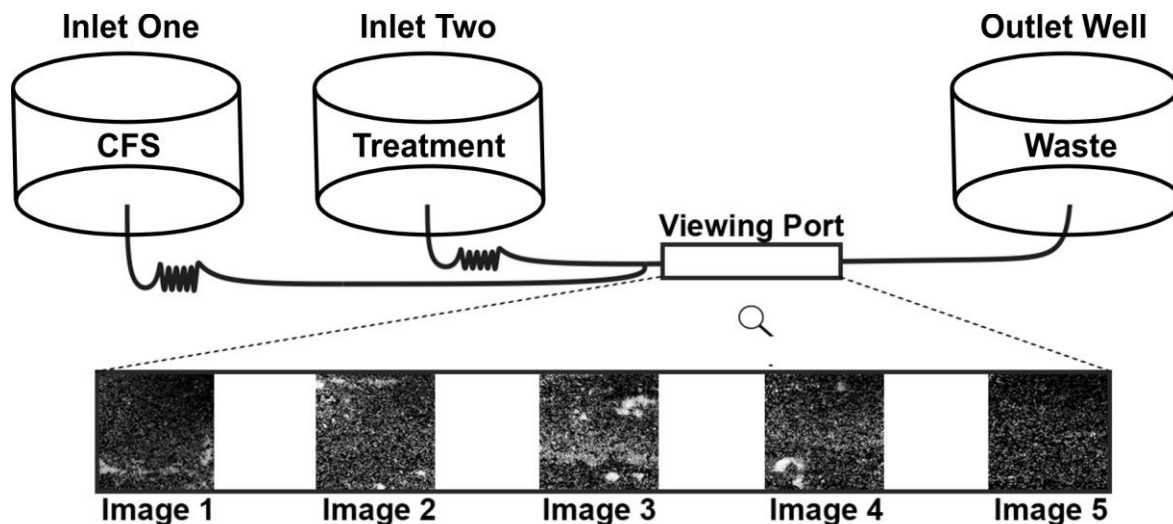
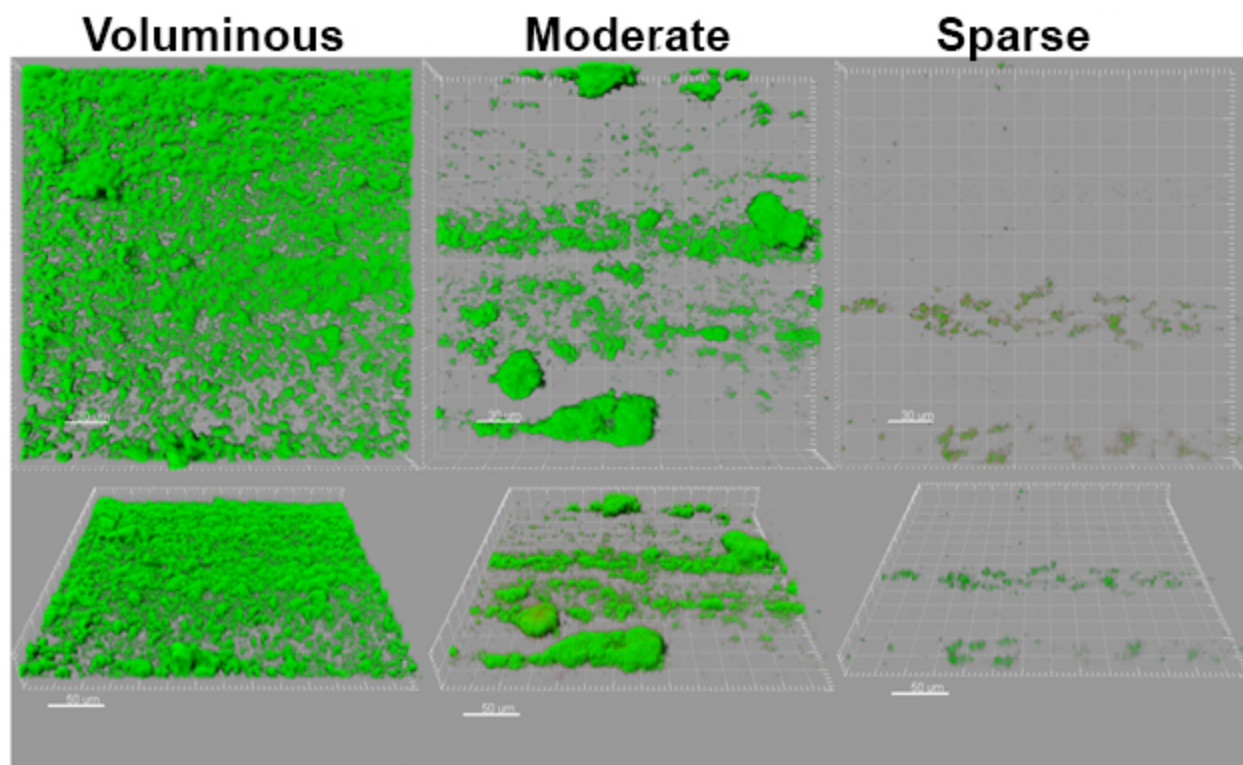


**Figure IV.3. Representation of the 24-well Bioflux™ Plate & Imaging Strategy.** An acquired pellicle was developed using cell-free saliva (CFS) prior to inoculation with cell-containing saliva (CCS). CFS serves as media and is flowed constantly at  $0.4 \text{ dynes/cm}^2$ . Varying concentrations of  $\text{SnF}_2$  treatment or placebo treatment were added to treatment well. Treatment regimen was set at  $2.0 \text{ dynes/cm}^2$  for two minutes. Biofilm growth was captured by imaging five locations evenly distributed across the viewing port.



Outcome	Voluminous	Moderate	Sparse
Biovolume	1,928,598	697,727	2,463
# of Objects	16,336	6,419	430
Surface Area	2,558,792	890,712	9,570
Fluffiness	1.33	1.28	3.89
Connectivity	118.06	108.70	5.73
Convex Hull Porosity	0.70	0.69	0.50
Viability	0.9975	0.9937	0.9984

**Figure IV.4. Validation of BAIT Using Three Confocal Oral Biofilm Images.** Three images were chosen to represent voluminous, moderate, and sparse amount of visible biofilm material. The images were rendered in shadow projection with Imaris after applying BEM threshold. All three images served as input to BAIT and results were assessed. Measurements from BAIT are biologically feasible based on expectations.

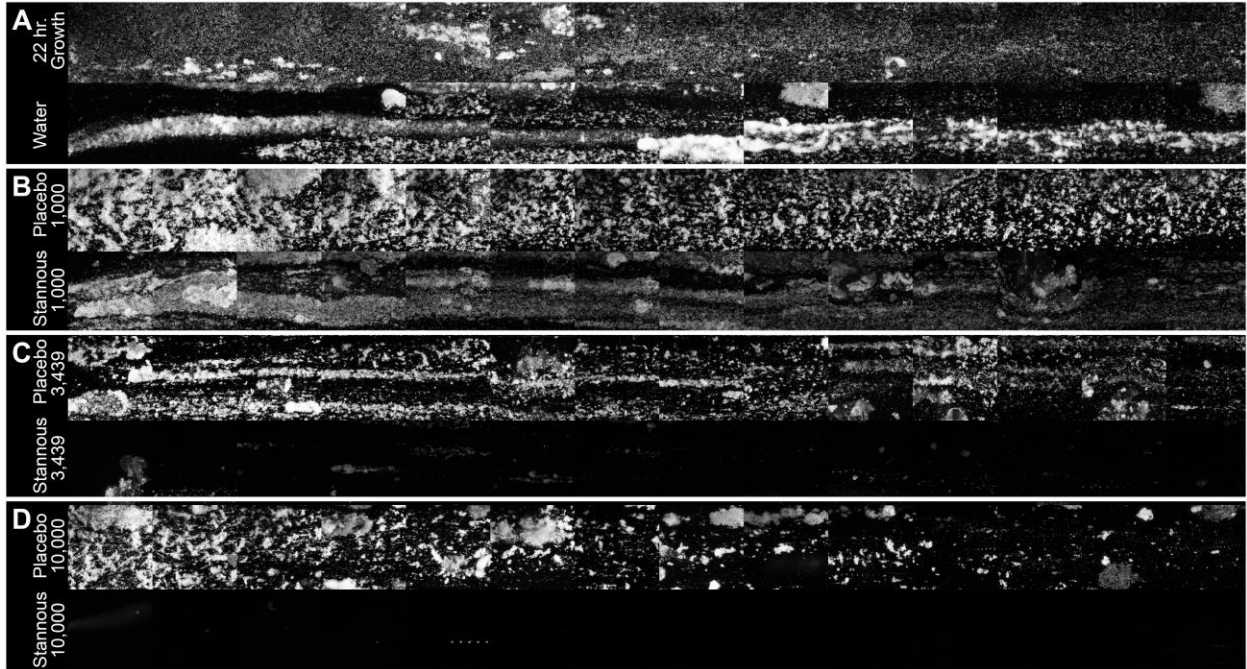


**Figure IV.5. Stitched Images of Representative Biofilms by Group.** Stitched images of entire viewing port reveal biofilm destabilization effects from periodic exposure to higher concentrations of stannous fluoride. Stannous 1,000 PPM was insufficient to inhibit biofilm development, but visual signs of fragmentation and streaking were present, particularly in the second half of the viewing port. Flow of CFS was from left to right.

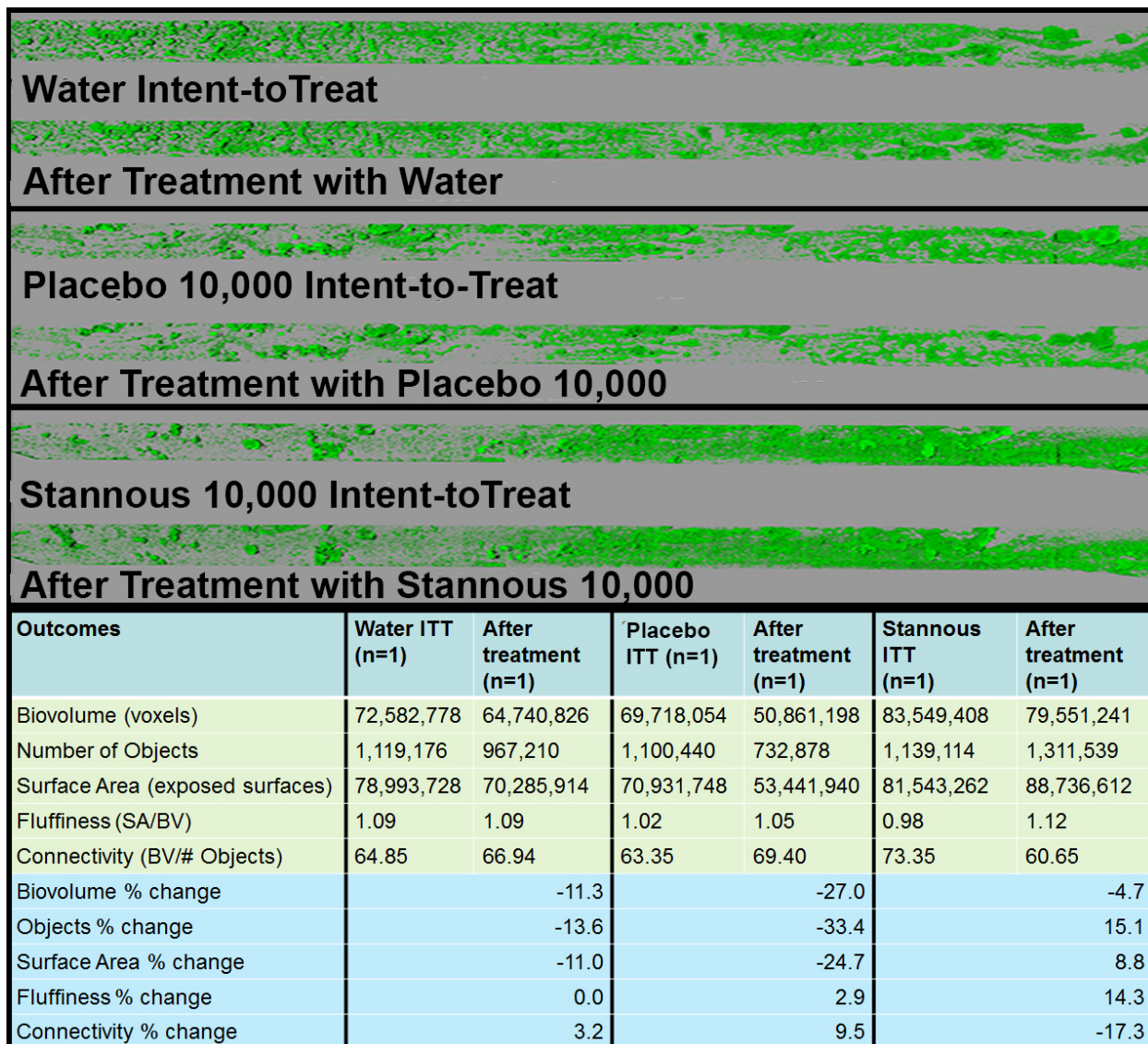


**Figure IV.6. Immediate Effects of Treatments.** End stage treatments were applied with three treatment groups (water, placebo 10,000, and stannous 10,000). Three intent-to-treat biofilms were developed over 22 hours and imaged across the entire viewing port. Biofilms were then treated for 2 minutes at 2.0 dynes/cm<sup>2</sup> with water, placebo 10,000, or stannous 10,000 and imaged again using the same coordinates. Post-treated biofilms were then compared to its pre-treated counterpart. Stannous 10,000 treatment did not eradicate biofilm to the extent observed in intermittent exposure study. However, end-stage treatment with stannous 10,000 showed precursors of biofilm fragmentation with increased # of objects, surface area, fluffiness, and decreased connectivity.

## Chapter V

### Concluding Remarks & Future Directions

#### Conclusions

Oral diseases, such as caries and periodontal disease are a contemporary public health challenge. These two diseases, as well as many other oral maladies, are highly influenced by biofilm or dental plaque accumulation on hard surfaces within the intraoral cavity. Thus, strategies limiting biofilm activity and plaque accumulation could decrease incidence of caries and periodontal disease and reduce billions in estimated annual healthcare costs (Sheiham, Williams et al. 2015).

*In vitro* biofilm model systems are widely used in dental biofilm research. Their appeal to investigators have been reinvigorated the past few decades due to newer models and techniques that enable better *in vivo* mimicry. In chapter II, a historical distillation of *in vitro* biofilm model systems is given, with a focus on model systems that are relevant to dental biofilm research today. Additionally, a discussion of integrated technologies, such as confocal laser scanning microscopy (CLSM) and 16S rRNA community profiling was included. These technologies enable investigators access to

non-traditional biofilm outcomes, such as biofilm architecture and community structure. Assisted by integrative technologies, recent developments in model system techniques and equipment have increased generalizability of results gathered from *in vitro* biofilm models. Ultimately, the goal of *in vitro* dental biofilm research is to generate representative results in order to provide the foundational impetus for continuing with clinical trials or further *in vivo* work.

There are few standard protocols for developing dental *in vitro* microcosm biofilms seeded from salivary milieu. We adapted the 24-well Bioflux™ model system to develop overnight microcosm biofilms representing early supragingival plaque. The protocol was standardized to include the secondary inlet well, which was utilized as the treatment delivery well. The resulting biofilm can be non-destructively imaged with a confocal laser scanning microscope (CLSM) to fully characterize its natural architecture. An objective imaging strategy was devised to eliminate operator subjectivity in selecting the best field of view to image. Biofilms with and without treatment regimens can be reliably duplicated using the 24-well Bioflux™ system, demonstrating its utility for *in vitro* microcosm biofilm studies.

Thresholding is a necessary image pre-processing step to distinguish background noise from foreground signal. Thresholding can be performed manually or automatically with algorithms. Traditional thresholding algorithms used in biofilm research include Otsu's method and iterative selection. These algorithms are shown to be rather aggressive in their classification of fluorescent noise, potentially leading to removal of

biomass signal. In Chapter III, we developed the biovolume elasticity method (BEM) designed for thresholding fluorescent CLSM images. The BEM is a sensitive alternative that captures more biomass. Three-dimensional renders of a singular dental biofilm image after applying each algorithm and manual threshold averages reveal that true biomass of low intensity is removed by Otsu's, iterative selection, and manual methods. The BEM was the only method sensitive enough to capture streptococcal chains and individual microcolonies. Thresholding strategies can have massive implications for downstream quantification and measurements and choice of algorithm can affect interpretation of results.

Few software packages capable of analyzing confocal stacks exist. The ones that do are focused on quantification of biomass material and not dedicated to the characterization of biofilm architecture. In Chapter IV, we developed a software package, named Biofilm Architecture Inference Tool (BAIT), for the calculation of biofilm architecture outcomes. The software is designed to be automated and can analyze confocal archives containing multiple images with little user supervision. The BAIT package features the BEM automatic thresholding method as well as Otsu's method and iterative selection. Biofilm architectural outcomes included in bait are: biovolume, surface area, total number of objects, viability, connectivity, fluffiness, and convex hull porosity. These outcomes were chosen because changes in each of these measures could inform investigators how efficacious a treatment is at biofilm control. This construct is not limited to reduction in biovolume, but other measures that could prime a biofilm to be more receptive to treatment. For example, increased fluffiness indicates more biofilm surface area that is exposed to the bulk-liquid phase, making it more vulnerable to future drug

delivery. We envision BAIT to be the standard software package for biofilm control studies that utilizes fluorescent signal.

## **Future Directions**

### **Textural, Spatial, & Temporal Outcomes in BAIT**

At its current stage in development, BAIT is capable of measuring biofilm architecture outcomes from binary image files after a threshold is applied. These outcomes: biovolume, surface area, number of objects, viability, connectivity, fluffiness, and convex hull porosity belong to an outcome set called areal parameters (Yang, Beyenal et al. 2000). Future versions of BAIT will include areal parameters. Areal measurements seek to characterize biofilm morphology and measures the size and shape of cell clusters (connectivity, fluffiness, number of objects) or interstitial space (convex hull porosity). Textural measurements, on the other hand, focuses on microscale heterogeneity of biofilm. Qualitatively, texture of a biofilm can be described as coarse, smooth, random, or irregular. Quantitatively, its measurement relies on the grayscale intensity value for each pixel in 2-dimensional images or voxel in 3-dimensional images for calculation. In an 8-bit image, each pixel/voxel value can range from 0-255. A 12-bit image can store values from 0-4095 for each pixel/voxel. The rate and direction of change in chromatic gradients can be used to calculate entropy, homogeneity, and energy. Textural entropy, for example, is calculated from the variation in grayscale values. Higher variation confers higher entropy, which indicates a heterogeneous biofilm.

Another outcome set we envision to be a part of the finalized BAIT package are spatial outcomes. Within the same channel, these outcomes relate distances between objects calculated by the objects' centroids. This average distance measure can provide an estimate of biomass density (Drescher, Dunkel et al. 2016). Signal from other potential channels will also be incorporated for outcomes such as colocalization and other proximity analyses. This functionality will be extremely useful in fluorescent labeling of specific taxa where a single channel can indicate presence of a certain genus. One such application is combinatorial labeling and spectral imaging – fluorescent *in situ* hybridization (CLASI-FISH), shown in **Figure V.1** (Valm, Mark Welch et al. 2012). Spatial presence of one genus relative to another can indicate how certain bacteria interact with one another, given its presence in a complex or microcosm community. Outcomes of interest include colocalization (Zijngel, van Leeuwen et al. 2010), whether signal from one channel occupies the same pixel-voxel space as signal from another channel, and average distances (Reighard, Hill et al. 2015) between biomass of the same color vs. another.

Another parameter of interest that can be added to BAIT and fluorescence microscopy is time. The confocal laser scanning microscope can be configured to take images at multiple time points, creating a time series of confocal stacks. This feature had been used for single-molecule and protein tracking (Han, Kiss et al. 2012), but had not been implemented in biofilm growth studies due to the technical limitations of integrating a Bioflux™ heating stage to a confocal stage. This has significant implications to the future

of *in vitro* dental biofilm studies. With the ability to capture digital data and render in real-time how the physical biofilm responds to treatment, investigators can observe the mechanism of action of proven anti-biofilm agents and generate new hypotheses on an optimal delivery regimen.

### **16S rRNA Community Profiling of *In Vitro* Dental Biofilms**

Dental biofilms developed in the 24-well Bioflux™ system may also be harvested by pulsating water back and forth between the inlet and outlet wells. The harvested cells can then be extracted for genomic DNA and sequenced with a next-generation sequencing platform. The bacterial community measured from 16S rRNA profiling is a cross-sectional snapshot of the biofilm community at the time of harvest. Unfortunately, there exists no technology that can interrogate a developing biofilm for their community composition in real-time. Community outcomes include alpha diversity, beta diversity, community types, and relative abundance by taxonomic depth. Alpha diversity is the measure of within sample diversity, or how many operational taxonomic units constitute a sample. Beta diversity is a measure of community dissimilarity between samples. Community types are clustering assignments made by Dirichlet multinomial models based off of operational taxonomic unit data (Holmes, Harris et al. 2012). Relative abundance data shows the percent composition by taxonomic level. All outcomes can be of particular interest for dental biofilm research, especially with treatments that shift the community or reduce the burden of established pathogenic taxa. A full demonstration of

16S rRNA community analysis is demonstrated on oral specimen collection and storage techniques (Luo, Srinivasan et al. 2016).

### **Synthesizing All Outcomes**

Traditionally, *in vitro* dental biofilm studies have for many years focused on single-species or consortia-species biofilms to gain understanding into a complex ecosystem. Today, the technology exists for investigators to pursue dental health research with a population-level approach. After all, biofilm function is largely attributable to that of the ecosystem contained within. We have the model systems to synthetically develop representative plaque; we have the microscopy techniques to capture high-resolution images of biofilms over time; we have the 'omics' technology to puzzle together the composition of an undefined community that sprouted from a microcosm; and finally, we have the computational capacity to perform analyses on big data. The challenge remains to put together this treasure trove of community and architectural data, decipher their interplay and associations with each other, and approach biofilm control from a combinatorial approach.

### **Personal Comments**

This five year journey has personally been the most challenging academic years of my life, and while at the same time, the most rewarding. I've always approached education: from grade school, to undergraduate, to Masters, with the same misguided

effort. To show up to class, learn the rigid curriculum, and take exams. Those years provided me with the fundamental knowledge, but not the applied skills to be successful. I was qualified on paper, but not competent. It only took independent study courses where, quoting my supervisor Alex, “the world is your oyster,” did I discover that learning is dynamic and adaptable with no curriculum. For example, under my own initiative, I became proficient at R coding, MatLab programming, software development, metagenomics techniques, and advanced microscopy. These skills are very technical and I had my fair share of troubleshooting and frustration. But every annoying coding bug or command line error fixed with persistence, was met with a lopsided feeling of accomplishment and satisfaction. I became a problem solver, whether simply brute-forcing syntax to see if it works, or using online resources, I was able to eventually navigate to a solution. To me, that is a far superior form of learning than anything I have engaged in, and much more gratifying than any objective test score.

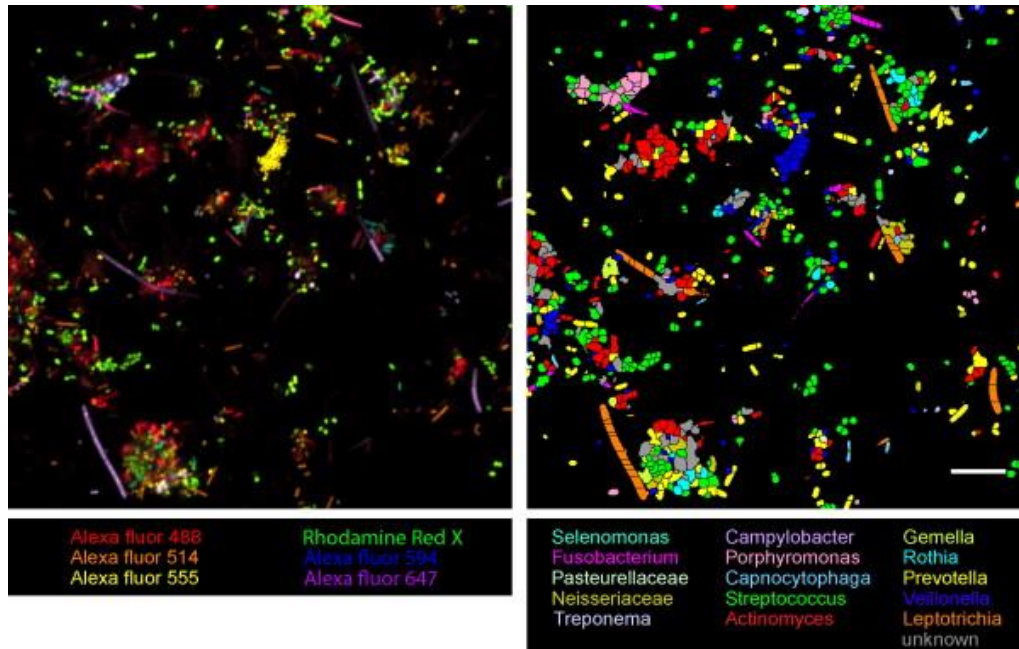


**Figure V.1. Potential Application of BAIT to CLASI-FISH.** 6 pairwise fluorophore combinations were used to create 15 different colors, each labeling a different genus present in the oral cavity. Each color signal indicates spatial presence of a genus. Spatial analysis of multiple signals can provide insight on how genera in the oral cavity interact with each other. Image acquired with permission from Valm et al. (Valm, Mark Welch et al. 2012).

## **APPENDICES**

## **APPENDIX A**

### **Protocol using 24-well Bioflux™ to Develop Dental Biofilms**

#### **Preparation of Pooled Saliva as Inoculum & Medium**

Saliva to be used as a growth media, cell-free saliva (CFS) will be collected, pooled, and prepared according to previously published protocols (Nance, Dowd et al. 2013). Saliva collected will be from healthy volunteers and from individuals with active caries. A portion of the saliva collected will be appropriated as cell-containing saliva (CCS) to be used as inoculum within the microfluidics system. The laboratory protocol will be as follows:

1. Recruit >5 healthy/caries-active individuals for saliva donation. Individuals must not be ill, have taken oral antibiotics in the past 3 months, or have consumed food or liquid, with the exception of water, in the previous 2 hours before donation.
2. Instruct individuals to donate saliva in 50 mL plastic tubes. Pool the collected saliva in a plastic beaker. Pipette 24 mL saliva and transfer to a 50 mL tube. Transfer the plastic beaker with the remaining pool of saliva on ice. Do not use glass as polymers in the saliva will adhere to the internal glass surfaces.

3. Add 8 mL autoclaved glycerol to the tube containing 24 mL pooled saliva to yield 3:1 part saliva:glycerol stock inoculum. Aliquot out to 4 mL into 15 mL tubes for single use cell containing saliva (CCS) inoculum for use per 24-well Bioflux™ run. Add Dithiothreitol (DTT) to the pooled saliva in the plastic beaker to a final concentration of 2.5 mM. Stir or shake for 10 min in a plastic beaker on ice.
4. Centrifuge the pooled saliva for 30 min at 17,500 x g to pellet particulate matter.
5. Dilute the supernatant saliva with 3 volumes of autoclaved deionized water to give one-fourth concentrated saliva.
6. Filter-sterilize saliva using a 0.22 µm polyethersulfone (PES), low protein binding filter. Keep saliva in a plastic container on ice while filtering.
7. Aliquot 25 mL of pooled saliva into 50 mL tubes. Freeze single use aliquots at –80° until needed for use. Each plastic tube is for one use only and should contain no more than 25 mL as each microfluidic well holds a maximum of 3 mL (3 mL x 8 wells = 24 mL) and space is needed in each tube as saliva expands during freezing.

For use, thaw the pooled saliva at room temperature. Once thawed, filter-sterilize once more using 0.22 µm polyethersulfone, low protein binding filter to remove any precipitates.

### **Growth of Dental Microcosm Biofilms**

Biofilms are developed overnight with a growth period of 22 hours. Automated treatment regimens can be implemented using the Bioflux™ software interface. The laboratory protocol will be as follows:

### 1. *CFS pre-treatment*

1. First coat the Bioflux™ microfluidic channels with CFS. Add 1 mL of CFS to each outlet well. Using the Bioflux control software under manual mode, select columns C and F.
2. Set shear to 1.0 dyne/cm<sup>2</sup> and start flow for 2 min at room temperature to ensure homogenous distribution of the CFS throughout the channel. At the end, ensure there is fluid in both inlet wells of each channel to verify that CFS flowed through all channels evenly.
3. Incubate plate at room temperature for 20 min.
4. Remove the remaining CFS in the outlet wells and transfer to the first inlet well. Add 1 mL of treatment solution in the second inlet well. This total volume of 1 mL per inlet well will serve to balance against the pressure being applied to the inoculum from the outlet well.

### 2. *Inoculation*

1. To each outlet well, add 500 µl of CCS inoculum. Place the microfluidic plate on the 37°C heat plate. Enter manual mode within the software interface and set flow from outlet wells to the inlet wells at 1.0 dyne/cm<sup>2</sup> for exactly 12.0 sec.
2. Incubate the microfluidic plate at 37 °C for 45 minutes to allow for initial adherence and growth of the bacteria in the inoculum.

### 3. *Biofilm Development*

1. Enter automatic mode within the software interface. Customize run by ordering sequences. Each sequence can be custom made to select which column(s) will have shear force applied, the amount of force, and duration of force. Ordered sequences may be saved as protocols that will be fully automated after user hits start.
  2. Create a sequence that will introduce flow of CFS at 0.2 dyne/cm<sup>2</sup> for 8,10, and 4 hours from column A & column D (both inlet 1's).
  3. Create a sequence that will deliver a treatment at 2.0 dyne/cm<sup>2</sup> for 2 minutes from column E.
  4. Order sequences from step 2 and step 3 to create an automated protocol. For automated treatment regimens, it should be ordered as CFS 8 hours, treatment, CFS 10 hours, treatment, CFS 4 hours.
  5. Add more CFS to inlet wells as needed depending on the automated protocol length.
  6. Incubate the microfluidic plate at 37 °C, select automatic on the software interface and select automated protocol to run.
4. *Stain prewash*
1. Aspirate all fluid from the inlet and outlet wells and add 500 µl of PBS (pH 7.4) to each of the inlet wells. Flow from inlet 1 for 20 min at 0.2 dyne/cm<sup>2</sup>.
5. *Stain mixture addition*
1. For cell viability staining make 100 µl of stain mixture for each channel to be stained. Specifically, add 3 µl of SYTO 9 and 3 µl of propidium iodide per mL of PBS using commercial cell viability staining kit such as LIVE/DEAD™.

2. Aspirate the remaining PBS from the first inlet well and then add 100  $\mu\text{l}$  of the cell viability stain mixture to the center of each well. Set flow at 0.2  $\text{dyne}/\text{cm}^2$  and run the solution from inlet to outlet for 45 min at room temperature.
6. *Post-staining wash*
1. Aspirate the remaining stain in each of the inlet wells and add 500  $\mu\text{l}$  of PBS to each inlet well. Set to flow at 0.2  $\text{dyne}/\text{cm}^2$  and run the PBS solution from inlet to outlet for 20 min at room temperature to remove any excess stain.

### **Objective Imaging Strategy**

After staining with LIVE/DEAD™, biofilm samples will be imaged five times along the viewing port, as detailed in **Figure IV.3**. The confocal laser scanning microscope used is an adapted Leica SPE (Leica, Buffalo Grove, IL). Biofilms will be imaged using a 40X 1.25 NA HCX PL APO infinity-corrected oil objective. All renderings and quantification analyses will be performed on a computer equipped with an Intel i7 processor (Intel, Santa Clara, CA) supported with two Nvidia GTX 970m graphics cards in SLI (Nvidia, Santa Clara, CA). Captured renderings will be assembled in CORELDRAW v. X7 (Corel, Mountain View, CA). The protocol is as follows:

1. Before imaging, optimize the laser intensity, gain, offset, and digital zoom. For the LIVE/DEAD™ stain cocktail used, we used 15% laser intensity, 900 gain, -

- 7.6% offset, and 1.00x digital zoom. Additionally, the images were captured at 512x512 resolution and each Z-slice was taken 1 $\mu$ M apart.
2. Locate the viewing port containing the four samples within the plate's column. Locate the first sample's inlet junction and position the field of view so that the left side touches the intersection. At 1.00x digital zoom, the top and bottom of the field of view should capture nearly the entire Y-length of the channel.
  3. Image the height of the biofilm by setting Z-coordinates. If no biofilm is present, take a 10 $\mu$ M thick image.
  4. Move the microscope stage down to the second sample. The left side of the field of view should align with the inlet junction of the second sample. Image the biofilm and continue down to Sample 4.
  5. At sample four, move the x-axis knob counterclockwise one full rotation to move the stage to the left. The 2<sup>nd</sup> image of sample 4 should be taken now, followed by the 2<sup>nd</sup> image of sample 3, 2, and 1.
  6. Continue the imaging strategy in the described serpentine pattern until five images per sample have been captured.
  7. If necessary, image the 4 samples contained within the other half of the plate.
  8. Name each confocal stack so that it can be readily identified. Save the experiment in the native .lif archive offered by Leica.

### **Harvesting Biofilm Cells for 16S rRNA Community Profiling**

After all images had been captured, biofilm cells can be harvested for culture-independent analysis. This involves a wash protocol to ensure the waste well is cleansed of all effluent. The protocol for this is as follows:

1. Aspirate all remaining fluid from the 24 wells.
2. Add 1 mL of ultrapure water into each of the 24 wells and place plate on a shaker at 120 RPM for five minutes.
3. Repeat the wash with ultrapure water for a total of three washes.
4. At the end of the third wash, aspirate all water and add 500 $\mu$ L of water into columns C and F (outlet wells).
5. Pulse the water from outlet to the two inlets at 20.0 dyne/cm<sup>2</sup> for 20 minutes. At the end of the 20 minutes, pulse the water from the inlets back into the outlet well at 20.0 dyne/cm<sup>2</sup> for 20 minutes.
6. Collect the sample from the outlet well and freeze at -80°C until ready for DNA extraction.

### **Calculation of Weighted Viability**

The traditional method of calculating viability involves using the dynamic 8-bit range of image histograms in both the propidium iodide and Syto-9 channels. Since viability is calculated by weighing higher intensity signals, the terminology used will be weighted viability, which differs from unweighted viability calculated by BAIT. Weighted viability is calculated from the saved .lif file post-imaging. The .lif confocal archive will

need to be batch converted into .ome (open-microscopy environment) files to be read as input by ImageJ (Collins 2007). The protocol is as follows:

1. Open Imaris software (Bitplane, Zurich, Switzerland). Under File, select batch convert. Convert all confocal stacks into .ome files into a specified directory.
2. Open ImageJ. Under file, select open and navigate to the directory containing all .ome files. Select an .ome file and ensure the “Split Channels” checkbox is checked.
3. For both channels, hit ctrl+h to generate an intensity histogram for each channel (**Figure A.1**).
4. The intensity histogram distribution from 0-255 can be copied onto clipboard and pasted into a spreadsheet software for viability calculation.
5. Weighted viability is calculated as follows:

$$WV = \frac{\sum_{i=0}^{255} i * g(i)}{\sum_{i=0}^{255} i * r(i) + \sum_{i=0}^{255} i * g(i)}$$

Where  $i$  = intensity ranging from 0-255.

$g(i)$  = number of total green voxels with intensity value  $i$ .

$r(i)$  = number of total red voxels with intensity value  $i$ .

$WV$  = biofilm weighted viability as a proportion.

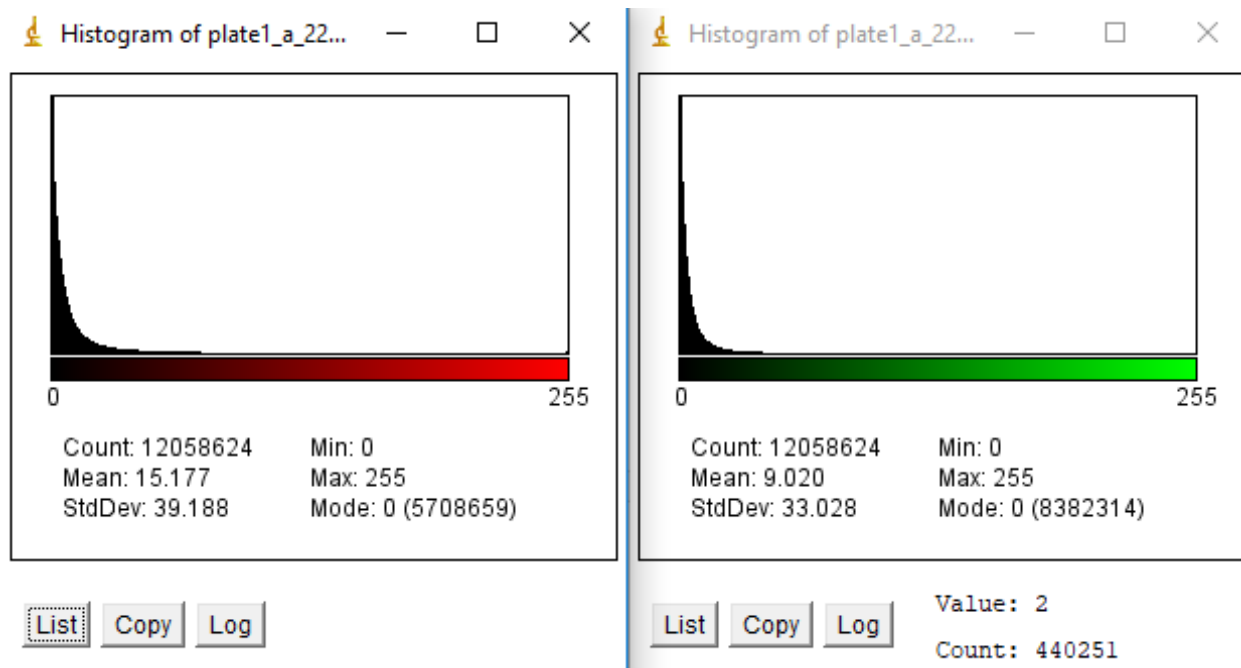


**Figure A.1. Intensity Histograms of Red & Green Channels.** The distribution of intensity signal is retrievable with ImageJ from an open microscopy environment (.ome) file. The distributions of both channels are used to calculate viability. Each voxel within the confocal image stack contains a 0-255 value indicating the brilliance of signal detected at that particular voxel space. 0 indicates no signal and 255 indicates the most brilliant. In the Syto-9 channel histogram on the right, 440,251 voxels contain the intensity value of 2.

## APPENDIX B

### Publications

- 1) Samarian, D. S., Jakubovics, N. S., **Luo, T. L.**, Rickard, A. H. Use of a high-throughput *in vitro* microfluidic system to develop oral multi-species biofilms. *Journal of Visualized Experiments* (94), e52467, doi:10.3791/52467 (2014).
- 2) Noe-Hays, A., Nace, K., Patel, N., Lahr, R.H., Goetsch, H.E., Mullen, R., Love, N.G., Aga, D.S., Bott, C.B., Foxman, B., Jimenez, J.A., **Luo, T.L.**, Ramadugu, K.R., Wigginton, K. Urine diversion for nutrient recovery and micropollutant management: results from a regional urine recycling program. *Proceedings of the Water Environment Federation (WEFTEC 2015: Session 203 – 209)*, doi: 10.2175/193864715819538921 (2015).
- 3) Goetsch, H.E., Mullen, R., Lahr, R.H., Noe-Hays, A., Aga, D.S., Bott, C.B., Foxman, B., Jimenez, J.A., Love, N.G., **Luo, T.L.**, Nace, K., Ramadugu, K.R., Wigginton, K. Fate of pharmaceutical and biological contaminants through the preparation and application of urine derived fertilizers. *Proceedings of the Water Environment Federation (WEFTEC 2015: Session 500-509)*, doi: 10.2175/193864715819541945 (2015).

- 4) **Luo, T.L.**, Rickard, A.H., Srinivasan, U., Kaye, K., Foxman, B. Association of *bla<sub>OXA-23</sub>* and *bap* with the persistence of *Acinetobacter baumannii* within a major healthcare system. *Frontiers in Microbiology* (6), doi: 10.3389/fmicb.2015.00182 (2015).
- 5) Stevens, M.R., **Luo, T.L.**, Vornhagen, J., Jakubovics, N.S., Gilsdorf, J., Marrs, C.F., Møretrø, T., Rickard, A.H. Coaggregation occurs between microorganisms from different environments. *FEMS Microbiology Ecology* (91), doi: 10.1093/femsec/fiv123 (2015).
- 6) Ismail, M.D., **Luo, T.L.**, McNamara, S.E., Lansing, B., Koo, E., Mody, L., Foxman, B. Long-term carriage of ciprofloxacin-resistant *Escherichia coli* isolates in high-risk nursing home residents. *Infection Control and Hospital Epidemiology* (4), doi: 10.1017/ice.2015.326 (2016).
- 7) Foxman, B., **Luo, T.L.**, Srinivasan, U., Ramadugu, K., Wen, A., Goldberg, D., Shedden, K., Crout, R., McNeil, D.W., Weyant, R.J., Marazita, M.L. The effects of family, dentition, and dental caries on salivary microbiome. *Annals of Epidemiology* (26), doi: 10.1016/j.annepidem.2016.03.006 (2016).
- 8) **Luo, T.L.**, Srinivasan, U., Ramadugu, K., Shedden, K., Trumble, E.L., Li, J., Neiswanger, K., Crout, R., McNeil, D., Weyant, R.J., Marazita, M.L., Foxman, F. Validation of Specimen Collection Methods for 16S Oral Microbial Community Analysis. *Applied and Environmental Microbiology* (82), doi: 10.1128/AEM.01132-16 (2016).
- 9) Lahr, R.H., Goetsch, H.E., Haig, S., Noe-Hays, A., Love, N.G., Aga, D.S., Bott, C.B., Foxman, B., Jimenez, J.A., **Luo, T.L.**, Nace, K., Ramadugu, K., Wigginton,

- K.R. Urine bacterial community convergence through fertilizer production: storage, pasteurization, and struvite precipitation. *Environmental Science & Technology* (50), doi: 10.1021/acs.est.6b02094 (2016).
- 10) Rostami, N., Shields, R.C., Yassin, S., Hawkins, A.R., Bowen, L., **Luo, T.L.**, Rickard, A.H., Holliday, R., Preshaw, P.M., Jakubovics, N.S. A critical role for extracellular DNA in dental plaque formation. *Journal of Dental Research* (96), doi: 10.1177/0022034516675849 (2016).
- 11) Shin, J.M., **Luo, T.L.**, Kamarajan, P., Fenno, J.C., Rickard, A.H., Kapila, Y.L. Microbial communities associated with primary and metastatic head and neck squamous cell carcinoma – a high Fusobacterial and low Streptococcal signature. *Nature Scientific Reports* (7), doi: 10.1038/s41598-017-09786-x (2017).

## APPENDIX C

### Posters

- 1) **Luo, T.L.**, Rickard, A.H., Foxman, B., Kaye, K., Srinivasan, U. Antibiotic resistance and biofilm-forming ability mediate dissemination of *Acinetobacter baumannii* strains within a healthcare system. ICAAC 2014.
- 2) **Luo, T.L.**, Srinivasan, U., Ramadugu, K., Shedden, K., Trumble, E.L., Li, J., Neiswanger, K., Crout, R., McNeil, D., Weyant, R.J., Marazita, M.L., Foxman, F. Validation of Specimen Collection Methods for Oral Microbial Community Analysis. IADR 2015.
- 3) **Luo, T.L.**, Zsiska, M., Circello, B.T., Eisenberg, M., Gonzalez-Cabezas, C., Foxman, B., MARRS, C.F., Rickard, A.H. *In vitro* inhibition of oral biofilm development by stannous fluoride. BSODR 2017.
- 4) **Luo, T.L.**, Eisenberg, M., Hayashi, M., Gonzalez-Cabezas, C., Foxman, B., MARRS, C.F., Rickard, A.H. A sensitive thresholding method for confocal laser scanning microscope image stacks of microbial biofilms. University of Michigan School of Dentistry Research Day 2018.

## References

- Aas, J. A., A. L. Griffen, S. R. Dardis, A. M. Lee, I. Olsen, F. E. Dewhirst, E. J. Leys and B. J. Paster (2008). "Bacteria of dental caries in primary and permanent teeth in children and young adults." J Clin Microbiol **46**(4): 1407-1417.
- Abdulkareem, E. H., K. Memarzadeh, R. P. Allaker, J. Huang, J. Pratten and D. Spratt (2015). "Anti-biofilm activity of zinc oxide and hydroxyapatite nanoparticles as dental implant coating materials." J Dent **43**(12): 1462-1469.
- Agnello, M., L. Cen, N. C. Tran, W. Shi, J. S. McLean and X. He (2017). "Arginine Improves pH Homeostasis via metabolism and microbiome modulation." J Dent Res **96**(8): 924-930.
- Akers, K. S., K. Mende, K. A. Cheatle, W. C. Zera, X. Yu, M. L. Beckius, D. Aggarwal, P. Li, C. J. Sanchez, J. C. Wenke, A. C. Weintrob, D. R. Tribble, and C. K. Murray (2014). "Biofilms and persistent wound infections in United States military trauma patients: a case-control analysis." BMC Infect Dis **14**: 190.
- Anolik, R., R. J. Berkowitz, J. M. Campos and A. D. Friedman (1981). "*Actinobacillus* endocarditis associated with periodontal disease." Clin Pediatr (Phila) **20**(10): 653-655.
- Arce, S. H., P. H. Wu and Y. Tseng (2013). "Fast and accurate automated cell boundary determination for fluorescence microscopy." Sci Rep **3**: 2266.
- Axelsson, P., B. Nystrom and J. Lindhe (2004). "The long-term effect of a plaque control program on tooth mortality, caries and periodontal disease in adults. Results after 30 years of maintenance." J Clin Periodontol **31**(9): 749-757.
- Azevedo, N. F., S. P. Lopes, C. W. Keevil, M. O. Pereira and M. J. Vieira (2009). "Time to "go large" on biofilm research: advantages of an omics approach." Biotechnol Lett **31**(4): 477-485.
- Baehni, P. C. and Y. Takeuchi (2003). "Anti-plaque agents in the prevention of biofilm-associated oral diseases." Oral Dis **9 Suppl 1**: 23-29.
- Bakke, R., Olsson, P.Q. (1986). "Biofilm thickness measurements by light microscopy." J Microb Met **5**(2): 93-98.
- Bang, H. and C. E. Davis (2007). "On estimating treatment effects under non-compliance in randomized clinical trials: Are intent-to-treat or instrumental variables analyses perfect solutions?" Statistics in Medicine **26**(5): 954-964.

- Baradez, M. O., McGuckin, C.P., Forraz, N., Pettengell, R., Hoop, A. (2003). "Robust and automated unimodal histogram thresholding and potential applications." Pattern Recognition **37**(6): 1131-1148.
- Battin, T. J., L. A. Kaplan, J. D. Newbold, X. Cheng and C. Hansen (2003). "Effects of current velocity on the nascent architecture of stream microbial biofilms." Appl Environ Microbiol **69**(9): 5443-5452.
- Baveye, P. (2002). "Comment on 'Evaluation of biofilm image thresholding methods'." Water Res **36**(3): 805-807.
- Behjati, S. and P. S. Tarpey (2013). "What is next generation sequencing?" Arch Dis Child Educ Pract Ed **98**(6): 236-238.
- Beikler, T. and T. F. Flemmig (2011). "Oral biofilm-associated diseases: trends and implications for quality of life, systemic health and expenditures." Periodontol 2000 **55**(1): 87-103.
- Benoit, M. R., C. G. Conant, C. Ionescu-Zanetti, M. Schwartz and A. Martin (2010). "New device for high-throughput viability screening of flow biofilms." Appl Environ Microbiol **76**(13): 4136-4142.
- Bergouignan, L., M. Chupin, Y. Czechowska, S. Kinkingnehun, C. Lemogne, G. Le Bastard, M. Lepage, L. Garnero, O. Colliot and P. Fossati (2009). "Can voxel based morphometry, manual segmentation and automated segmentation equally detect hippocampal volume differences in acute depression?" Neuroimage **45**(1): 29-37.
- Berry, C. W. and C. A. Henry (1977). "The effect of adsorption on the acid production of caries and noncaries-producing streptococci." J Dent Res **56**(10): 1193-1200.
- Bester, E., O. Kroukamp, M. Hausner, E. A. Edwards and G. M. Wolfaardt (2011). "Biofilm form and function: carbon availability affects biofilm architecture, metabolic activity and planktonic cell yield." J Appl Microbiol **110**(2): 387-398.
- Beyenal, H., C. Donovan, Z. Lewandowski and G. Harkin (2004). "Three-dimensional biofilm structure quantification." J Microbiol Methods **59**(3): 395-413.
- Beyenal, H., Z. Lewandowski and G. Harkin (2004). "Quantifying biofilm structure: facts and fiction." Biofouling **20**(1): 1-23.
- Blanc, V., S. Isabal, M. C. Sanchez, A. Llama-Palacios, D. Herrera, M. Sanz and R. Leon (2014). "Characterization and application of a flow system for *in vitro* multispecies oral biofilm formation." J Periodontal Res **49**(3): 323-332.
- Bomchil, N., P. Watnick and R. Kolter (2003). "Identification and characterization of a *Vibrio cholerae* gene, *mbaA*, involved in maintenance of biofilm architecture." J Bacteriol **185**(4): 1384-1390.

- Borrell, L. N. and N. D. Crawford (2012). "Socioeconomic position indicators and periodontitis: examining the evidence." Periodontol 2000 **58**(1): 69-83.
- Bradshaw, D. J. and R. J. Lynch (2013). "Diet and the microbial aetiology of dental caries: new paradigms." Int Dent J **63 Suppl 2**: 64-72.
- Bradshaw, D. J., P. D. Marsh, G. K. Watson and C. Allison (1998). "Role of *Fusobacterium nucleatum* and coaggregation in anaerobe survival in planktonic and biofilm oral microbial communities during aeration." Infect Immun **66**(10): 4729-4732.
- Brambilla, E., A. Ionescu, A. Mazzoni, M. Cadenaro, M. Gagliani, M. Ferraroni, F. Tay, D. Pashley and L. Breschi (2014). "Hydrophilicity of dentin bonding systems influences *in vitro* *Streptococcus mutans* biofilm formation." Dent Mater **30**(8): 926-935.
- Brambilla, E., Ionescu, A.C., Cazzaniga, G., Ottobelli, M., Mazzonni, A., Cadenaro, M., Gagliani, M., Tay, F.R., Pashley, D.H., Breschi, L. (2017). "*In vitro* *Streptococcus mutans* biofilm formation on surfaces of chlorhexidine-containing dentin bonding systems." Internat J Adhesion Adhesives **75**: 23-30.
- Bridier, A., F. Dubois-Brissonnet, A. Boubetra, V. Thomas and R. Briandet (2010). "The biofilm architecture of sixty opportunistic pathogens deciphered using a high throughput CLSM method." J Microbiol Methods **82**(1): 64-70.
- Bridier, A., T. Meylheuc and R. Briandet (2013). "Realistic representation of *Bacillus subtilis* biofilms architecture using combined microscopy (CLSM, ESEM and FESEM)." Micron **48**: 65-69.
- Caicedo, J. C., S. Cooper, F. Heigwer, S. Warchal, P. Qiu, C. Molnar, A. S. Vasilevich, J. D. Barry, H. S. Bansal, O. Kraus, M. Wawer, L. Paavolainen, M. D. Herrmann, M. Rohban, J. Hung, H. Hennig, J. Concannon, I. Smith, P. A. Clemons, S. Singh, P. Rees, P. Horvath, R. G. Linington and A. E. Carpenter (2017). "Data-analysis strategies for image-based cell profiling." Nat Methods **14**(9): 849-863.
- Camosci, D. A. and N. Tinanoff (1984). "Anti-bacterial determinants of stannous fluoride." J Dent Res **63**(9): 1121-1125.
- Casanova, L., F. J. Hughes and P. M. Preshaw (2014). "Diabetes and periodontal disease: a two-way relationship." Br Dent J **217**(8): 433-437.
- Cenci, M. S., T. Pereira-Cenci, J. A. Cury and J. M. Ten Cate (2009). "Relationship between gap size and dentine secondary caries formation assessed in a microcosm biofilm model." Caries Res **43**(2): 97-102.
- Cheng, X., J. Liu, J. Li, X. Zhou, L. Wang, J. Liu and X. Xu (2017). "Comparative effect of a stannous fluoride toothpaste and a sodium fluoride toothpaste on a multispecies biofilm." Arch Oral Biol **74**: 5-11.

Chukkapalli, S. S., M. Easwaran, M. F. Rivera-Kweh, I. M. Velsko, S. Ambadapadi, J. Dai, H. Larjava, A. R. Lucas and L. Kesavalu (2017). "Sequential colonization of periodontal pathogens in induction of periodontal disease and atherosclerosis in LDLRnull mice." Pathog Dis **75**(1).

Chun, J., K. Y. Kim, J. H. Lee and Y. Choi (2010). "The analysis of oral microbial communities of wild-type and toll-like receptor 2-deficient mice using a 454 GS FLX Titanium pyrosequencer." BMC Microbiol **10**: 101.

Coenye, T., K. De Prijck, B. De Wever and H. J. Nelis (2008). "Use of the modified Robbins device to study the *in vitro* biofilm removal efficacy of NitrAdine, a novel disinfecting formula for the maintenance of oral medical devices." J Appl Microbiol **105**(3): 733-740.

Coenye, T. and H. J. Nelis (2010). "*In vitro* and *in vivo* model systems to study microbial biofilm formation." J Microbiol Methods **83**(2): 89-105.

Collins, T. J. (2007). "ImageJ for microscopy." Biotechniques **43**(1 Suppl): 25-30.

Costerton, J. W., K. J. Cheng, G. G. Geesey, T. I. Ladd, J. C. Nickel, M. Dasgupta and T. J. Marrie (1987). "Bacterial biofilms in nature and disease." Annu Rev Microbiol **41**: 435-464.

Costerton, J. W., G. G. Geesey and K. J. Cheng (1978). "How bacteria stick." Sci Am **238**(1): 86-95.

Coulter, W. A. and C. Russell (1976). "pH and Eh in single and mixed culture bacterial plaque in an artificial mouth." J Appl Bacteriol **40**(1): 73-87.

Davies, D. (2003). "Understanding biofilm resistance to antibacterial agents." Nat Rev Drug Discov **2**(2): 114-122.

de Carvalho, C. C. and M. M. da Fonseca (2007). "Assessment of three-dimensional biofilm structure using an optical microscope." Biotechniques **42**(5): 616, 618-620.

de Chaumont, F., S. Dallongeville, N. Chenouard, N. Herve, S. Pop, T. Provoost, V. Meas-Yedid, P. Pankajakshan, T. Lecomte, Y. Le Montagner, T. Lagache, A. Dufour and J. C. Olivo-Marin (2012). "Icy: an open bioimage informatics platform for extended reproducible research." Nat Methods **9**(7): 690-696.

Deng, D. M. and J. M. ten Cate (2004). "Demineralization of dentin by *Streptococcus mutans* biofilms grown in the constant depth film fermentor." Caries Res **38**(1): 54-61.

Deng, D. M., C. van Loveren and J. M. ten Cate (2005). "Caries-preventive agents induce remineralization of dentin in a biofilm model." Caries Res **39**(3): 216-223.

Derlon, N., A. Grutter, F. Brandenberger, A. Sutter, U. Kuhlicke, T. R. Neu and E. Morgenroth (2016). "The composition and compression of biofilms developed on ultrafiltration membranes determine hydraulic biofilm resistance." Water Res **102**: 63-72.

Dewhirst, F. E., T. Chen, J. Izard, B. J. Paster, A. C. Tanner, W. H. Yu, A. Lakshmanan and W. G. Wade (2010). "The human oral microbiome." J Bacteriol **192**(19): 5002-5017.

Dhadse, P., D. Gattani and R. Mishra (2010). "The link between periodontal disease and cardiovascular disease: How far we have come in last two decades?" J Indian Soc Periodontol **14**(3): 148-154.

Diaz, P. I. (2012). "Microbial diversity and interactions in subgingival biofilm communities." Front Oral Biol **15**: 17-40.

Diaz, P. I., N. I. Chalmers, A. H. Rickard, C. Kong, C. L. Milburn, R. J. Palmer, Jr. and P. E. Kolenbrander (2006). "Molecular characterization of subject-specific oral microflora during initial colonization of enamel." Appl Environ Microbiol **72**(4): 2837-2848.

Dibdin, G. H., R. P. Shellis and C. M. Wilson (1976). "An apparatus for the continuous culture of micro-organisms on solid surfaces with special reference to dental plaque." J Appl Bacteriol **40**(3): 261-268.

Dige, I., H. Nilsson, M. Kilian and B. Nyvad (2007). "*In situ* identification of streptococci and other bacteria in initial dental biofilm by confocal laser scanning microscopy and fluorescence *in situ* hybridization." Eur J Oral Sci **115**(6): 459-467.

Ding, Y., W. Wang, M. Fan, Z. Tong, R. Kuang, W. Jiang and L. Ni (2014). "Antimicrobial and anti-biofilm effect of Bac8c on major bacteria associated with dental caries and *Streptococcus mutans* biofilms." Peptides **52**: 61-67.

Dombrowsky, M., A. Kirschner and R. Sommer (2013). "PVC-piping promotes growth of *Ralstonia pickettii* in dialysis water treatment facilities." Water Sci Technol **68**(4): 929-933.

Drescher, K., J. Dunkel, C. D. Nadell, S. van Teeffelen, I. Grnja, N. S. Wingreen, H. A. Stone and B. L. Bassler (2016). "Architectural transitions in *Vibrio cholerae* biofilms at single-cell resolution." Proc Natl Acad Sci U S A **113**(14): E2066-2072.

Dufour, D., Leung, Vincent, Lévesque, Céline M. (2010). "Bacterial biofilm: structure, function, and antimicrobial resistance." Endodontic Topics **22**(1).

Dye, B. A. (2012). "Global periodontal disease epidemiology." Periodontol 2000 **58**(1): 10-25.

Edlund, A., Y. Yang, A. P. Hall, L. Guo, R. Lux, X. He, K. E. Nelson, K. H. Neilson, S. Yooseph, W. Shi and J. S. McLean (2013). "An *in vitro* biofilm model system maintaining a highly reproducible species and metabolic diversity approaching that of the human oral microbiome." Microbiome **1**(1): 25.

- Egland, P. G., R. J. Palmer, Jr. and P. E. Kolenbrander (2004). "Interspecies communication in *Streptococcus gordonii*-*Veillonella atypica* biofilms: signaling in flow conditions requires juxtaposition." Proc Natl Acad Sci U S A **101**(48): 16917-16922.
- Ellingsen, J. E., B. Svaton and G. Rolla (1980). "The effects of stannous and stannic ions on the formation and acidogenicity of dental plaque *in vivo*." Acta Odontol Scand **38**(4): 219-222.
- Elliott, D., J. Pratten, M. Edwards, J. Crowther, A. Petrie and M. Wilson (2005). "Bacterial biofilm development on hydroxyapatite-coated glass." Curr Microbiol **51**(1): 41-45.
- Fan, Y., Z. T. Wen, S. Liao, T. Lallier, J. L. Hagan, J. T. Twomley, J. F. Zhang, Z. Sun and X. Xu (2012). "Novel amelogenin-releasing hydrogel for remineralization of enamel artificial caries." J Bioact Compat Polym **27**(6): 585-603.
- Feldman, M., J. Shenderovich, E. Lavy, M. Friedman and D. Steinberg (2017). "A sustained-release membrane of thiazolidinedione-8: effect on formation of a *Candida*/bacteria mixed biofilm on hydroxyapatite in a continuous flow model." Biomed Res Int **2017**: 3510124.
- Fernandez, C. E., M. B. Aspiras, M. W. Dodds, C. Gonzalez-Cabezas and A. H. Rickard (2017). "The effect of inoculum source and fluid shear force on the development of *in vitro* oral multispecies biofilms." J Appl Microbiol **122**(3): 796-808.
- Flemming, H. C. and J. Wingender (2010). "The biofilm matrix." Nat Rev Microbiol **8**(9): 623-633.
- Foley, I. and P. Gilbert (1996). "Antibiotic resistance of biofilms." Biofouling **10**(4): 331-346.
- Foster, J. S. and P. E. Kolenbrander (2004). "Development of a multispecies oral bacterial community in a saliva-conditioned flow cell." Appl Environ Microbiol **70**(7): 4340-4348.
- Foster, J. S., Pan, P.C., Kolenbrander, P.E. (2004). "Effects of antimicrobial agents on oral biofilms in a saliva-conditioned flowcell." Biofilms **1**(1): 5-12.
- Fritz, J. V., M. S. Desai, P. Shah, J. G. Schneider and P. Wilmes (2013). "From meta-omics to causality: experimental models for human microbiome research." Microbiome **1**(1): 14.
- Gabrilska, R. A. and K. P. Rumbaugh (2015). "Biofilm models of polymicrobial infection." Future Microbiol **10**(12): 1997-2015.
- Geismar, K., K. Stoltze, B. Sigurd, F. Gyntelberg and P. Holmstrup (2006). "Periodontal disease and coronary heart disease." J Periodontol **77**(9): 1547-1554.
- Genco, R. J. and W. S. Borgnakke (2013). "Risk factors for periodontal disease." Periodontol 2000 **62**(1): 59-94.

- Gilbert, P., D. G. Allison, D. J. Evans, P. S. Handley and M. R. Brown (1989). "Growth rate control of adherent bacterial populations." Appl Environ Microbiol **55**(5): 1308-1311.
- Graves, D. T., J. Kang, O. Andriankaja, K. Wada and C. Rossa, Jr. (2012). "Animal models to study host-bacteria interactions involved in periodontitis." Front Oral Biol **15**: 117-132.
- Grembowski, D., D. A. Conrad and P. Milgrom (1987). "Dental care demand among children with dental insurance." Health Serv Res **21**(6): 755-775.
- Gross, E. L., C. J. Beall, S. R. Kutsch, N. D. Firestone, E. J. Leys and A. L. Griffen (2012). "Beyond *Streptococcus mutans*: dental caries onset linked to multiple species by 16S rRNA community analysis." PLoS One **7**(10): e47722.
- Guggenheim, B., E. Giertsen, P. Schupbach and S. Shapiro (2001). "Validation of an *in vitro* biofilm model of supragingival plaque." J Dent Res **80**(1): 363-370.
- Guggenheim, B., R. Gmur, J. C. Galicia, P. G. Stathopoulou, M. R. Benakanakere, A. Meier, T. Thurnheer and D. F. Kinane (2009). "*In vitro* modeling of host-parasite interactions: the 'subgingival' biofilm challenge of primary human epithelial cells." BMC Microbiol **9**: 280.
- Haffajee, A. D. and S. S. Socransky (2006). "Introduction to microbial aspects of periodontal biofilm communities, development and treatment." Periodontol 2000 **42**: 7-12.
- Hajishengallis, G. and R. J. Lamont (2012). "Beyond the red complex and into more complexity: the polymicrobial synergy and dysbiosis (PSD) model of periodontal disease etiology." Mol Oral Microbiol **27**(6): 409-419.
- Hall-Stoodley, L., J. W. Costerton and P. Stoodley (2004). "Bacterial biofilms: from the natural environment to infectious diseases." Nat Rev Microbiol **2**(2): 95-108.
- Han, J. J., C. Kiss, A. R. Bradbury and J. H. Werner (2012). "Time-resolved, confocal single-molecule tracking of individual organic dyes and fluorescent proteins in three dimensions." ACS Nano **6**(10): 8922-8932.
- Harford, J. and S. Chrisopoulos (2012). "Productivity losses from dental problems." Aust Dent J **57**(3): 393-397.
- Harriott, M. M. and M. C. Noverr (2011). "Importance of *Candida*-bacterial polymicrobial biofilms in disease." Trends Microbiol **19**(11): 557-563.
- Henrici, A. T. (1933). "Studies of freshwater bacteria: I. a direct microscopic technique." J Bacteriol **25**(3): 277-287.
- Heydorn, A., A. T. Nielsen, M. Hentzer, C. Sternberg, M. Givskov, B. K. Ersboll and S. Molin (2000). "Quantification of biofilm structures by the novel computer program COMSTAT." Microbiology **146** ( Pt 10): 2395-2407.

- Hill, K. E., S. Malic, R. McKee, T. Rennison, K. G. Harding, D. W. Williams and D. W. Thomas (2010). "An *in vitro* model of chronic wound biofilms to test wound dressings and assess antimicrobial susceptibilities." J Antimicrob Chemother **65**(6): 1195-1206.
- Hodgson, A. E., S. M. Nelson, M. R. Brown and P. Gilbert (1995). "A simple *in vitro* model for growth control of bacterial biofilms." J Appl Bacteriol **79**(1): 87-93.
- Hojo, K., S. Nagaoka, T. Ohshima and N. Maeda (2009). "Bacterial interactions in dental biofilm development." J Dent Res **88**(11): 982-990.
- Holm, E. R., M. P. Schultz, E. G. Haslbeck, W. J. Talbott and A. J. Field (2004). "Evaluation of hydrodynamic drag on experimental fouling-release surfaces, using rotating disks." Biofouling **20**(4-5): 219-226.
- Holmes, I., K. Harris and C. Quince (2012). "Dirichlet multinomial mixtures: generative models for microbial metagenomics." PLoS One **7**(2): e30126.
- Honraet, K. and H. J. Nelis (2006). "Use of the modified robbins device and fluorescent staining to screen plant extracts for the inhibition of *S. mutans* biofilm formation." J Microbiol Methods **64**(2): 217-224.
- Hope, C. K., K. Bakht, G. Burnside, G. C. Martin, G. Burnett, E. de Josselin de Jong and S. M. Higham (2012). "Reducing the variability between constant-depth fermenter experiments when modelling oral biofilm." J Appl Microbiol **113**(3): 601-608.
- Hope, C. K., D. Clements and M. Wilson (2002). "Determining the spatial distribution of viable and nonviable bacteria in hydrated microcosm dental plaques by viability profiling." J Appl Microbiol **93**(3): 448-455.
- Hu, M., Zhang, T.C., Stansbury, J., Neal, J., Garboczi, E.J. (2013). "Determination of porosity and thickness of biofilm attached on irregular-shaped media." J Environ Engin **139**(7): 923-931.
- Huang, R., M. Li and R. L. Gregory (2011). "Bacterial interactions in dental biofilm." Virulence **2**(5): 435-444.
- Jakubovics, N. S. and P. E. Kolenbrander (2010). "The road to ruin: the formation of disease-associated oral biofilms." Oral Dis **16**(8): 729-739.
- Janda, J. M. and S. L. Abbott (2007). "16S rRNA gene sequencing for bacterial identification in the diagnostic laboratory: pluses, perils, and pitfalls." J Clin Microbiol **45**(9): 2761-2764.
- Johnston, M. D., Jones, M.V. (1995). "Disinfection tests with intact biofilms: combined use of the modified Robbins device with impedance detection." J Microb Met **21**(1): 15-26.
- Joo, H. S. and M. Otto (2012). "Molecular basis of *in vivo* biofilm formation by bacterial pathogens." Chem Biol **19**(12): 1503-1513.

- Kantarci, A., H. Hasturk and T. E. Van Dyke (2015). "Animal models for periodontal regeneration and peri-implant responses." Periodontol 2000 **68**(1): 66-82.
- Kassebaum, N. J., E. Bernabe, M. Dahiya, B. Bhandari, C. J. Murray and W. Marcenes (2015). "Global burden of untreated caries: a systematic review and metaregression." J Dent Res **94**(5): 650-658.
- Kim, H. Y. (2013). "Statistical notes for clinical researchers: evaluation of measurement error 1: using intraclass correlation coefficients." Restor Dent Endod **38**(2): 98-102.
- Kinniment, S. L., J. W. Wimpenny, D. Adams and P. D. Marsh (1996). "Development of a steady-state oral microbial biofilm community using the constant-depth film fermenter." Microbiology **142 ( Pt 3)**: 631-638.
- Kistler, J. O., M. Pesaro and W. G. Wade (2015). "Development and pyrosequencing analysis of an *in-vitro* oral biofilm model." BMC Microbiol **15**: 24.
- Kolderman, E., D. Bettampadi, D. Samarian, S. E. Dowd, B. Foxman, N. S. Jakubovics and A. H. Rickard (2015). "L-arginine destabilizes oral multi-species biofilm communities developed in human saliva." PLoS One **10**(5): e0121835.
- Kolenbrander, P. E., R. J. Palmer, Jr., A. H. Rickard, N. S. Jakubovics, N. I. Chalmers and P. I. Diaz (2006). "Bacterial interactions and successions during plaque development." Periodontol 2000 **42**: 47-79.
- Koo, T. K. and M. Y. Li (2016). "A guideline of selecting and reporting intraclass correlation coefficients for reliability research." J Chiropr Med **15**(2): 155-163.
- Koopman, J. E., M. J. Buijs, B. W. Brandt, B. J. Keijser, W. Crielaard and E. Zaura (2016). "Nitrate and the origin of saliva influence composition and short chain fatty acid production of oral microcosms." Microb Ecol **72**(2): 479-492.
- Koopman, J. E., W. F. Roling, M. J. Buijs, C. H. Sissons, J. M. ten Cate, B. J. Keijser, W. Crielaard and E. Zaura (2015). "Stability and resilience of oral microcosms toward acidification and *Candida* outgrowth by arginine supplementation." Microb Ecol **69**(2): 422-433.
- Krespi, Y. P., M. G. Shrimel and A. Kacker (2006). "The relationship between oral malodor and volatile sulfur compound-producing bacteria." Otolaryngol Head Neck Surg **135**(5): 671-676.
- Krithikadatta, J., V. Gopikrishna and M. Datta (2014). "CRIS Guidelines (Checklist for Reporting *In-vitro* Studies): A concept note on the need for standardized guidelines for improving quality and transparency in reporting *in-vitro* studies in experimental dental research." J Conserv Dent **17**(4): 301-304.

- Larimer, C., E. Winder, R. Jeters, M. Prowant, I. Nettleship, R. S. Addleman and G. T. Bonheyo (2016). "A method for rapid quantitative assessment of biofilms with biomolecular staining and image analysis." Anal Bioanal Chem **408**(3): 999-1008.
- Ledder, R. G., T. Madhwani, P. K. Sreenivasan, W. De Vizio and A. J. McBain (2009). "An *in vitro* evaluation of hydrolytic enzymes as dental plaque control agents." J Med Microbiol **58**(Pt 4): 482-491.
- Ledder, R. G. and A. J. McBain (2012). "An *in vitro* comparison of dentifrice formulations in three distinct oral microbiotas." Arch Oral Biol **57**(2): 139-147.
- Ledder, R. G., P. K. Sreenivasan, W. DeVizio and A. J. McBain (2010). "Evaluation of the specificity and effectiveness of selected oral hygiene actives in salivary biofilm microcosms." J Med Microbiol **59**(Pt 12): 1462-1468.
- Li, Y., C. G. Zou, Y. Fu, Y. Li, Q. Zhou, B. Liu, Z. Zhang and J. Liu (2016). "Oral microbial community typing of caries and pigment in primary dentition." BMC Genomics **17**: 558.
- Liljemark, W. F. and C. Bloomquist (1996). "Human oral microbial ecology and dental caries and periodontal diseases." Crit Rev Oral Biol Med **7**(2): 180-198.
- Lockhart, P. B., M. T. Brennan, M. Thornhill, B. S. Michalowicz, J. Noll, F. K. Bahrani-Mougeot and H. C. Sasser (2009). "Poor oral hygiene as a risk factor for infective endocarditis-related bacteremia." J Am Dent Assoc **140**(10): 1238-1244.
- Luo, T., U. Srinivasan, K. Ramadugu, K. A. Shedden, K. Neiswanger, E. Trumble, J. J. Li, D. W. McNeil, R. J. Crout, R. J. Weyant, M. L. Marazita and B. Foxman (2016). "Effects of specimen collection methodologies and storage conditions on the short-term stability of oral microbiome taxonomy." Appl Environ Microbiol **82**(18): 5519-5529.
- Luo, T. L., Eisenberg, M.C., Hayashi, M. Gonzalez-Cabezas, C., Foxman, B., Marrs, C.F., Rickard, A.H. (2018). "A sensitive thresholding method for confocal laser scanning microscope image stacks of microbial biofilms." Nature Scientific Reports.
- Luo, T. L., A. H. Rickard, U. Srinivasan, K. S. Kaye and B. Foxman (2015). "Association of *bla*<sub>OXA-23</sub> and *bap* with the persistence of *Acinetobacter baumannii* within a major healthcare system." Front Microbiol **6**: 182.
- Mah, T. F. and G. A. O'Toole (2001). "Mechanisms of biofilm resistance to antimicrobial agents." Trends Microbiol **9**(1): 34-39.
- Mansoor, A., V. Patsekin, D. Scherl, J. P. Robinson and B. Rajwa (2015). "A statistical modeling approach to computer-aided quantification of dental biofilm." IEEE J Biomed Health Inform **19**(1): 358-366.
- Marcenes, W., N. J. Kassebaum, E. Bernabe, A. Flaxman, M. Naghavi, A. Lopez and C. J. Murray (2013). "Global burden of oral conditions in 1990-2010: a systematic analysis." J Dent Res **92**(7): 592-597.

Marsh, P. D. (2006). "Dental diseases--are these examples of ecological catastrophes?" Int J Dent Hyg **4 Suppl 1**: 3-10; discussion 50-12.

Marsh, P. D. (2006). "Dental plaque as a biofilm and a microbial community - implications for health and disease." BMC Oral Health **6 Suppl 1**: S14.

Marsh, P. D. (2010). "Controlling the oral biofilm with antimicrobials." J Dent **38 Suppl 1**: S11-15.

Marsh, P. D., A. Moter and D. A. Devine (2011). "Dental plaque biofilms: communities, conflict and control." Periodontol 2000 **55**(1): 16-35.

Martin-Kerry, J. M., T. J. Lamont, A. Keightley, H. Calache, R. Martin, R. Floate, K. Princi and A. M. de Silva (2015). "Practical considerations for conducting dental clinical trials in primary care." Br Dent J **218**(11): 629-634.

McBain, A. J. (2009). "Chapter 4: *In vitro* biofilm models: an overview." Adv Appl Microbiol **69**: 99-132.

McBain, A. J., R. G. Bartolo, C. E. Catrenich, D. Charbonneau, R. G. Ledder and P. Gilbert (2003). "Effects of a chlorhexidine gluconate-containing mouthwash on the vitality and antimicrobial susceptibility of *in vitro* oral bacterial ecosystems." Appl Environ Microbiol **69**(8): 4770-4776.

McBain, A. J., R. G. Bartolo, C. E. Catrenich, D. Charbonneau, R. G. Ledder and P. Gilbert (2003). "Growth and molecular characterization of dental plaque microcosms." J Appl Microbiol **94**(4): 655-664.

McBain, A. J., C. Sissons, R. G. Ledder, P. K. Sreenivasan, W. De Vizio and P. Gilbert (2005). "Development and characterization of a simple perfused oral microcosm." J Appl Microbiol **98**(3): 624-634.

McCoy, W. F., J. D. Bryers, J. Robbins and J. W. Costerton (1981). "Observations of fouling biofilm formation." Can J Microbiol **27**(9): 910-917.

Metcalf, D., C. Robinson, D. Devine and S. Wood (2006). "Enhancement of erythrosine-mediated photodynamic therapy of *Streptococcus mutans* biofilms by light fractionation." J Antimicrob Chemother **58**(1): 190-192.

Milferstedt, K., M. N. Pons and E. Morgenroth (2008). "Textural fingerprints: a comprehensive descriptor for biofilm structure development." Biotechnol Bioeng **100**(5): 889-901.

Milferstedt, K., M. N. Pons and E. Morgenroth (2009). "Analyzing characteristic length scales in biofilm structures." Biotechnol Bioeng **102**(2): 368-379.

Millioni, R., S. Sbrignadello, A. Tura, E. Iori, E. Murphy and P. Tessari (2010). "The inter- and intra-operator variability in manual spot segmentation and its effect on spot

quantitation in two-dimensional electrophoresis analysis." Electrophoresis **31**(10): 1739-1742.

Mueller, L. N., J. F. de Brouwer, J. S. Almeida, L. J. Stal and J. B. Xavier (2006). "Analysis of a marine phototrophic biofilm by confocal laser scanning microscopy using the new image quantification software PHLIP." BMC Ecol **6**: 1.

Mulcahy, L. R., V. M. Isabella and K. Lewis (2014). "*Pseudomonas aeruginosa* biofilms in disease." Microb Ecol **68**(1): 1-12.

Murray, C. J., M. Ezzati, A. D. Flaxman, S. Lim, R. Lozano, C. Michaud, M. Naghavi, J. A. Salomon, K. Shibuya, T. Vos, D. Wikler and A. D. Lopez (2012). "GBD 2010: design, definitions, and metrics." Lancet **380**(9859): 2063-2066.

Murray, C. J. L. and A. D. Lopez (2017). "Measuring global health: motivation and evolution of the Global Burden of Disease Study." Lancet **390**(10100): 1460-1464.

Nagaoka, S., K. Hojo, S. Murata, T. Mori, T. Ohshima and N. Maeda (2008). "Interactions between salivary *Bifidobacterium adolescentis* and other oral bacteria: *in vitro* coaggregation and coadhesion assays." FEMS Microbiol Lett **281**(2): 183-189.

Nance, W. C., S. E. Dowd, D. Samarian, J. Chludzinski, J. Delli, J. Battista and A. H. Rickard (2013). "A high-throughput microfluidic dental plaque biofilm system to visualize and quantify the effect of antimicrobials." J Antimicrob Chemother **68**(11): 2550-2560.

Newnham, J. P., Shub, A., Doherty, D., Sloboda, D.M., Nitsos, I., Moss, T.J.M. (2005). "Recent advances in understanding and preventing pre-term birth - the oral health connection." Reprod, Fert, Develop **17**(9): 64-66.

Ng, H. M., L. X. Kin, S. G. Dashper, N. Slakeski, C. A. Butler and E. C. Reynolds (2016). "Bacterial interactions in pathogenic subgingival plaque." Microb Pathog **94**: 60-69.

Noiri, Y., T. Katsumoto, H. Azakami and S. Ebisu (2008). "Effects of Er:YAG laser irradiation on biofilm-forming bacteria associated with endodontic pathogens *in vitro*." J Endod **34**(7): 826-829.

Otsu, N. (1979). "A threshold selection method from gray-level histograms." IEEE Transactions of Systems Man and Cybernetics **9**(1): 62-66.

Owens, G. J., R. J. M. Lynch, C. K. Hope, L. Cooper, S. M. Higham and S. P. Valappil (2017). "Evidence of an *in vitro* coupled diffusion mechanism of lesion formation within microcosm dental plaque." Caries Res **51**(3): 188-197.

Oz, H. S. and D. A. Puleo (2011). "Animal models for periodontal disease." J Biomed Biotechnol **2011**: 754857.

Palmer, R. J., Jr. (1999). "Microscopy flowcells: perfusion chambers for real-time study of biofilms." Methods Enzymol **310**: 160-166.

- Palmer, R. J., Jr. (2014). "Composition and development of oral bacterial communities." Periodontol 2000 **64**(1): 20-39.
- Palmer, R. J., Jr., K. Kazmerzak, M. C. Hansen and P. E. Kolenbrander (2001). "Mutualism versus independence: strategies of mixed-species oral biofilms *in vitro* using saliva as the sole nutrient source." Infect Immun **69**(9): 5794-5804.
- Palmer, R. J., Jr. and C. Sternberg (1999). "Modern microscopy in biofilm research: confocal microscopy and other approaches." Curr Opin Biotechnol **10**(3): 263-268.
- Palmer, R. J., Jr., Caldwell, D.E. (1995). "A flowcell for the study of plaque removal and regrowth." Journal of Microbiological Methods **24**(2): 171-182.
- Parahitiyawa, N. B., C. Scully, W. K. Leung, W. C. Yam, L. J. Jin and L. P. Samaranayake (2010). "Exploring the oral bacterial flora: current status and future directions." Oral Dis **16**(2): 136-145.
- Pavissich, J. P., I. T. Vargas, B. Gonzalez, P. A. Pasten and G. E. Pizarro (2010). "Culture dependent and independent analyses of bacterial communities involved in copper plumbing corrosion." J Appl Microbiol **109**(3): 771-782.
- Peters, A. C. and J. W. Wimpenny (1988). "A constant-depth laboratory model film fermentor." Biotechnol Bioeng **32**(3): 263-270.
- Petersen, P. E., D. Bourgeois, H. Ogawa, S. Estupinan-Day and C. Ndiaye (2005). "The global burden of oral diseases and risks to oral health." Bull World Health Organ **83**(9): 661-669.
- Peterson, S. N., E. Snesrud, J. Liu, A. C. Ong, M. Kilian, N. J. Schork and W. Bretz (2013). "The dental plaque microbiome in health and disease." PLoS One **8**(3): e58487.
- Pigman, W., J. Brasher and T. Koulourides (1962). "Cariogenicity of common sugars as evaluated in the artificial mouth." Nature **195**: 190-191.
- Pigman, W., H. C. Elliott, Jr. and R. O. Laffre (1952). "An artificial mouth for caries research." J Dent Res **31**(5): 627-633.
- Pigman, W., W. L. Hawkins, J. Watson, R. Powell and C. Gaston (1955). "The effect of the concentration of D-glucose on the attack of tooth substances in the artificial mouth." J Dent Res **34**(4): 537-545.
- Pigman, W. and E. Newbrun (1962). "Evaluation of anticaries agents by the use of the artificial mouth." J Dent Res **41**: 1304-1311.
- Polk, D. E., R. J. Weyant, R. J. Crout, D. W. McNeil, R. E. Tarter, J. G. Thomas and M. L. Marazita (2008). "Study protocol of the Center for Oral Health Research in Appalachia (COHRA) etiology study." BMC Oral Health **8**: 18.

- Reighard, K. P., D. B. Hill, G. A. Dixon, B. V. Worley and M. H. Schoenfisch (2015). "Disruption and eradication of *P. aeruginosa* biofilms using nitric oxide-releasing chitosan oligosaccharides." Biofouling **31**(9-10): 775-787.
- Reilly, C., K. Rasmussen, T. Selberg, J. Stevens and R. S. Jones (2014). "Biofilm community diversity after exposure to 0.4% stannous fluoride gels." J Appl Microbiol **117**(6): 1798-1809.
- Renslow, R., Z. Lewandowski and H. Beyenal (2011). "Biofilm image reconstruction for assessing structural parameters." Biotechnol Bioeng **108**(6): 1383-1394.
- Rickard, A. H., S. R. Campagna and P. E. Kolenbrander (2008). "Autoinducer-2 is produced in saliva-fed flow conditions relevant to natural oral biofilms." J Appl Microbiol **105**(6): 2096-2103.
- Rickard, A. H., P. Gilbert, N. J. High, P. E. Kolenbrander and P. S. Handley (2003). "Bacterial coaggregation: an integral process in the development of multi-species biofilms." Trends Microbiol **11**(2): 94-100.
- Ridler, T. W., Calvard, S. (1978). "Picture thresholding using an iterative selection method." IEEE Transactions of Systems Man and Cybernetics **8**(8): 630.
- Rivera, M. F., J. Y. Lee, M. Aneja, V. Goswami, L. Liu, I. M. Velsko, S. S. Chukkapalli, I. Bhattacharyya, H. Chen, A. R. Lucas and L. N. Kesavalu (2013). "Polymicrobial infection with major periodontal pathogens induced periodontal disease and aortic atherosclerosis in hyperlipidemic ApoE(null) mice." PLoS One **8**(2): e57178.
- Rojas, D., L. Rueda, A. Ngom, H. Hurrutia and G. Carcamo (2011). "Image segmentation of biofilm structures using optimal multi-level thresholding." Int J Data Min Bioinform **5**(3): 266-286.
- Romling, U. and C. Balsalobre (2012). "Biofilm infections, their resilience to therapy and innovative treatment strategies." J Intern Med **272**(6): 541-561.
- Rosin, P. L. (2001). "Unimodal thresholding." Pattern Recognition **34**(11): 2083-2096.
- Rudney, J. D., R. Chen, P. Lenton, J. Li, Y. Li, R. S. Jones, C. Reilly, A. S. Fok and C. Aparicio (2012). "A reproducible oral microcosm biofilm model for testing dental materials." J Appl Microbiol **113**(6): 1540-1553.
- Russell, C. and F. I. Ahmed (1978). "Interrelationships between lactobacilli and streptococci in plaque formation on a tooth in an artificial mouth." J Appl Bacteriol **45**(3): 373-382.
- Russell, C. and W. A. Coulter (1977). "Plaque formation by streptococci in an artificial mouth and factors influencing colonization." J Appl Bacteriol **42**(3): 337-344.

- Salli, K. M. and A. C. Ouwehand (2015). "The use of *in vitro* model systems to study dental biofilms associated with caries: a short review." J Oral Microbiol **7**: 26149.
- Samarian, D. S., N. S. Jakubovics, T. L. Luo and A. H. Rickard (2014). "Use of a high-throughput *in vitro* microfluidic system to develop oral multi-species biofilms." J Vis Exp(94).
- Sanders, A. E., G. D. Slade, S. Lim and S. T. Reisine (2009). "Impact of oral disease on quality of life in the US and Australian populations." Community Dent Oral Epidemiol **37**(2): 171-181.
- Sbordone, L. and C. Bortolaia (2003). "Oral microbial biofilms and plaque-related diseases: microbial communities and their role in the shift from oral health to disease." Clin Oral Investig **7**(4): 181-188.
- Schwendicke, F., C. E. Dorfer, P. Schlattmann, L. Foster Page, W. M. Thomson and S. Paris (2015). "Socioeconomic inequality and caries: a systematic review and meta-analysis." J Dent Res **94**(1): 10-18.
- Selwitz, R. H., A. I. Ismail and N. B. Pitts (2007). "Dental caries." Lancet **369**(9555): 51-59.
- Sheiham, A., D. M. Williams, R. J. Weyant, M. Glick, S. Naidoo, J. L. Eisele and H. S. Selikowitz (2015). "Billions with oral disease: A global health crisis--a call to action." J Am Dent Assoc **146**(12): 861-864.
- Shin, J. M., I. Ateia, J. R. Paulus, H. Liu, J. C. Fenno, A. H. Rickard and Y. L. Kapila (2015). "Antimicrobial nisin acts against saliva derived multi-species biofilms without cytotoxicity to human oral cells." Front Microbiol **6**: 617.
- Shukla, S. K. and T. S. Rao (2013). "Effect of calcium on *Staphylococcus aureus* biofilm architecture: a confocal laser scanning microscopic study." Colloids Surf B Biointerfaces **103**: 448-454.
- Sissons, C. H. (1997). "Artificial dental plaque biofilm model systems." Adv Dent Res **11**(1): 110-126.
- Sliepen, I., M. Van Essche, M. Quirynen and W. Teughels (2010). "Effect of mouthrinses on *Aggregatibacter actinomycetemcomitans* biofilms in a hydrodynamic model." Clin Oral Investig **14**(3): 241-250.
- Stewart, P. S. (2003). "Diffusion in biofilms." J Bacteriol **185**(5): 1485-1491.
- Stoodley, P., K. Sauer, D. G. Davies and J. W. Costerton (2002). "Biofilms as complex differentiated communities." Annu Rev Microbiol **56**: 187-209.
- Strathdee, F. and A. Free (2013). "Denaturing gradient gel electrophoresis (DGGE)." Methods Mol Biol **1054**: 145-157.

- Struillou, X., H. Boutigny, A. Soueidan and P. Layrolle (2010). "Experimental animal models in periodontology: a review." Open Dent J **4**: 37-47.
- Taani, D. Q. (2002). "Relationship of socioeconomic background to oral hygiene, gingival status, and dental caries in children." Quintessence Int **33**(3): 195-198.
- Takahashi, N. and B. Nyvad (2008). "Caries ecology revisited: microbial dynamics and the caries process." Caries Res **42**(6): 409-418.
- Takenaka, S., M. Iwaku and E. Hoshino (2001). "Artificial *Pseudomonas aeruginosa* biofilms and confocal laser scanning microscopic analysis." J Infect Chemother **7**(2): 87-93.
- Tan, C. H., K. W. Lee, M. Burmolle, S. Kjelleberg and S. A. Rice (2017). "All together now: experimental multispecies biofilm model systems." Environ Microbiol **19**(1): 42-53.
- Tang, G., H. K. Yip, T. W. Cutress and L. P. Samaranayake (2003). "Artificial mouth model systems and their contribution to caries research: a review." J Dent **31**(3): 161-171.
- Tavares, M., K. A. Lindefjeld Calabi and L. San Martin (2014). "Systemic diseases and oral health." Dent Clin North Am **58**(4): 797-814.
- Taylor, B. and J. Greenman (2010). "Modelling the effects of pH on tongue biofilm using a sorbarod biofilm perfusion system." J Breath Res **4**(1): 017107.
- Team, B. (2015). "Global oral health burden amounts to \$442 billion." Br Dent J **219**(7): 311.
- Thompson, H., A. Rybalka, R. Moazzez, F. E. Dewhirst and W. G. Wade (2015). "*In vitro* culture of previously uncultured oral bacterial phylotypes." Appl Environ Microbiol **81**(24): 8307-8314.
- Tinanoff, N. (1995). "Progress regarding the use of stannous fluoride in clinical dentistry." J Clin Dent **6 Spec No**: 37-40.
- Tinanoff, N., J. Hock, D. Camosci and L. Hellden (1980). "Effect of stannous fluoride mouthrinse on dental plaque formation." J Clin Periodontol **7**(3): 232-241.
- Tonetti, M. S., P. Eickholz, B. G. Loos, P. Papapanou, U. van der Velden, G. Armitage, P. Bouchard, R. Deinzer, T. Dietrich, F. Hughes, T. Kocher, N. P. Lang, R. Lopez, I. Needleman, T. Newton, L. Nibali, B. Pretzl, C. Ramseier, I. Sanz-Sanchez, U. Schlegelhauf and J. E. Suvan (2015). "Principles in prevention of periodontal diseases: consensus report of group 1 of the 11th European Workshop on Periodontology on effective prevention of periodontal and peri-implant diseases." J Clin Periodontol **42 Suppl 16**: S5-11.
- Torpy, J. M., A. E. Burke and R. M. Glass (2008). "JAMA patient page. Periodontal disease." JAMA **299**(5): 598.

- Unnikrishnan, R., C. Pantofaru and M. Hebert (2007). "Toward objective evaluation of image segmentation algorithms." IEEE Trans Pattern Anal Mach Intell **29**(6): 929-944.
- Valm, A. M., J. L. Mark Welch and G. G. Borisy (2012). "CLASI-FISH: principles of combinatorial labeling and spectral imaging." Syst Appl Microbiol **35**(8): 496-502.
- van Aarle, W., K. J. Batenburg and J. Sijbers (2011). "Optimal threshold selection for segmentation of dense homogeneous objects in tomographic reconstructions." IEEE Trans Med Imaging **30**(4): 980-989.
- Vieira, A. R., A. Modesto and M. L. Marazita (2014). "Caries: review of human genetics research." Caries Res **48**(5): 491-506.
- Vogtmann, E., X. Hua, L. Zhou, Y. Wan, S. Suman, B. Zhu, C. L. Dagnall, A. Hutchinson, K. Jones, B. D. Hicks, R. Sinha, J. Shi and C. C. Abnet (2018). "Temporal variability of oral microbiota over 10 months and the implications for future epidemiologic studies." Cancer Epidemiol Biomarkers Prev.
- Vyas, N., R. L. Sammons, O. Addison, H. Dehghani and A. D. Walmsley (2016). "A quantitative method to measure biofilm removal efficiency from complex biomaterial surfaces using SEM and image analysis." Sci Rep **6**: 32694.
- Wade, W. G. (2013). "The oral microbiome in health and disease." Pharmacol Res **69**(1): 137-143.
- Wall, T., Nasseh, K., & Vujcic, M. (2014). "U.S. dental spending remains flat through 2012." American Dental Association(Health Policy Resources Center Research Brief): 1-11.
- Walter, J., C. Schwab, D. M. Loach, M. G. Ganzle and G. W. Tannock (2008). "Glucosyltransferase A (GtfA) and inulosucrase (Inu) of *Lactobacillus reuteri* TMW1.106 contribute to cell aggregation, *in vitro* biofilm formation, and colonization of the mouse gastrointestinal tract." Microbiology **154**(Pt 1): 72-80.
- Weiss, E. I., R. Lev-Dor, Y. Kashamn, J. Goldhar, N. Sharon and I. Ofek (1998). "Inhibiting interspecies coaggregation of plaque bacteria with a cranberry juice constituent [published erratum appear in J Am Dent Assoc 1999 Jan;130(1):36 and 1999 Mar;130(3):332]." J Am Dent Assoc **129**(12): 1719-1723.
- Whitmore, S. E. and R. J. Lamont (2011). "The pathogenic persona of community-associated oral streptococci." Mol Microbiol **81**(2): 305-314.
- Williams, D. L., R. T. Epperson, J. P. DeGrauw, M. B. Nielsen, N. B. Taylor and R. D. Jolley (2017). "Effect of silver-loaded PMMA on *Streptococcus mutans* in a drip flow reactor." J Biomed Mater Res A **105**(9): 2632-2639.
- Wimpenny, J. (2009). "Microbial metropolis." Adv Microb Physiol **56**: 29-84.

- Wimpenny, J., W. Manz and U. Szewzyk (2000). "Heterogeneity in biofilms." FEMS Microbiol Rev **24**(5): 661-671.
- Wood, S. R., J. Kirkham, P. D. Marsh, R. C. Shore, B. Nattress and C. Robinson (2000). "Architecture of intact natural human plaque biofilms studied by confocal laser scanning microscopy." J Dent Res **79**(1): 21-27.
- Wu, Y. M., F. Ren, L. L. Chen, W. L. Sun, J. Liu, L. H. Lei, J. Zhang and Z. Cao (2014). "Possible socioeconomic and oral hygiene behavioural risk factors for self-reported periodontal diseases in women of childbearing age in a Chinese population." Oral Health Prev Dent **12**(2): 171-181.
- Xiao, J., A. T. Hara, D. Kim, D. T. Zero, H. Koo and G. Hwang (2017). "Biofilm three-dimensional architecture influences *in situ* pH distribution pattern on the human enamel surface." Int J Oral Sci **9**(2): 74-79.
- Xu, K. D., P. S. Stewart, F. Xia, C. T. Huang and G. A. McFeters (1998). "Spatial physiological heterogeneity in *Pseudomonas aeruginosa* biofilm is determined by oxygen availability." Appl Environ Microbiol **64**(10): 4035-4039.
- Xu, X., J. He, J. Xue, Y. Wang, K. Li, K. Zhang, Q. Guo, X. Liu, Y. Zhou, L. Cheng, M. Li, Y. Li, Y. Li, W. Shi and X. Zhou (2015). "Oral cavity contains distinct niches with dynamic microbial communities." Environ Microbiol **17**(3): 699-710.
- Xu, Z., Y. Liang, S. Lin, D. Chen, B. Li, L. Li and Y. Deng (2016). "Crystal violet and XTT assays on *Staphylococcus aureus* biofilm quantification." Curr Microbiol **73**(4): 474-482.
- Xue, J., Zhang, YJ. (2012). "Ridler and Calvard's, Kittler and Illingworth's and Otsu's methods for image thresholding." Pattern Recognition Letters **33**(6): 793-797.
- Yaari, A. and B. G. Bibby (1976). "Production of plaques and initiation of caries *in vitro*." J Dent Res **55**(1): 30-36.
- Yang, L., Y. Liu, H. Wu, N. Hoiby, S. Molin and Z. J. Song (2011). "Current understanding of multi-species biofilms." Int J Oral Sci **3**(2): 74-81.
- Yang, X., H. Beyenal, G. Harkin and Z. Lewandowski (2000). "Quantifying biofilm structure using image analysis." J Microbiol Methods **39**(2): 109-119.
- Yang, X., H. Beyenal, G. Harkin and Z. Lewandowski (2001). "Evaluation of biofilm image thresholding methods." Water Res **35**(5): 1149-1158.
- Yassin, S. A., M. J. German, S. L. Rolland, A. H. Rickard and N. S. Jakubovics (2016). "Inhibition of multispecies biofilms by a fluoride-releasing dental prosthesis copolymer." J Dent **48**: 62-70.

Yerly, J., Y. Hu, S. M. Jones and R. J. Martinuzzi (2007). "A two-step procedure for automatic and accurate segmentation of volumetric CLSM biofilm images." J Microbiol Methods **70**(3): 424-433.

Yoon, N. A. and C. W. Berry (1979). "The antimicrobial effect of fluorides (acidulated phosphate, sodium and stannous) on *Actinomyces viscosus*." J Dent Res **58**(8): 1824-1829.

Zanin, I. C., R. B. Goncalves, A. B. Junior, C. K. Hope and J. Pratten (2005). "Susceptibility of *Streptococcus mutans* biofilms to photodynamic therapy: an *in vitro* study." J Antimicrob Chemother **56**(2): 324-330.

Zaura-Arite, E., J. van Marle and J. M. ten Cate (2001). "Conofocal microscopy study of undisturbed and chlorhexidine-treated dental biofilm." J Dent Res **80**(5): 1436-1440.

Zaura, E., B. J. Keijser, S. M. Huse and W. Crielaard (2009). "Defining the healthy "core microbiome" of oral microbial communities." BMC Microbiol **9**: 259.

Zhang, T. (2017). "Modeling biofilms: from genes to communities." Processes **5**(1): 17.

Zijngel, V., M. B. van Leeuwen, J. E. Degener, F. Abbas, T. Thurnheer, R. Gmur and H. J. Harmsen (2010). "Oral biofilm architecture on natural teeth." PLoS One **5**(2): e9321.

Zobell, C. E. and E. C. Allen (1935). "The significance of marine bacteria in the fouling of submerged surfaces." J Bacteriol **29**(3): 239-251.